UNIVERSIDADE FEDERAL DE PERNAMBUCO
CENTRO DE TECNOLOGIA E GEOCIÊNCIAS
DEPARTAMENTO DE ENGENHARIA MECÂNICA
PROGRAMA DE PÓS-GRADUAÇÃO EM ENGENHARIA MECÂNICA

LUIS CARLOS FABRÍCIO FILHO

A STUDY ON HULL FORM DESIGN OF A SHIP

Recife
2020

LUIS CARLOS FABRÍCIO FILHO

A STUDY ON HULL FORM DESIGN OF A SHIP

Thesis submitted to the Graduate Program in Mechanical Engineering of the Federal University of Pernambuco in partial fulfillment of the requirements for the degree of Master in Mechanical Engineering.

Field of concentration: Materials and Manufacturing Engineering.

Advisor: Prof. Dr. Armando Hideki Shinohara.

Co-advisor: Prof. Dr. Tadao Yamano.

Recife

2020

Catalogação na fonte
Bibliotecária Margareth Malta, CRB-4 / 1198

F126s Fabrício Filho, Luis Carlos.
A study on hull form design of a ship / Luis Carlos Fabrício Filho. - 2020.
121 folhas, il., gráfs., tabs.

Orientador: Prof. Dr. Armando Hideki Shinohara.
Coorientador: Prof. Dr. Tadao Yamano.

Dissertação (Mestrado) – Universidade Federal de Pernambuco. CTG. Programa de Pós-Graduação em Engenharia Mecânica, 2020.
Inclui Referências.
Texto em Inglês

1. Engenharia Mecânica. 2. Redução da resistência de formação de ondas. 3. Método de projeto de forma de proa. 4. Ensaio de resistência ao avanço em CWC. 5. Navio-modelo. I. Shinohara, Armando Hideki (Orientador). II. Yamano, Tadao (Coorientador). III. Título.

UFPE

621 CDD (22. ed.) BCTG/2020-89

LUIS CARLOS FABRÍCIO FILHO

A STUDY ON HULL FORM DESIGN OF A SHIP

Thesis submitted to the Graduate Program in Mechanical Engineering of the Federal University of Pernambuco in partial fulfillment of the requirements for the degree of Master in Mechanical Engineering.

Approved in: 02 / 03 / 2020.

THESIS COMMITTEE

_____

Prof. Dr. Armando Hideki Shinohara (Advisor)
Federal University of Pernambuco

_____

Prof. Dr. Cezar Henrique Gonzalez (Internal Committee Member)
Federal University of Pernambuco

_____

Profº. Drº. Shuji Aihara (External Committee Member)
The University of Tokyo (Emeritus Professor)

This master’s thesis is dedicated to professor Tadao Yamano, whose contribution was essencial for the development of the studies here reported, without which this master’s thesis would not be possible. I am greatly indebted to him.

ACKNOWLEDGMENTS

The study described in Chapter 4 has been conducted as a cooperative study between Federal University of Pernambuco and Oshima Shipbuilding Co., Ltd. Thanks are given to Dr. Junichi Man, General Manager of Design Department, Oshima Shipbuilding Co., Ltd. and Prof. Cezar H. Gonzalez, Coordinator of the Graduate Program of Mechanical Engineering – PPGEM/UFPE, for their understanding the significance of the cooperative study and their contribution to its realization. Special thanks are given to Prof. Armando H. Shinohara and prof. Tadao Yamano, my supervisors. Thanks are also extended to CAPES/MEC, for the financial support through the master's scholarship and to prof. Kleber Gonçalves B. Alves, for his kindness to the approval of the examination board in a short time due to carnival holidays.

ABSTRACT

It goes without saying that energy saving is important now for our world. The study carried out for this master's thesis has the theme of energy saving a ship. This master's thesis reports two studies that share the same theme: hull form design of a ship, with a focus on reduction of wave-making resistance by the hull form improvement. In both studies, the importance of the bow form for reduction of wave-making resistance, which my undergraduate thesis has clarified, is a base. In the first study, a bow form design method for a full ship has been developed and its usefulness has been confirmed by model tests. In the second study, a new resistance test method for a fine ship in a CWC (Circulating Water Channel) has been developed to solve the issues present in the traditional resistance test method in a small CWC concerning accuracy in resistance measurement and model ship manufacture. The new method increases the value of the measured total resistance of the most important part of hull by 216 times compared with that of Traditional Resistance Test Method. The models and connection system necessary for the confirmation test of the method in the CWC have been designed. A study on the model manufacture for the test in a CWC was also conducted, in which material, paint and resin were studied from the viewpoints of strength, water tightness and manufacture easiness by actually manufacturing a partial model and by testing it.

Keywords: Reduction of Wave-making resistance. Bow form design method. Resistance test in CWC. Model ship.

RESUMO

É indiscutível a importância da economia de energia para o mundo atual. O estudo realizado para esta dissertação de mestrado tem como tema economia de energia de um navio. Esta dissertação apresenta dois estudos que compartilham do mesmo tema: projeto da forma do casco de um navio, com foco na redução da resistência de formação de ondas pela melhoria da forma do casco. Em ambos os estudos, a importância da forma da proa para a redução da resistência de formação de ondas, que foi esclarecida no meu trabalho de conclusão de curso, é tomada como base. No primeiro estudo, um método de projeto de forma de proa para um navio de formas cheias foi desenvolvido e sua utilidade foi comprovada por ensaios de resistência ao avanço de navios-modelo. No segundo estudo, um novo método de ensaio de resistência ao avanço para um navio formas finas em um CWC (Canal de Água Circulante, do inglês *circulating water channel*) foi desenvolvido a fim de solucionar os problemas presentes no método tradicional de ensaio de resistência ao avanço em um CWC de pequeno porte no que diz respeito à precisão da medição da resistência ao avanço e à confecção de navios-modelo. O novo método aumenta o valor da resistência ao avanço total medida da parte mais importante do casco em 216 vezes em comparação com o método tradicional de ensaio de resistência ao avanço. Os modelos e o sistema de conexão necessários para o teste de comprovação do método no CWC foram projetados. Foi realizado também um estudo sobre a confecção de um modelo para ensaio em CWC, no qual o material, a tinta e a resina foram estudados sob os pontos de vista de resistência, impermeabilidade e facilidade de confecção, através da confecção e teste de um modelo parcial.

Palavras-chave: Redução da resistência de formação de ondas. Método de projeto de forma de proa. Ensaio de resistência ao avanço em CWC. Navio-modelo.

LIST OF ILLUSTRATIONS

LIST OF TABLES

LIST OF ABBREVIATIONS

AP	Aft perpendicular
BHP	Brake horsepower
CFD	Computational fluid dynamics
CWC	Circulating water channel
DWT	Deadweight tonnage
EHP	Effective horsepower
FP	Fore perpendicular
LPG	Liquefied petroleum gas
LWL	Load waterline
NOR BHP	Normal break horsepower
OB, OF, M1B etc.:	First 1 or 2 letters = Bow form; O Original, M1 Modified 1, M2 Modified 2, Last 1 letter = Condition; F Full load, H Half load, B Ballast
SS	Square station: SS 0 = AP, SS 10 = FP
VLCC	Very large crude carrier

LIST OF SYMBOLS

B	Breadth molded (m)
B/d	Breadth-draft ratio (-)
b_e	Imaginary half breadth of fore end of waterline on water surface (m)
$C(\theta), S(\theta)$	Amplitude functions of elementary wave (m/rad)
C_b	Block coefficient (-)
d	Draft molded (m)
d_a	Aft draft (m)
d_f	Fore draft (m)
d_{ls}	Depth of a line source (m)
d_m	Mean draft (m)
EHP	Effective horsepower, $EHP = R_{ts}V_s/75$ (hp)
F_n	Froude number, $F_n = V/\sqrt{g \cdot L_{LWL}}$ (-)
g	Gravity acceleration (m/s^2)
i_e	Entrance half angle of waterline on water surface (deg)
i_r	Stem rake angle on water surface (deg)
k	Form factor (-)
ℓ	$\ell = L_{pp}/2$ (m)
L/B	Length-breadth ratio (-)
l_{cb}	Center of buoyancy from midship (%L_{pp})
l_f	Bow profile from FP (m)
L_{LWL}	Length on load waterline (m)
L_{oa}	Length over all (m)
L_{pp}	Length between perpendiculars (m)
n	Counter for a divided unit of a raked stem (-)
N	Total number of draft-ward divided units of a raked stem (-)
r_f	Frictional resistance coefficient, $r_f = R_f/\rho\nabla^{2/3}V^2$ (-)
R_f	Frictional resistance (kgf)
R_v	Form resistance (kgf)
r_w	Wave-making resistance coefficient, $r_w = R_w/\rho\nabla^{2/3}V^2$ (-)

R_w	Wave-making resistance (kgf)
sr	Steradian
V	Ship speed (m/s)
V'	Ship speed (knot)
∇	Displacement volume (m^3)
Δ	Displacement weight (t)
ΔC_f	Friction correction (-)
$\delta\tau$	$\delta\tau = \tau/N$ (-)
ε_{ls}	Line source position from fore-end, $\varepsilon ls(z)=y(lf(z),z)/\ \pi$ (m)
ζ	$\zeta = z/\ell$ (-)
ξ	$\xi = x/\ell$ (-)
θ	Advancing direction of an elementary wave from x axis (rad)
ρ	Water density ($kgf{\cdot}s^2/m^4$)
σ	Singularity distribution density (m/(s·sr) on a surface, m^2/(s·sr) on a line)
τ	$\tau = d/\ell$ (-)
χ	$\chi = g/V^2$ (m^{-1})
χ_0	$\chi_0 = l\chi$ (-)
x, y, z	Coordinate system (m)

X_s: Subscript s:	Quantity X related to full-scale ship
X_m: Subscript m:	Quantity X related to model ship
$C = \frac{R}{\frac{1}{2}\rho S V^2}$	resistance coefficient
$\frac{R_{ws}}{\rho_s V_s^2}$	Wave-making resistance proportional to R_{ws} at a ship speed V_s (m^2)

SUMMARY

1 INTRODUCTION

The world’s economy is undergoing a profound transition. The driving factors of the transition are population growth, rising incomes, decreasing natural resources, and a climate change scenario. Shipping is an ocean-based industry. It is responsible for carrying approximately 90% of global trade (OECD, 2016). Shipbuilding is another ocean-based industry and is responsible for providing ships for the shipping industry.

The economic importance of shipping activities is attested by the UN (2017): “Sea-borne trade is of strategic economic importance, as it accounts for over 80 per cent of world merchandise trade by volume and more than 70 per cent of its value”.

Ships mostly use fossil fuel as energy resource. However, it goes without saying that the carbon emissions caused by the burning of fossil fuels have severely impacted the ocean. The increase of atmospheric CO_2 since the industrial revolution has induced ocean acidification “ten times faster than at any time in the las 55 million years” (OECD, 2016).

The fuel oil combustion generates not only CO_2, but also other products such as NO_x, SO_x, CO, HC (which, together with CO_2, are the so-called greenhouse gases, GHG), and particulate materials. The exhaust gases are emitted into the atmosphere from the ship's exhaust and are diluted with the ambient air. These emissions can alter regionally and globally the composition of the atmosphere, impacting the climate (Eyring *et al*., 2005, apud Schiller, 2017).

The IMO estimated that the fuel consumption used by the world fleet doubled between the years 1990 and 2007, ranging from 170 million to more than 340 million tons per year (IMO, 2008, apud Schiller, 2017). This shows that the demand for fuel oil is also increasing, which threatens the sustainable use of natural resources.

In such a scenario, it is indispensable to design resource-efficient and climate-friendly ships. The study carried out for this master’s thesis has the theme of energy saving a ship. This master’s thesis reports two studies that share the same theme, which is based on my undergraduate thesis results. In section 1.1, the theme is presented. In section 1.2, the importance of the theme is presented. In section 1.3, the structure of this master’s thesis is reported.

1.1 THEME

The definition of the theme of this master's thesis and its two studies needs the understanding of technical terms such as hull form, full ship, fine ship, model test, CWC, and wave-making resistance. For this understanding, the reader may refer to chapter 2.

The theme of this master's thesis is hull form design of a ship, with a focus on reduction of wave-making resistance by the hull form improvement.

In the first study, "Study 1" hereafter, a bow form design method for a full ship has been developed and its usefulness has been confirmed by model tests. In the second study, "Study 2" hereafter, a new resistance test method for a fine ship in a CWC has been developed to solve the issues present in the traditional resistance test method in a smaller CWC concerning accuracy in resistance measurement and model ship manufacture.

1.2 IMPORTANCE OF THE THEME

When a shipowner requests a ship to a shipbuilder, the shipowner provides only two design conditions: ship speed and cargo weight. The shipbuilder realizes all the work of design and construction to complete the ship, and hull form design is one of the designs. The hull form design decides the main engine horsepower of a ship, which is very important because it decides fuel consumption. And, fuel consumption decides the ship's operation economy, which is related to energy saving. So, it is important to minimize the main engine horsepower. To do that, the hull form design tries to realize minimum resistance, highest propeller efficiency and best interaction between the hull and the propeller.

From the resistance point of view, the main purpose of the hull form design is to design a hull form with minimum wave-making resistance. To do that, it is necessary to understand the relation between hull form and wave-making resistance. However, this relation is not yet completely clear. So, three methods can be used to help understanding this relation:

a) Wave-making resistance theory (theoretical approach)
b) Model test (experimental approach)
c) Accumulated model test results (past, history)

"Study 1" uses methods "a)" and "c)" to develop a bow form design method for a full ship, and method "b)" for confirmation. "Study 2", is concerned with solving a problem present in method "b)".

1.3 STRUCTURE OF THIS MASTER'S THESIS

Chart 1 below presents the structure of the two studies of this master's thesis, which are referred to as "Study 1" and "Study 2".

Chart 1 – Structure of the two studies of this master's thesis

	"Study 1"	"Study 2"
Title of the study	Development of a bow form design method for a full ship	Development of a new resistance test method for a fine ship in a CWC
Location (Chapter)	Chapter 4	Chapter 5
Target ship kind	Full ships with F_n around 0.15	Fine ships with $F_n \geq 0.20$
Issues to be solved	• To clarify the reason why the wave-making resistance at Ballast condition of the subject ship is so large. • To reduce the large resistance at ballast condition of the subject Panamax bulk carrier • Absence of a bow form design method that: can be used for any bow form; is effective at Full and ballast condition; can be used even for full ships with C_b around 0.9 and can be used to solve the above issues	• Low accuracy in resistance measurement and model manufacture in traditional resistance test method in a small CWC. • Lack of model ship suppliers.
Base finding for study	• Undergraduate thesis results.	• Undergraduate thesis results.
Base data for study	• Resistance test results on a 7m-long model ship of a Panamax bulk carrier at 21 drafts by Yamano (1994)	• Hull form data of a 354,000ft³ refrigerated cargo ship
CWC to be used for confirmation test	• A CWC with B more than 2m (Finally, that of Oshima Shipbuilding Co. Ltd. has been used)	• CWC with observation part with dimensions length × breadth × height =2.00m×0.50m×0.50m installed in the university

Basic idea for study	1) The base data give us 21 data on the relation between bow form and wave-making resistance for a full ship. 2) To clarify the relation by detailed analysis of base data “1)” 3) From “2)”, to derive an equation to estimate wave-making resistance. 4) From “3)”, to develop a bow form design method for a full ship The most important study is at step “2)”.	1) To realize such a model test in a small CWC in that only an important part of a hull is tested. 2) By the test “1)”, we can use larger scale partial model. 3) The larger scale partial model brings 1. Larger resistance and higher measurement accuracy 2. Higher accuracy of model manufacture The most important study is how to realize step “1)”.
Results of study	1) A bow form design method for a full ship has been developed. 2) By the method, the reason why the wave-making resistance at Ballast condition of the subject ship is so large has been clarified. 3) By the method, the large wave-making resistance at Ballast condition of the subject ship has been reduced.	1) Models including connection system to be used for the confirmation test in the CWC have been designed. 2) Materials and manufacturing procedures for the models have been clarified.
Confirmation of usefulness of developed method	• Modified bow form designed by the developed bow form design method was tested using 2m-long model ship in the CWC of Oshima Shipbuilding Co. Ltd. • The result showed a EHP reduction of 5.5% by the modified bow M2 as the average value in the F_n range from 0.10 to 0.18. • This value is practically large enough. • As a result, we have concluded that the developed bow form design method for a full ship is useful for practical design.	• Confirmation test was not conducted, because the CWC is not in such a condition we can use it normally.

Source: The Author (2019).

1.4 GENERAL OBJECTIVE

To further clarify the relation between hull form and wave-making resistance of full ships and fine ships and develop new technologies to design hull form with less wave-making resistance based on the results of the studies.

1.5 SPECIFIC OBJECTIVES

The specific objectives are stated in the following for each of the studies: “Study 1” and “Study 2”.

1.5.1 For “Study 1”

(1) To clarify the relation between the bow form parameters and the wave-making resistance of a full ship

(2) To derive an equation to estimate the wave-making resistance of a full ship at any draft and any Froude number F_n, using the relation got in “(1)”

(3) To confirm the usefulness of the equation derived in “(2)” by applying the equation for reducing the larger wave-making resistance at Ballast condition of a Panamax bulk carrier.

(4) Based on “(1)”, “(2)” and “(3)”, to derive a practical bow form design method for a full ship which we can apply to any bow form including that of such a very full ship as with block coefficient C_b of around 0.9.

1.5.2 For “Study 2”

(1) To confirm the reliability of the result of the undergraduate thesis (FABRÍCIO FILHO, L.C., 2018) that has pointed out the outstanding importance of bow form of a fine ship in wave-making resistance at Froude number below 0.26

(2) Based on the result got in “(1)”, to develop a new resistance test method for a fine ship in a CWC which improves the demerit of a small CWC: low accuracy in resistance measurement and model manufacture.

(3) To clarify the issues and the ways how to solve the issues regarding the confirmation model test of the new model test method.

2 THEORETICAL FUNDAMENTALS

This chapter presents and explains fundamental concepts necessary to understand this master's thesis. In section 2.1, important technical terms used in this master's thesis are explained. In section 2.2, the resistance problem is presented. In section 2.3, model test, Froude number and Froude's law of similarity, which is the base of model test, are explained. In section 2.4, the types of resistance are presented. In section 2.5, the wave-making resistance is explained. In section 2.6, the linear wave-making resistance theory is presented.

2.1 EXPLANATION OF IMPORTANT TECHNICAL TERMS

In the following, the technical terms hull form, full ship, fine ship and CWC, which are used in this master's thesis, are explained in sections 2.1.1 to 2.1.4. In section 2.1.5, a hull form description (hull forms dimensions, AP, FP, C_b) is done.

2.1.1 Hull form

Hull form is the form of the ship's body. The hull form is represented by hull lines (Figure 1): body plan (transverse sections), buttock lines (longitudinal sections) and waterlines (horizontal sections). The fore part of the hull is called bow, shown in the figure.

Figure 1 – Hull Lines

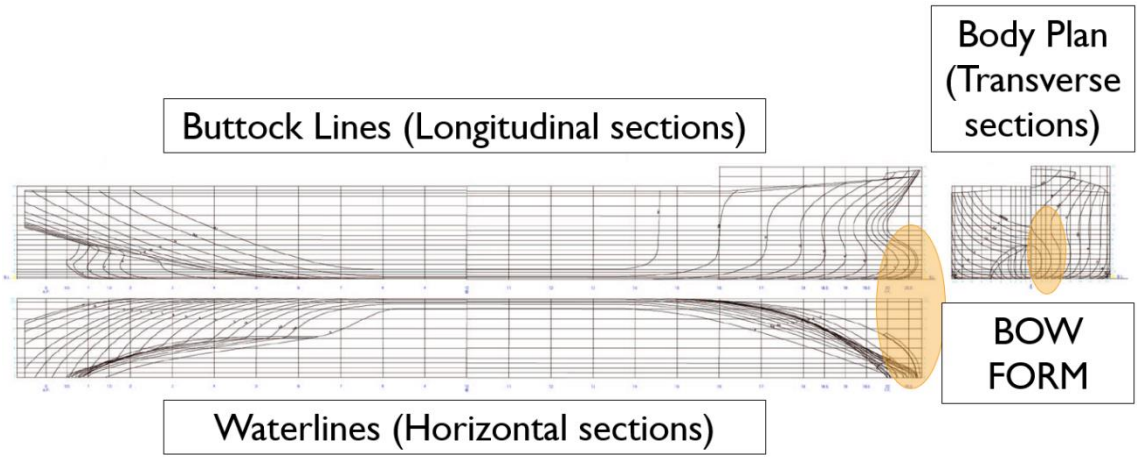

Source: RESEARCHGATE (2009). Adapted.

2.1.2 Full ship

Full ship is a low-speed ship, with a full-bodied form and Froude number around 0.15 (Froude number will be explained in 2.3.1), such as bulk carriers and oil tankers. Figure 2 shows an example of full ship, a bulk carrier. The bow is shown in the figure. The lines of full load condition and ballast condition (the present condition) are also shown. The full load condition is that of the fully loaded ship. The ballast condition is that of the unloaded ship, where only the ballast tanks are filled with water to provide the ship enough stability.

Figure 2 – An example of full ship.

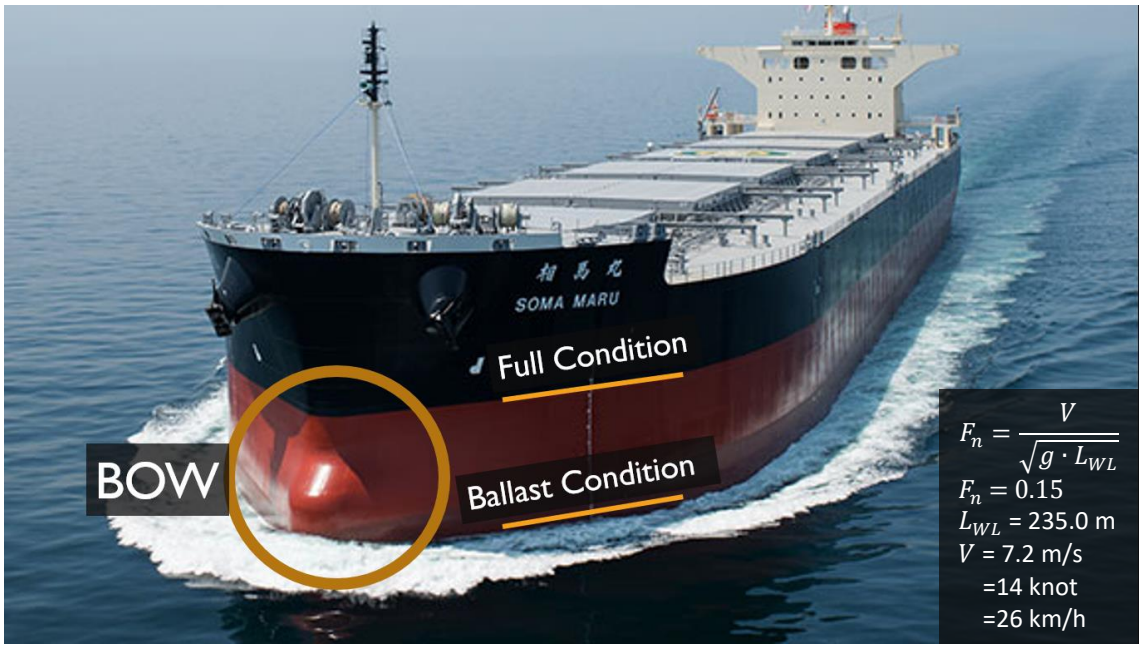

Source: WORLDCOAL (2014). Adapted.

2.1.3 Fine ship

Fine ship is a high-speed ship, with a fine form and Froude number larger than 0.20, such as container ships and pure car carriers. Figure 3 shows an example of fine ship, a container ship. The bow is shown in the figure. The lines of full load condition and ballast condition (the present condition) are also shown.

Figure 3 – An example of fine ship.

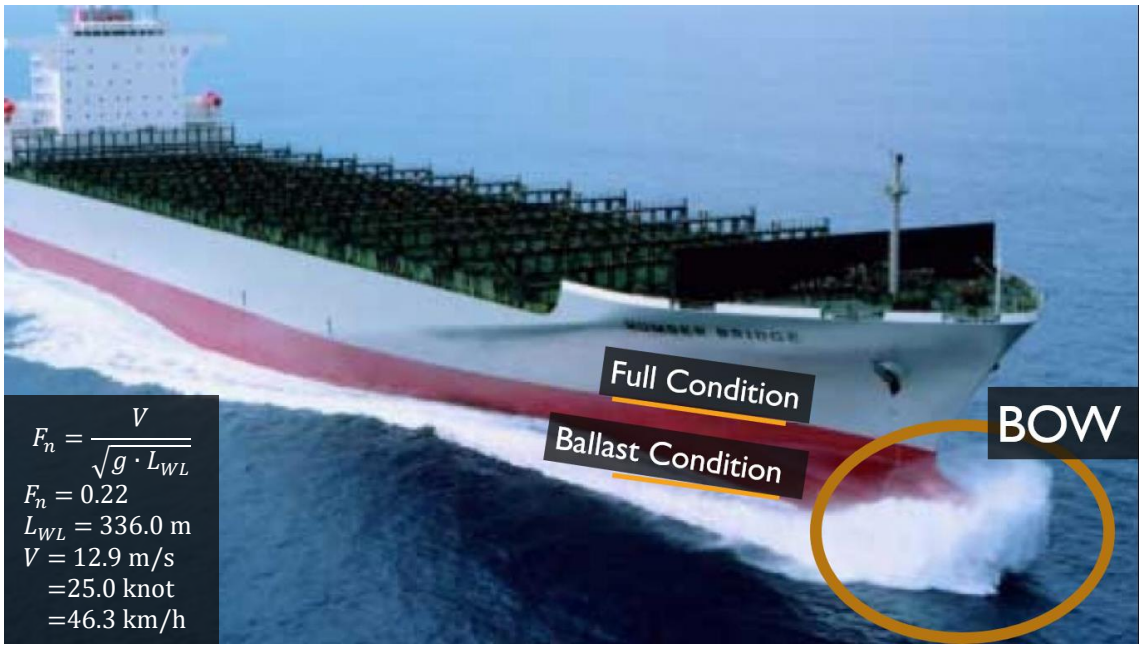

Source: SEATRADE MARITIME (2013). Adapted.

2.1.4 CWC

A CWC – circulating water channel – is shown in Figure 4. It is a device that has a channel, which is filled with water, and an impeller in it circulates the water (Figure 4). It has an observation section (Figure 4), where some object is set and the flow around the object can be observed, or, the resistance of the object can be measured. CWC can be used for resistance test with a model ship.

Figure 4 – CWC

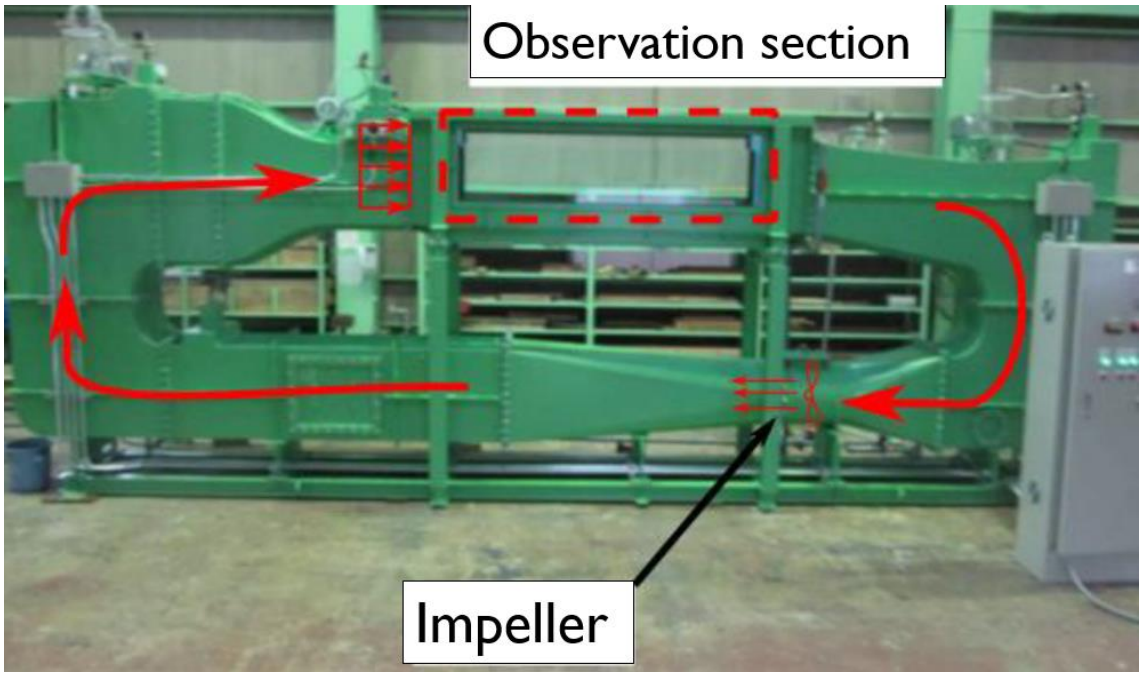

Source: FEL (2015), adapted.

2.1.5 Hull form description

Figure 5 shows important hull dimensions. B is the breadth molded. d draft molded. d_f fore draft. d_a aft draft. L_{pp} length between perpendiculars (perpendiculars: AP – aft perpendicular, on the center of the rudder shaft; FP – fore perpendicular, on the cross point of LWL (load waterline) and bow profile). L_{WL} length on the waterline. L_{OA} length overall.

Figure 6 shows the definition of C_b, the block coefficient. C_b expresses how much of the volume of a box with dimensions $L_{pp} \cdot B \cdot d$ is occupied by the hull form. The closest to 1, the fuller is the ship. That is, C_b expresses the fullness of a ship's hull form.

Figure 5 – Hull dimensions

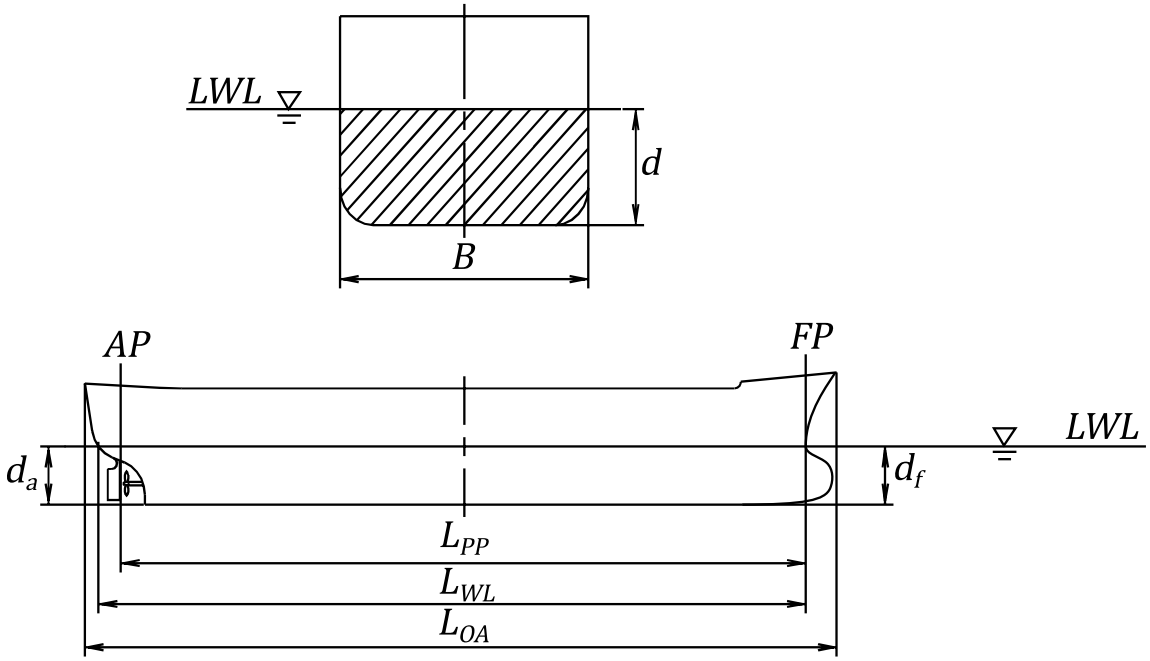

Source: MAN DIESEL & TURBO (2011).

Figure 6 – Definition of C_b

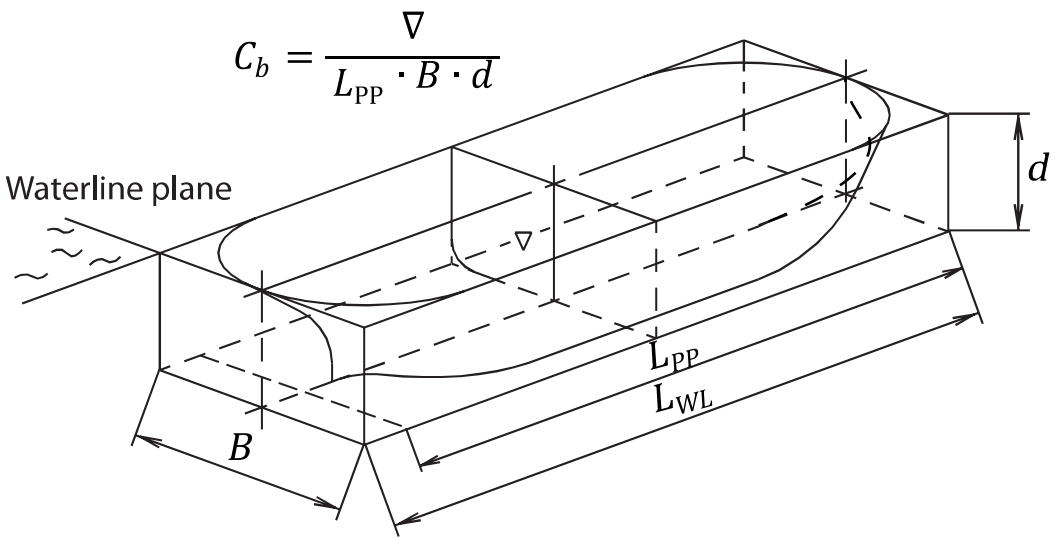

Source: MAN DIESEL & TURBO (2011).

2.2 RESISTANCE

Daily experience shows that it is necessary to put force on a solid so that it moves at a certain speed in the fluid medium: that is, when moving in this medium, the solid feels resistance. The intuitive concept of resistance probably came into

existence as soon as it was built. Builders, since antiquity, found that certain forms were more favorable to navigation than others, although they did not know how to explain the reason (LAP, 1958).

Over thousands of years, shipbuilding had been developing quite slowly. One could experiment with full-scale ships without much concern. With the Industrial Revolution, the daily life of the Western World began to demand rapidity in several areas, and the naval sector was not left out. The use of propellers and steel allowed the construction of new types of ships, with higher speeds and larger sizes (and also more expensive), with which the designers had no experience (LAP, 1958).

After several attempts at construction, some forms did not permit the design speed to be reached at installed main engine horsepower, and in other cases, a speed can be achieved in a fraction of the installed main engine horsepower. This motivated the development of a method that allows determining beforehand the main engine horsepower that a ship should have to reach a certain speed (LAP, 1958).

In the course of the 19th century, then, many notable scientists turned their attention to this problem. In the search for solutions, many of them turned to the preparation of model tests. It so happens that, at that time, there was a lack of understanding of the physical phenomenon of flow in a moving ship, which meant that model tests were discredited by the shipyards of the time. (LAP, 1958).

2.3 MODEL TESTS: RESISTANCE TEST

The resistance problem came to have its first solutions with the English naval architect William Froude, the pioneer of experimental techniques for investigating hull forms and propellers, after obtaining fundamental explanations of the phenomenon discussed in the previous section. He obtained support from the British Admiralty (institution that was formerly responsible for the British Royal Navy), which resulted in the construction of the world's first towing tank for model experiment in Torquay, around 1870. The method developed by W. Froude is still used today in model tests (LAP, 1958).

One of the experiments done with models is called resistance test. If done in a towing tank, the resistance test is as follows: a model is guided through the water and along the tank with the help of a towing cart or a long wire. The force required to move the model at a certain speed is measured. If done in a CWC, the model ship is set in water flow with a certain speed and the force with which the model ship is

pushed by the water flow is measured. From the measurements at resistance test, with the aid of the method proposed by Froude, it is possible to calculate the resistance of the full-scale ship corresponding to the model ship tested (LAP, 1958).

A perhaps more important fact about model tests is the possibility of making comparative tests with different models designed for the same ship. This makes it possible for designers, using the method developed by Froude, to test various models until reaching the form that best meets the resistance criteria (LAP, 1958).

2.3.1 Froude number

W. Froude found that the resistance depends on the hull form, the speed and the properties of the fluid, as expressed in equation (1) (LAP, 1958).

$$R = f\left(\text{hull form}, \frac{V}{\sqrt{gL}}, \frac{\rho VL}{\nu}\right) \quad (1)$$

Where V is the ship speed, ρ is the specific density, ν is the viscosity, g is the gravitacional acceleration, and L is the waterline length of a ship.

The parameter $\frac{\rho VL}{\nu}$ is the Reynolds number, which represents the ratio between the inertial force of the water and the frictional force.

The parameter $\frac{\mathrm{V}}{\sqrt{gL}}$ is the Froude number, which represents the ratio between the inertial force of the water and the gravitational force to the water.

Usually, Froude number is based on L_{WL}. So, we use Froude number as equation (2):

$$F_n = \frac{V}{\sqrt{gL_{WL}}} \quad (2)$$

2.3.2 Froude's law of similarity

The Reynolds number decides the frictional coefficient C_f. In a model test, the Reynolds number is different between the model ship and full-scale ship. So, to

estimate the frictional resistance of the full-scale ship, C_f of a flat plate is used (and a correction factor ΔC_f got from sea trial results).

However, in a model test, the model ship speed is set so that its Froude number is same as that of full-scale ship because, at the same Froude number, the wave by a model ship becomes similar to that of its full-scale ship. So, the wave-making resistance coefficient is also same between the model ship and full-scale ship. This is called Froude's law of similarity and is the reason why model ships can be used for a test.

2.4 TYPES OF RESISTANCE

Resistance has three components: frictional resistance (R_f), form resistance (R_V), and wave-making resistance (R_w). The total resistance (R_t) is the sum of the components, as shown in equation (3).

$$R_t = R_f + R_V + R_w \tag{3}$$

A resistance component R can be non-dimensionalized by $\rho\nabla^{2/3}V^2$:

$$r_t = \frac{R_t}{\rho\nabla^{2/3}V^2}, \qquad r_f = \frac{R_f}{\rho\nabla^{2/3}V^2}, \qquad k \cdot r_f = \frac{R_V}{\rho\nabla^{2/3}V^2}, \qquad r_w = \frac{R_w}{\rho\nabla^{2/3}V^2}$$

Where r_t is the total resistance coefficient, r_f is the frictional resistance coefficient, r_w is the wave-making resistance coefficient, and k is the form factor. ρ is the water density, ∇ is the displacement volume, and V is the speed.

Writing equation (1) in terms of the resistance coefficients and the form factor k, we have:

$$r_t = r_f + k \cdot r_f + r_w$$

$$r_t = (1 + k)r_f + r_w \tag{4}$$

2.5 WAVE-MAKING RESISTANCE

For bodies completely immersed in a fluid, such as an airplane moving in the air or a submarine moving in the water, only the frictional resistance and the form resistance are present. However, a ship moves between the boundary of the two fluids, air and water. Since the density of water is about 800 times larger than that of air, as the ship moves on the boundary, the boundary moves up and down. This movement of the boundary is wave made by the ship. To make the wave, the ship loses energy to the water. The ship feels the energy loss as a force from the water. This is wave-making resistance.

Therefore, the total resistance of a ship has the three components: frictional resistance, form resistance, and wave-making resistance. Figure 7 shows the resistance components of an airplane, a submarine, and a ship.

Figure 7 – Resistance components of an airplane, a submarine, and a ship.

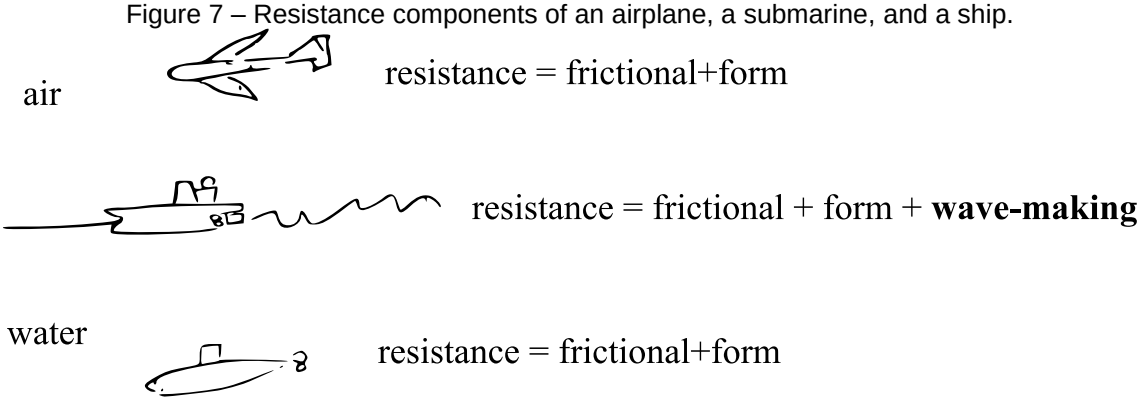

Source: The Author (2019)..

Lord Kelvin is credited with the first considerations regarding the ship's wave system. He observed that for a pressure point moving at a uniform speed, in a straight line, on the water surface, waves generated by the point combined to form a specific pattern. This pattern consists of a system of transverse waves following behind the point, along with a series of divergent waves radiated from the point. The complete system is limited by two straight lines that start from the point and make an angle of 19°28'on each side of the movement line, as shown in Figure 8 (VAN MANEN, 1988).

Figure 8 – Kelvin’s wave pattern

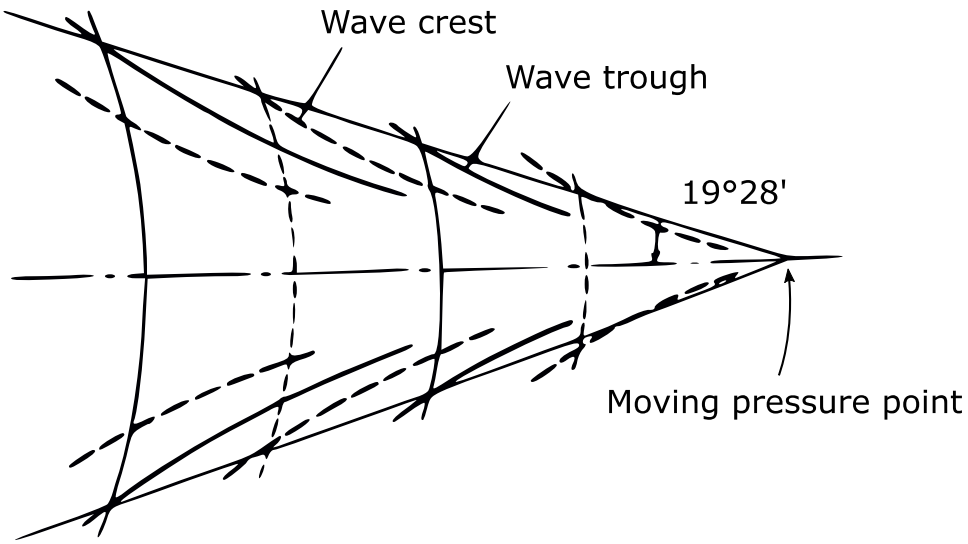

Source: VAN MANEN (1988, p. 16).

The Kelvin’s wave pattern illustrates and explains many of the characteristics of a ship's wave system (see Figure 9). (VAN MANEN, 1988).

Figure 9 – Ship’s wave pattern

Source: MFAME TEAM (2016).

2.6 THE LINEAR WAVE-MAKING RESISTANCE THEORY

The design of the hull form became, after Froude, very dependent on model tests. Even though it is not possible to get rid of model test to use only a theoretical method, theoretical treatments can provide valuable information regarding the phenomenon. The combination of a theoretical approach with purely empirical investigations can guide the designer towards the optimization of his project (LAP, 1958).

The linear wave-making resistance theory was first formulated by Michell (MICHELL, 1898) and was developed by authors such as Havelock and Lunde (HAVELOCK, 1932, 1934, 1924; LUNDE, 1951). It has great utility in the design of thin ships with a higher Froude number, in which the wave-making resistance represents the largest portion of the total resistance (YAMANO, 2018).

At the forefront of the hull form design is Computational Fluid Dynamics (CFD). CFD directly solves the equations of motion of a fluid (Euler or Navier-Stokes equation) through numerical realization. Nonlinear factors are even taken into account, which allows obtaining more accurate data than a linear approach, such as the linear wave-making resistance theory (YAMANO, 2018).

Despite the advantage of precision, CFD is not a theory, but a numerical method and, therefore, does not, in itself, present the relation between results (for instance, resistance) and input parameters (for instance, hull form). Thus, CFD can be considered a method similar to model tests, which provides an accurate result, without, however, explaining the relation between hull form and resistance (YAMANO, 2018).

The linear wave-making resistance theory, on the other hand, although it does not provide results as accurate as CFD, shows the relation between hull form and wave-making resistance, which is quite useful to assist in the design (YAMANO, 2018).

2.6.1 Equations to calculate wave-making resistance

The wave-making resistance, according to the linear wave-making resistance theory, can be calculated by equation (5) (HAVELOCK, 1934):

$$R_w = \pi\rho V^2 \int_0^{\pi/2} [S^2(\theta) + C^2(\theta)] \cos^3\theta \, d\theta \tag{5}$$

In equation (5), R_w [kgf] is the wave-making resistance; V [m/s] is the ship speed; ρ [kgf s^2/m^4] is the water density; $S(\theta)$ and $C(\theta)$ are called amplitude function of, respectively, a sine elementary wave and a cosine elementary wave, advancing in the direction θ (see Figure 10).

Figure 10 – Coordinate system

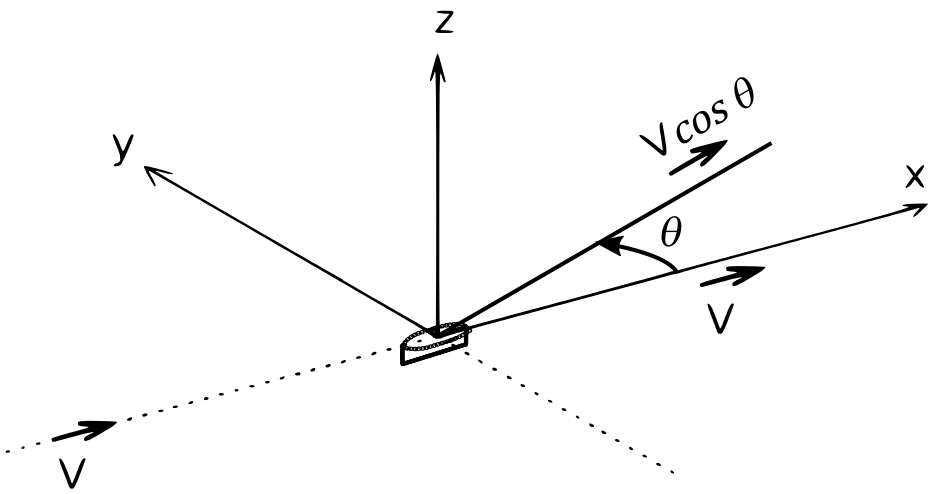

Source: The Author (2019).

The linear wave-making resistance theory is based on a principle in which the ship wave can be expressed with the superposition of innumerable elementary waves (two-dimensional waves) advancing to the direction θ from $-\pi/2$ to $\pi/2$.

According to the linear wave-making resistance theory, for a coordinate system as in Figure 10, the functions $S(\theta)$ and $C(\theta)$ can be calculated by equation (6) (HAVELOCK, 1934):

$$\left.\begin{matrix} C(\theta) \\ S(\theta) \end{matrix}\right\} = \frac{4V\chi^2}{g} \sec^3\theta \cdot \int_{x_1}^{x_2} \int_{z_1}^{z_2} \sigma(x,z) e^{z\chi \sec^2\theta} \begin{matrix} \cos \\ \sin \end{matrix} (\chi x \sec\theta) dz \, dx \tag{6}$$

In equation (6), $\chi = g/V^2$, where g is the gravitaty acceleration; $\sigma(x,z)$ is called singularity distribution density. The singularity distribution is a distribution of sources and/or sinks, over a plane, a line or a point, that represents a hull form.

2.6.2 Representation of a hull form with singularities

The relation between hull form and singularity distribution density $\sigma(x,z)$ in equation (6) can be expressed according to the next two points (YAMANO, 2018):

a) main hull: singularity density with distribution given by equation (7):

$$\sigma(x,z) = \frac{V}{2\pi}\frac{\partial y(x,z)}{\partial x} \tag{7}$$

Where:

$y(x,z)$: main hull half-breadth as a function of x and z

b) bulbous bow: for the following three cases:

(i) Stem with breadth $2b_e$ in Figure 11 (i), at $x = x_e$: line source with density given by equation (8).

$$\sigma(x_e,z) = \frac{V}{2\pi}b_e \tag{8}$$

(ii) Bulb similar to a longitudinal cylinder with radius r_s and rounded head in Figure 11 (ii), at $x = x_s,\ z = z_s$: point source with density given by equation (9).

$$\sigma(x_s,z_s) = \frac{V}{4}r_s^2 \tag{9}$$

(iii) Bulb similar to a ball with radius r_b (Figure 11 (iii)) at $x = x_b,\ z = z_b$: doublet with density given by equation (10):

$$\sigma(x_b,z_b) = \frac{V}{2}r_b^3 \tag{10}$$

Figure 11 – Relations of singularity density for bulbous bow

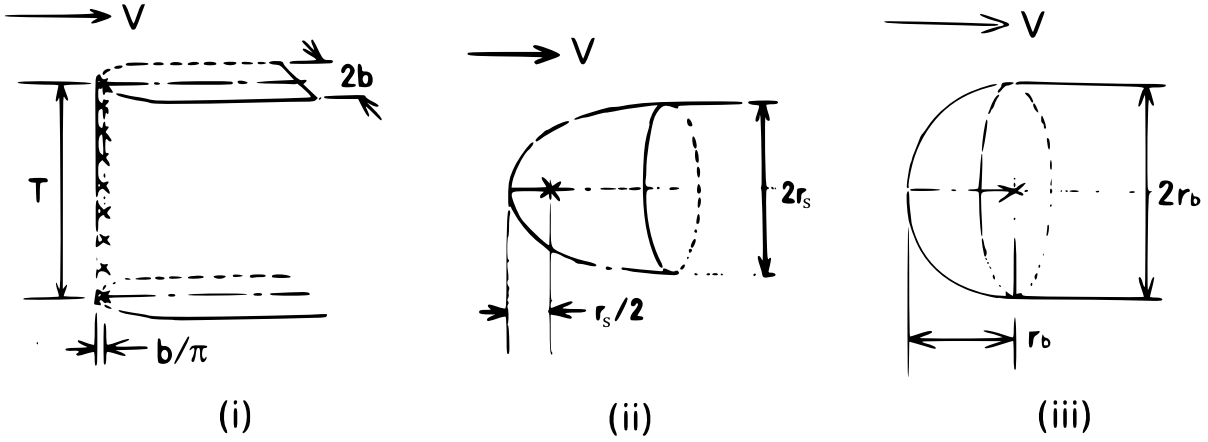

Source: YAMANO (2018). Adapted.

2.6.3 Effect of immersion in wave-making resistance

In equation (6), the term $e^{z\chi \sec^2\theta}$ shows the effect of immersion. In the resistance equation (5), this term becomes $e^{2z\chi \sec^2\theta}$. For example, consider a ship at draft of d = 11m, V'= 25 knots (V = 12.86m/s). For these values, with gravity acceleration g = 9.8 m/s^2 and θ = 0, $\chi = g/V^2$ = 0.05926. The graph in Figure 12 shows that the effect on load waterline (LWL, z = 0), which is the largest, drops to approximately half at $z = ½\ (-d)$ and to about 1/3 at the bottom ($z = -d$) (YAMANO, 2018).

Figure 12 – Effect of immersion in wave-making resistance

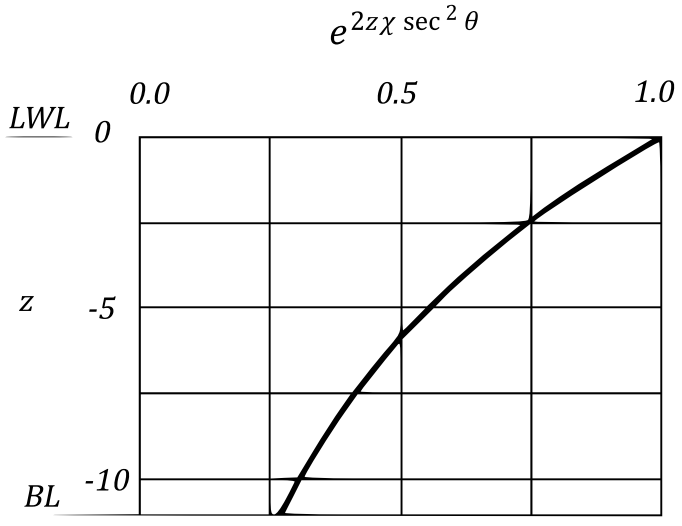

Source: The Author (2019).

3 METHODOLOGY

The methodologies of “Study 1” and “Study 2” are described in this chapter, in sections 3.1 and 3.2, respectivelly.

3.1 FOR “STUDY 1”

In this section, the methodology of “Study 1” is presented. In 3.1.1, the base data adopted for “Study 1” is presented. In 3.1.2, the form to express wave-making resistance in “Study 1” and the reason for using such a form are explained. In 3.1.3, the theory used to analyze the data in “Study 1” is presented.

In “Study 1”, first, a preliminary study was conducted. In 3.1.4, the methodology of the preliminary study is presented. Then, a detailed study was conducted. In 3.1.5, the methodology of the detailed study is presented.

3.1.1 Base data

As the base data for the “Study 1”, we adopted the results of resistance test by Yamano (1994), with a 7m-long model ship of a Panamax bulk carrier (Ship ISNI) in a towing tank with length 200m, breadth 13m, and water depth 6.5m. The characteristic point of the data is that the resistance test was conducted at as many as 21 drafts, from a shallow draft (d_f = 2.68 m) to an over-full draft (d_f = 14.66 m). With the change of draft, the waterline form at water surface, which is the most important hull parameter for wave-making resistance, changes. Therefore, despite the data are those of only a ship, the value of the resistance test data for our present study is almost equivalent to that of resistance test results on 21 different bow forms.

3.1.2 Expression of wave-making resistance in the form $\frac{R_{ws}}{\rho_s V_s^2}$

The displacement volumes at 21 drafts vary widely from the smallest one $0.34\nabla_{Full}$ to the largest one $1.20\nabla_{Full}$. However, the hull form parameter that is most important for wave-making resistance is not ∇ but the waterline form on the water surface. Therefore, the form $r_w = \frac{R_w}{\rho \nabla^{2/3} V^2}$ is not preferable for us to compare wave-making resistance at a draft to those at other drafts. So, we use the form $\frac{R_{ws}}{\rho_s V_s^2}$, which is proportional to R_{ws} at a ship speed.

3.1.3 Linear wave-making resistance theory

As the method to describe the relation between bow form and wave-making resistance, we use the linear wave-making resistance theory. The application of the linear theory to a full ship might cause lower quantitative accuracy. However, the theory has a merit that it not only gives us the calculation result but also it explains the relation between input data (bow form) for calculation and calculation result. This is the reason why we use the linear theory.

3.1.4 Preliminary study

In a preliminary study, using the base data described in 3.1.1 and the theory in 3.1.3, we clarified the relation between bow form and wave-making resistance, concluding that wave-making resistance is strongly related with the far fore end of the bow, from fore end to 0.5% L_{pp} aft. The means by which we could get such a result is described in 3.1.4.1. The way of the analysis is presented in 3.1.4.2.

3.1.4.1 Means for analysis

As a means to analyze the base data described in 3.1.1 in the preliminary study, we developed an algorithm using the software Octave GNU to calculate wave-making resistance by a bow based on the linear wave-making resistance theory. One of the characteristics of the developed algorithm is that a bow form, input data for the algorithm to calculate wave-making resistance, is divided draft-wise into many units. Each unit has an upper side waterline and lower side one. These waterlines are approximated with polynomials for calculation. Each transverse section of the unit has a form of trapezoid. We can select the draft-wise depth of each unit and number of the units between BL and water surface according to the form of a transverse section or the profile of the bow. With such an algorithm, we can input the details of the bow form to calculate its wave-making resistance.

3.1.4.2 Analysis

We analyze the base data described in 3.1.1 using the algorithm developed in 3.1.4.1 from the viewpoints of 1) clarifying the relation between a bow form of a full ship and its wave-making resistance and 2) clarifying the most important part of a bow for its wave-making resistance.

3.1.5 Detailed study

Based on the results of the “Preliminary study” described in 3.1.4, we further studied in order to find the bow form parameters which are most strongly related with wave-making resistance. As a result, we find such bow form parameters (3.1.5.1), derive an equation to estimate the wave-making resistance of a full ship (3.1.5.2), apply the derived equation to design new bow forms and estimate their wave-making resistance (3.1.5.3), confirm the usefulness of the equation by model test of the design new bow forms (3.1.5.4), and, finally, develop a bow form design method for a full ship (3.1.5.5).

3.1.5.1 Investigation of bow form parameters

We use the base data described in 3.1.1 and the theory in 3.1.3 to investigate the effect of the bow form parameters “b_e”, “i_r” and “i_e” on wave-making resistance of a full ship.

3.1.5.2 Derivation of an equation to estimate wave-making resistance of the subject ship

Through the findings of the investigation described above, we derive an equation to estimate the wave-making resistance of a full ship, at any draft, at any Froude number F_n.

3.1.5.3 Application of the derived equation to bow form design

For reducing the larger wave-making resistance at Ballast condition of the subject ship (Ship ISNI), from the original bow form of Ship ISNI (which we call bow form “O”, original), we design modified bow forms “M1” and “M2”. Then, we estimate the reduction of wave-making resistance by the designed modified bow forms “M1” and “M2” and estimate their wave-making resistance using the equation we derived, described above.

3.1.5.4 Confirmation of the derived equation by model test

We conduct resistance test by using 2m-long model ships of the three bow models: “O”, “M1” and “M2”, in order to confirm the EHP reduction by the modified bow forms “M1” and “M2”, which are designed as described above.

3.1.5.5 Development of a bow form design method for a full ship

Based on the procedures above, we derive a practical bow form design method for a full ship which we can apply to any bow form including that of such a very full ship as with C_b of around 0.9, with design Froude number F_n below 0.17.

3.2 FOR STUDY 2

In this section, the methodology of “Study 2” is presented.

3.2.1 Base findings of the new resistance test method

Two findings support the new resistance test method (we call “Finding 1” and “Finding 2”). “Finding 1” is that of the results of my undergraduate thesis and other works by Yamano: that most of the wave-making resistance is generated by the bow (YAMANO *et al*., 1996, 1997; FABRÍCIO FILHO *et al*., 2018, 2019a). “Finding 2” is that most of the wave-making resistance by the bow is due to wave-breaking near the bow (YAMANO *et al*, 1996, 1997).

We confirm the reliability of the undergraduate thesis result by:

1) additional theoretical analysis: We try to clarify the relation between hull form and wave-making resistance by analyzing a 354,000ft³ refrigerated cargo ship (a fine ship). The linear wave-making resistance theory (Havelock, 1924; 1932) is used for the analysis. Using the linear theory, we can understand how each part of the forebody of the refrigerated cargo ship affects the wave-making resistance. In our previous study (Fabrício Filho *et al*., 2018), calculations are made for the overall forebody. In our present study, calculations are made only for the bow. Both results are compared and discussed.

2) discussion with related other model test results: We have searched for other model test results which we can use to confirm our previous study result and found the paper written by Yamano *et al*. (1996). It has two model test results which are useful for us to discuss our previous study result.

3.2.2 The new resistance test method

We propose the new resistance test method for a fine ship in a CWC to solve the current issue of low accuracy in resistance measurement and model manufacture present in the traditional resistance test method in a smaller CWC due to smaller scale model ship. We design models according to our developed new resistance test method and design a connection system to connect the models to the measuring apparatus of UFPE's CWC.

3.2.3 Study of manufacture of a model for the test in a CWC

In our university, there was no experience of manufacture of a model for a test in a CWC. Further, we found some difficulties in asking the manufacture to some makers around us, even to those who work with 3D Print or NC Cutting. In such a condition, the best and most practical way we should take to achieve our objective is to manufacture the model by ourselves first. The reason is that through our manufacturing the model, we can find the issues in the manufacture and they can be studied the ways how to solve them. So, we design and manufacture a partial model for a test in a CWC.

4 DEVELOPMENT OF A BOW FORM DESIGN METHOD FOR A FULL SHIP

The study reported in this chapter is designated “Study 1”. Here, we report the development of a bow form design method for a full ship, which can be applied to any bow form. In section 4.1, the background necessary to understand “Study 1” is reported. In section 4.1.3, the base data for “Study 1” – the results of resistance test with a 7m-long model of a Panamax bulk carrier (Ship ISNI) is reported. In section 4.3, the results of resistance test by Yamano (1994) are directly compared with the bow form. In section 4.4, the theoretical analysis through which the study was conducted is reported. In section 4.5, the investigation of important bow parameters and the derivation of an equation to estimate the wave-making resistance of a full ship is reported. In section 4.6, the design of new bow forms to reduce wave-making resistance at ballast condition of Ship ISNI using the derived equation is reported. In section 4.7, the resistance tests of the designed bow forms conducted with 2m-long models to confirm the usefulness of the derived equation is reported. In section 4.8, the discussion of the results of “Study 1” is reported. In section 4.9, the developed design bow form method is stated.

4.1 BACKGROUND

This section presents a background of “Study 1”. In 4.1.1, a review of the studies on bow form design of a full ship is presented. In 4.1.3, the importance of wave-making resistance for a full ship is discussed. In 4.1.2, the outline of “Study 1” is presented.

4.1.1 Review of the studies on bow form design of a full ship

In the following: 4.1.1.1 studies on the flow around a bow, 4.1.1.2 studies on bow form design, 4.1.1.3 the remaining issues on bow form design.

4.1.1.1 Studies on the flow around a bow

As characteristics of the flow around the bow of a full ship, Taneda (1975) found that wave-breaking occurs there. The wave-breaking is important for the ship’s resistance because it accompanies larger momentum loss. Takekuma and Kayo (1981) pointed out that the flow speed at the water surface just before a bow largely influences the wave-breaking. Baba (1969) pointed out that the bulbous bow has an

effect of reducing bow wave-breaking of a full ship. Ueura, Hino and Suzuki (2014) studied CFD application to a full ship with C_b = 0.95, L/B = 5 and F_n = 0.1 and pointed that, in order to get correct results from CFD application to such a full ship, it is essential to establish a model for wave-breaking.

4.1.1.2 Studies on bow form design

If L_{pp} is required to keep a given value, a protruding bulbous bow is an effective method to reduce wave-making resistance of a full ship. Inui (1962) proposed a theoretical bulbous bow design method where the bulb size and position are selected so that amplitude functions of elementary waves due to a bulb well cancel those of the bow. The method was applied to a fast and fine passenger ship and was proved effective by a full-scale ship sea trial by Shigemitsu and Kai (1961). Kracht (1978) proposed a practical design method of a bulbous bow. It was derived as a result of analysis of many model test results. It selects the main parameters of a bulbous bow. Yamano (1995) pointed out that the load waterline fore end form is especially important for wave-making resistance and its importance increases with the decrease of F_n. Sharma and Sha (2005) proposed a practical and hydrodynamic bulbous bow design method based on both theory and model test data. Their basic idea was that, even if CFD is used for the optimization of a bulbous bow, its start point affects its goal. Therefore, its start point is important, and his proposed method is for the design of the start point. However, these methods are for a fine ship with Froude number higher than about 0.2. Similar bulbous bow or stem design methods for a full ship with F_n of around 0.15 have not been proposed yet. On the other hand, many model tests on bulbous bow for a full ship including cylindrical bow, for example by Muntjewerf (1967), have been conducted.

If L_{oa} is required to keep a given value, we can take other method to reduce wave-making resistance of a full ship. Ebira, Iwasaki and Komura (2004), to reduce the wave-making resistance of an LPG carrier where the necessary minimum hull breadth at the bottom fore end corner of the fore-most LPG tank was always a great restriction against hull form design, extended the fore end of every waterline to the fore end of L_{oa} and reduced wave-making resistance by 6% of total resistance.

4.1.1.3 Remaining issues

First one is the method how to design a bulbous bow that is effective at both conditions of Full load and Ballast, for the ships that run at Ballast condition for out-bound and at Full load condition for return. Second is the bow form design method which we can apply even for a very full ship whose C_b is increasing up to around 0.9. Third is the method which we can apply to any bow form, with a bulbous bow or straight vertical stem.

4.1.2 Importance of wave-making resistance for a full ship

The importance of wave-making resistance is presented in the following by discussing the results of the resistance test with a 7m-long model of Ship ISNI, by Yamano (1994). In 4.1.2.1, the components of the full-scale resistance for a full ship (using Ship ISNI) are presented. In 4.1.2.2, it is presented what surprised us much by looking at the results of wave-making resistance on a full ship (using Ship ISNI) that motivated us to conduct this study.

4.1.2.1 Components of the full-scale resistance

From the adopted base data: results of resistance test with a 7m-long model of Ship ISNI, by Yamano (1994), the full-scale resistance was estimated by using the friction correction ΔC_f shown in Table 1. The ΔC_f : at other conditions were interpolated or extrapolated from the values at the two conditions on the assumption that ΔC_f linearly changes with Δ/Δ_{Full}.

Table 1 – ΔC_f used for estimation of full-scale resistance

Condition	Δ/Δ_{Full}	$\Delta C_f \cdot 10^3$
Full	1	0.13
Ballast	0.424	0.28

Source: FABRÍCIO FILHO, SHINOHARA; YAMANO (2019b).

The comparison of the amount of the three components of the full-scale resistance – frictional resistance, form resistance, and wave-making resistance – at F_n = 0.15, in the forms $\frac{R_{fs}}{\rho_s V_s^2}$, $\frac{R_{vs}}{\rho_s V_s^2}$, and $\frac{R_{ws}}{\rho_s V_s^2}$, respectively, is shown in Figure 13.

At the Design (Full load) condition of d_a/d_f = 12.4 m / 12.4 m, the ratio between the wave-making resistance R_{ws} and the total resistance R_{ts} is 6.3 %. On

the other hand, the same ratio is 12.9% at the Ballast condition of d_a/d_f = 6.5 m / 4.69 m. This data shows that, at Ballast condition, there is still room for improvement of propulsive performance by reducing the wave-making resistance.

Figure 13 – Comparison of amount of three components of full-scale resistance at F_n=0.15 (7m-long model ship, tested by Yamano (1994)).

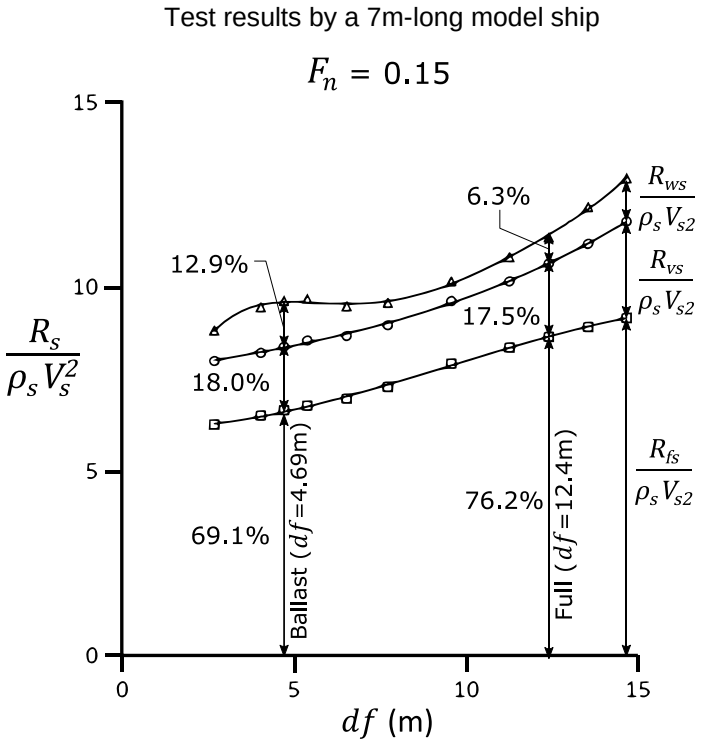

Source: FABRÍCIO FILHO, SHINOHARA; YAMANO (2019b).

4.1.2.2 What surprised us much

From the results got by Yamano (1994), the wave-making resistance measured in the resistance test with a 7m-long model of Ship ISNI is correlated with the fore draft d_f in Figure 14.

We were much surprised at Figure 14 in the point that R_{ws} at Ballast condition is about 1.5 times larger than that at Full condition, because we know that the hull at Ballast condition ($0.424\ \Delta_{Full}$) is finer than that at Full load condition.

Then we had the following question and issue:

Why is the resistance at Ballast condition so large?

There is room to reduce wave-making resistance at Ballast condition. How can we reduce it?

These are our motivation for the present study.

Figure 14 – $d_f - R_{ws}/\rho_s V_s^2$ at F_n = 0.15 (7m-long model ship, tested by Yamano (1994))

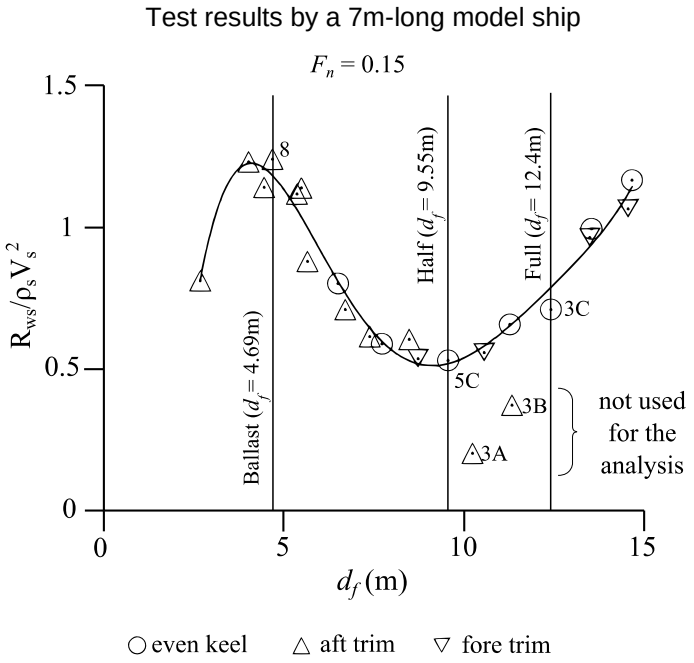

Source: FABRÍCIO FILHO, SHINOHARA; YAMANO (2019b).

4.1.3 Outline of “Study 1”

We start by clarifying the relation between bow form and wave-making resistance. For doing that, we apply the linear wave-making resistance theory to the results got by Yamano (1994), of resistance tests at 21 drafts with a 7m-long model of a Panamax bulk carrier Ship ISNI. As a result, in a preliminary study, we find that wave-making resistance is strongly related with the far fore end of the bow, from fore end to 0.5% L_{pp} aft. In a detailed study, we clarify the bow form parameters which are most strongly related with wave-making resistance. Using the bow form parameters, we derive an equation to estimate the wave-making resistance of a full ship, at any draft, at any F_n. Then, we confirm the equation by model test with 2m-long models. Finally, using the equation, we derive a bow form design method for a full ship.

4.2 BASE DATA

This section presents the base data adopted for the “Study 1”: the results of the resistance test by Yamano (1994), with a 7m-long model ship of a Panamax bulk carrier (Ship ISNI) in a towing tank with length 200m, breadth 13m, and water depth 6.5m. In 4.2.1, the principal particulars of Ship ISNI are presented. In 4.2.2, the

results of the resistance test by Yamano (1994) are presented in a table. In 4.2.3, the check of the results of the resistance test by Yamano (1994) is reported.

4.2.1 Principal particulars of the subject ship

The principal particulars of the subject ship, a Panamax bulk carrier – Ship ISNI, are shown in Table 2 in full-scale. The size of the model ship used by Yamano (1994) for the resistance tests is L_{ppm} = 7.120 m (scale = 1/29.78).

Table 2 – Principal particulars of tested ship

Ship	Unit	ISNI
L_{LWL}	m	215.5
L_{pp}	m	212.0
B	m	32.2
d	m	12.4
L/B	-	6.584
B/d	-	2.597
C_b	-	0.823
l_{cb}	$\%L_{pp}$	-2.5

Source: YAMANO (1994).

4.2.2 Resistance test results on a 7m-long model of Panamax bulk carrier Ship ISNI by Yamano (1994)

The results of resistance test at 21 drafts with a 7m-long model of Ship ISNI by Yamano (1994) are shown below in Table 3.

Table 3 – Results of resistance test with a 7m-long model of Ship ISNI tested by Yamano (1994)

Condition	d_a (m)	d_m (m)	d_f (m)	trim ($\%L_{pp}$)	b_e (m)	i_e (deg)	i_r (deg)	Δ_s (t)	k	$r_w \cdot 10^3$	$r_w \cdot \nabla^{2/3}$	$k \cdot r_{fm}$
OF1*	14.66	14.66	14.66	0	1.58	32	-24	85715	0.3009	0.6107	1.168	5.350
OF2*	13.53	13.53	13.53	0	1.27	36.5	-13	78574	0.2703	0.5518	0.9958	4.600
3A	14.47	12.35	10.23	2	0.62	33.5	32.5	71437	0.3100	0.1200	0.2032	5.039
3B	13.44	12.38	11.32	1	0.74	37.8	17	71436	0.2800	0.2200	0.3726	4.550
3C*(Full)	12.4	12.4	12.4	0	1	37.8	0	71432	0.2500	0.4200	0.7113	4.062
3D	11.36	12.42	13.48	-1	1.27	36.5	-12.5	71428	0.2500	0.5700	0.9652	4.062
3E	10.3	12.42	14.54	-2	1.57	32.8	-23	71431	0.2500	0.6300	1.067	4.065
4*	11.26	11.26	11.26	0	0.75	37.8	17.8	64291	0.2354	0.4175	0.6590	3.640
5A	11.62	9.5	7.38	2	0.78	14.1	51.5	53533	0.2700	0.4400	0.6148	3.851
5B	10.59	9.53	8.47	1	0.62	20.2	52.5	53673	0.2450	0.4330	0.6060	3.500
5C* (Half)	9.55	9.55	9.55	0	0.6	28	40	53784	0.2450	0.3800	0.5326	3.504
5D	8.43	9.49	10.55	-1	0.66	35.7	27	53578	0.2450	0.4000	0.5592	3.470
6A	9.9	7.78	5.66	2	1.48	7.4	12	42928	0.3050	0.7300	0.8804	3.974
6B	8.82	7.76	6.7	1	1	10.2	40	42904	0.2850	0.5900	0.7113	3.697
6C*	7.72	7.72	7.72	0	0.68	15.8	53.5	42889	0.2650	0.4900	0.5906	3.416

6D	6.6	7.66	8.72	-1	0.6	21.8	51.5	42847	0.2623	0.4460	0.5372	3.400
7A	8.7	6.58	4.46	2	1.66	6.9	0	35734	0.3150	1.070	1.142	3.809
7B	7.6	6.54	5.48	1	1.53	7.2	7	35730	0.3100	1.070	1.142	3.744
7C*	6.51	6.51	6.51	0	1.08	9.4	36	35871	0.2850	0.7500	0.8024	3.459
8(Ballast)	6.5	5.6	4.69	0.85	1.65	6.9	0	30299	0.3100	1.300	1.243	3.545
9	6.5	5.94	5.37	0.53	1.57	7.2	3	32351	0.3100	1.120	1.119	3.626
10	6.5	5.26	4.02	1.17	1.6	7	0	28288	0.3100	1.350	1.233	3.460
11	6.5	4.59	2.68	1.80	1.4	7.6	-26	24261	0.3351	0.9864	0.8132	3.564

Source: YAMANO, T. (1994).

Remarks:
1. Mark *: even keel
2. Model basin: L = 200 m, B = 13 m, water depth = 6.5 m; Model ship: L_{ppm} = 7.120 m (scale = 1/29.78).
3. Water temperature at resistance tests: 16 °C.
4. Test results: k (form factor), r_w (wave-making resistance coefficient) at F_n = 0.15.
5. $r_w \cdot \nabla_s^{2/3} = \frac{R_w}{\rho_s V_s^2}$
6. $k \cdot r_{fm} \cdot \nabla_s^{2/3} = \left(\frac{R_V}{\rho_s V_s^2}\right)\left(\frac{r_{fm}}{r_{fs}}\right)$

4.2.3 Check of the resistance test results

In the analysis of the resistance test results, the value of the form factor $k = R_{vm}/R_{fm}$ is first decided and then the wave-making resistance coefficient $r_w = \frac{R_w}{\rho \nabla^{2/3} V^2}$ is derived using the value of the form factor k. The value of the wave-making resistance coefficient r_w is correlated with the value of the form factor k. So, the check of $\frac{R_{ws}}{\rho_s V_s^2} = r_w \cdot \nabla_{as}^{2/3}$ was conducted with the check of $k \cdot r_{fm} \cdot \nabla_{as}^{2/3} = \left(\frac{R_{vs}}{\rho_s V_s^2}\right)\left(\frac{r_{fm}}{r_{fs}}\right)$ at the same time.

The wave-making resistance is estimated to be largely related to the bow form, and the form factor, to the aft body. Based on such consideration, the wave-making resistance in the form $r_w \cdot \nabla_s^{2/3} = R_{ws}/\rho_s V_s^2$ at F_n = 0.15 at 21 drafts is plotted on a graph with abscissa of the fore draft d_f in Figure 15 and the form resistance in the form $k \cdot r_{fm} \cdot \nabla_s^{2/3} = \left(\frac{R_{vs}}{\rho_s V_s^2}\right)\left(\frac{r_{fm}}{r_{fs}}\right)$, on a graph with abscissa of the aft draft d_a in Figure 16.

From Figure 15, we know that, except for two points 3A and 3B, most data are on a trend line. Regarding these two points, we could not find the reason for such a large deviation. So, we put them out of our discussion.

From Figure 16, we know that the data at even keel drafts are on a trend line. The knuckle of the trend line at d_a = 11m coincides with the bottom of the aft end of the hull lines. The rapid increase of $k \cdot r_{fm} \cdot \nabla_s^{2/3}$ with the increase of d_a in the d_a

range deeper than 11m is estimated due to the increase of the dead-water after the stern end. The deviation of other points from the trend line for even keel drafts can be explained as the effect of trim as follows: from the data at a trimmed condition in the d_a range shallower than 11m, we could derive the trend lines for ±2% trim and ±1% trim. The trend lines for trimmed conditions also must have knuckles at d_a = 11m. They are shown in Figure 16. Trim effect derived from these lines at d_a = 6.5m, 9m and 11m is shown in Figure 17. In the d_a range deeper than 11 m, the number of trimmed condition data is too small for us to derive the trend lines for ±2% trim and ±1% trim.

Only the $\frac{R_{ws}}{\rho_s V_s^2}$ at conditions 3A and 3B largely deviates from the others. So, from the above discussion, we concluded that the $\frac{R_{ws}}{\rho_s V_s^2}$ data at 21 conditions besides 3A and 3B are reliable and can be used for our analysis.

Figure 15 – Correlation of wave-making resistance at F_n = 0.15 with fore draft d_f (7m-long model ship, tested by Yamano (1994)).

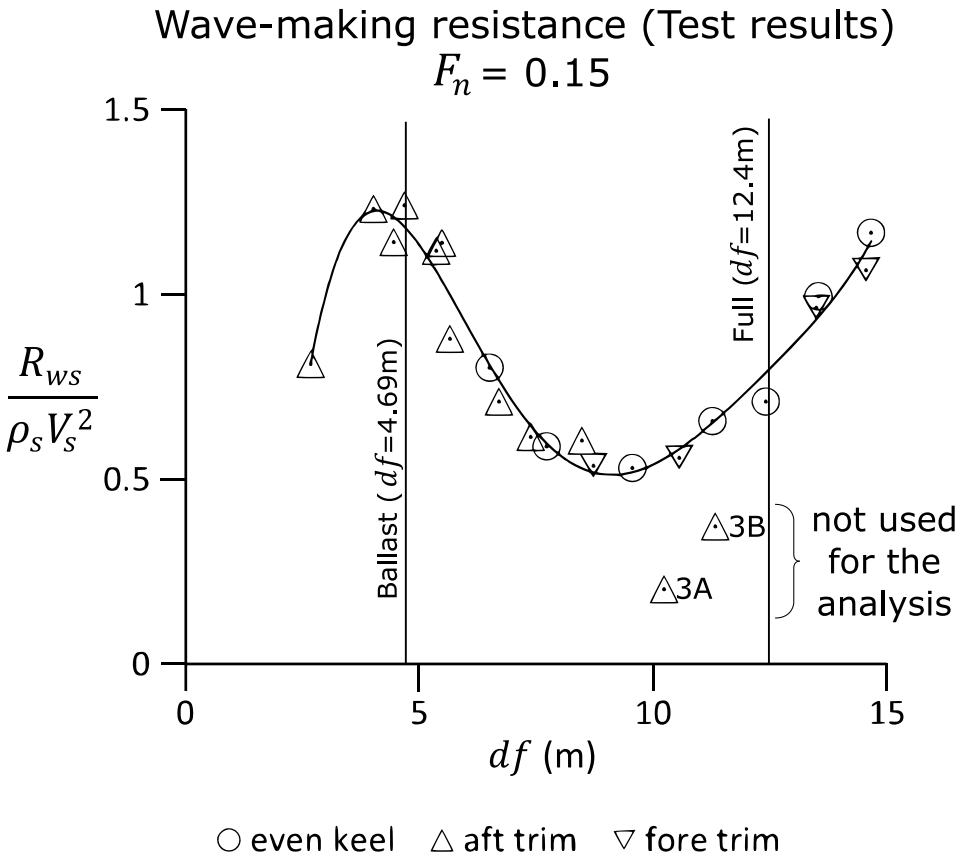

Source: FABRÍCIO FILHO, SHINOHARA; YAMANO (2019b).

Figure 16 – Correlation of form resistance with aft draft d_a (7m-long model ship, tested by Yamano (1994)).

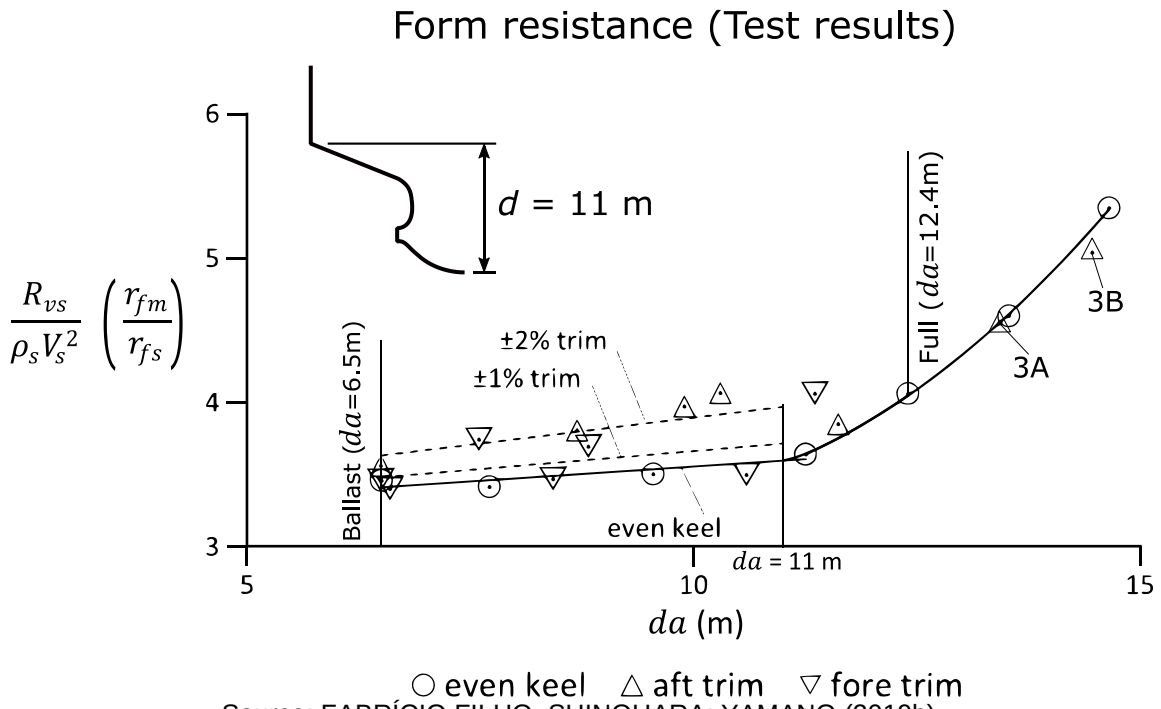

Source: FABRÍCIO FILHO, SHINOHARA; YAMANO (2019b).

Figure 17 – Correlation of form resistance with trim (7m-long model ship, tested by Yamano (1994)).

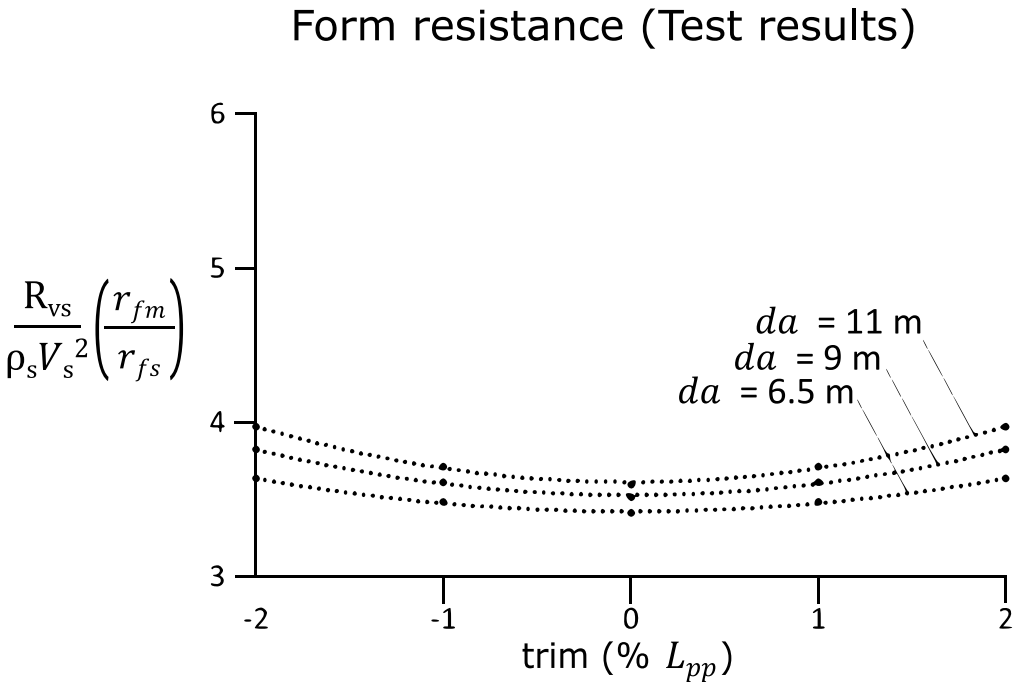

Source: FABRÍCIO FILHO, SHINOHARA; YAMANO (2019b).

4.3 DIRECT COMPARISON OF THE RESISTANCE TEST RESULTS BY YAMANO (1994) WITH THE BOW FORM

In Figure 18, the wave-making resistance measured at F_n = 0.15 obtained by the resistance test results of a 7m-long model of Ship ISNI (Yamano, 1994) is directly compared with the bow fore end form.

Figure 18 – Direct comparison of wave-making resistance at F_n=0.15 and bow fore end form (7m-long model ship, tested by Yamano (1994))

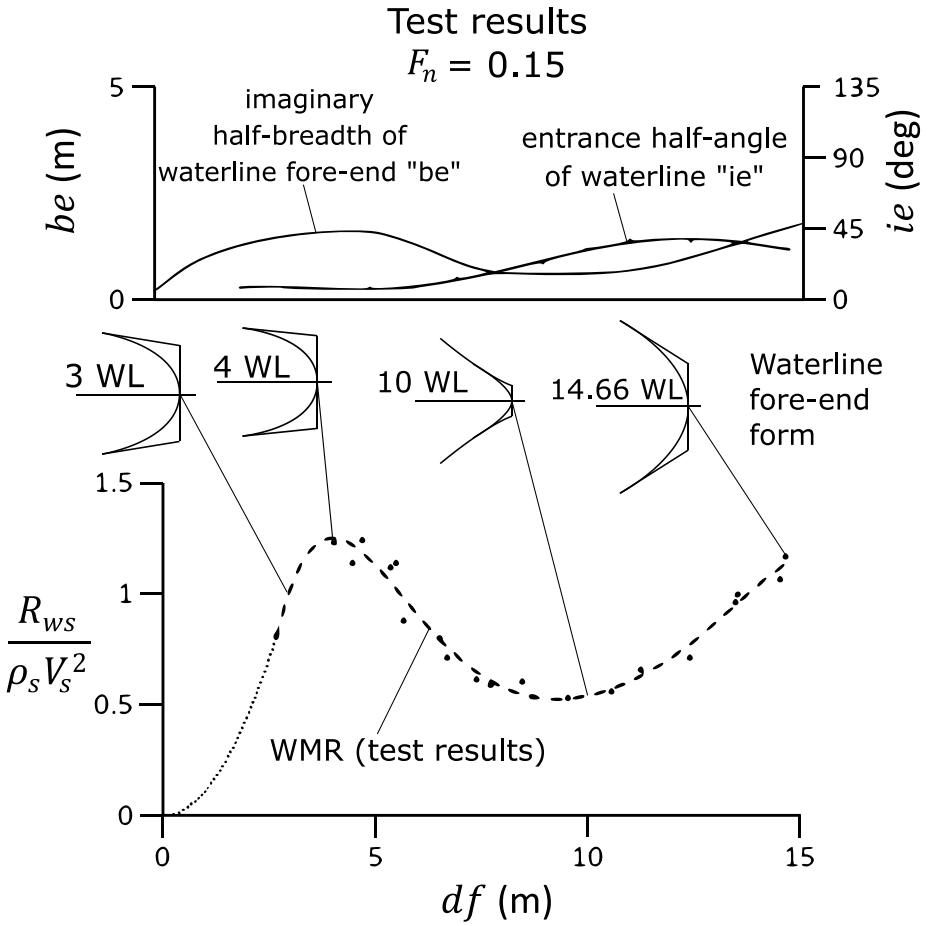

Source: FABRÍCIO FILHO, SHINOHARA; YAMANO (2019b).

The points of the measured wave-making resistance $\frac{R_{ws}}{\rho_s V_s^2}$ are almost on a line. This seems to show that the wave-making resistance is almost decided by the form of bow fore end.

The measured wave-making resistance $\frac{R_{ws}}{\rho_s V_s^2}$ curve has a peak near the Ballast condition (d_f = 4.69 m) and a bottom around d_f = 10 m. After the bottom, the wave-making resistance $\frac{R_{ws}}{\rho_s V_s^2}$ increases with the increase of fore draft d_f.

When we compare the wave-making resistance $\frac{R_{ws}}{\rho_s V_s^2}$ curve with the bow fore end form – the curves of the imaginary half breadth of the waterline fore end and waterline entrance half-angle – shown in Figure 18, we can estimate that:

a) The peak of the wave-making resistance $\frac{R_{ws}}{\rho_s V_s^2}$ curve near the Ballast condition seems to be caused by the largest imaginary half breadth of waterline fore end.

b) The bottom of the wave-making resistance $\frac{R_{ws}}{\rho_s V_s^2}$ curve around d_f = 10m seems to be caused by the smallest imaginary half breadth of the waterline fore end.

c) The increase of the wave-making resistance $\frac{R_{ws}}{\rho_s V_s^2}$ curve over d_f = 10m seems to be caused by the increase of the imaginary half breadth and also the entrance angle of the waterline fore end.

4.4 THEORETICAL ANALYSIS OF THE WAVE-MAKING RESISTANCE

This section reports the theoretical analysis of wave-making resistance conducted in the preliminary study of “Study 1”. In 4.4.1, the fundamentals of the theoretical analysis. In 4.4.2, the calculation procedures. In 4.4.3, the calculation results for the preliminary study. In 4.4.4, a discussion of the results of the preliminary study. In 4.4.5, implications of the results of preliminary study.

4.4.1 Fundamentals of the theoretical analysis of preliminary study

In 4.4.1.1, the used coordinate system is presented. In 4.4.1.2, the equations used to calculate wave-making resistance are presented. In 4.4.1.3, the representation of the hull form with singularities is presented.

4.4.1.1 Coordinate system

The used coordinate system “xyz, θ” is shown in Figure 19. The origin is at the FP section plane, hull centerline plane and water surface plane; the x-axis is on the intersection of the hull centerline plane with the water surface plane, and points to the aft of the ship; the y-axis, on the intersection of the FP section plane with the water surface plane, and points to the starboard direction; and the z-axis, on the intersection of the FP section plane with the hull centerline plane, and points to the

upward direction. We consider a uniform flow with speed V towards the positive direction of the x-axis.

Figure 19 – Coordinate system xyz, θ.

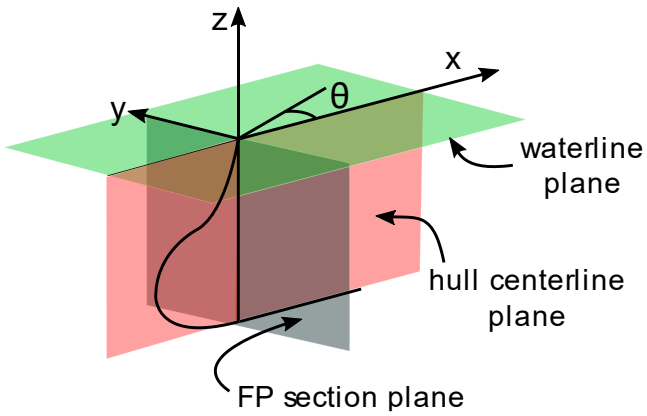

Source: FABRÍCIO FILHO, SHINOHARA; YAMANO (2019b).

4.4.1.2 Equations to calculate wave-making resistance

The wave-making resistance, according to the linear wave-making resistance theory, can be calculated by equations (5) and (6) (HAVELOCK, 1934):

$$R_w = \pi\rho V^2 \int_0^{\pi/2} [S^2(\theta) + C^2(\theta)]\, cos^3\,\theta\, d\theta \tag{5}$$

$$\left.\begin{matrix} C(\theta) \\ S(\theta) \end{matrix}\right\} = \frac{4V\chi^2}{g} sec^3\,\theta \cdot \int_{x_1}^{x_2}\int_{z_1}^{z_2} \sigma(x,z) e^{z\chi\, sec^2\,\theta} \begin{matrix} cos \\ sin \end{matrix} (\chi x\, sec\,\theta) dz\, dx \tag{6}$$

(Equations (5) and (6) are first presented in 2.6.2. For further explanation on these equations, the reader may refer to section 2.6).

4.4.1.3 Representation of a hull form with singularities

The bow part of a hull consists of many waterlines, like the one shown in Figure 20. We represent the bow part mathematically as follows (see Figure 20):

(a) Surface functions $y(x,z)$, representing the side hull;

(b) Straight segments $y(l_f(z),z)$, representing the imaginary fore end breadth.

Figure 20 – Definition of waterline fore end.

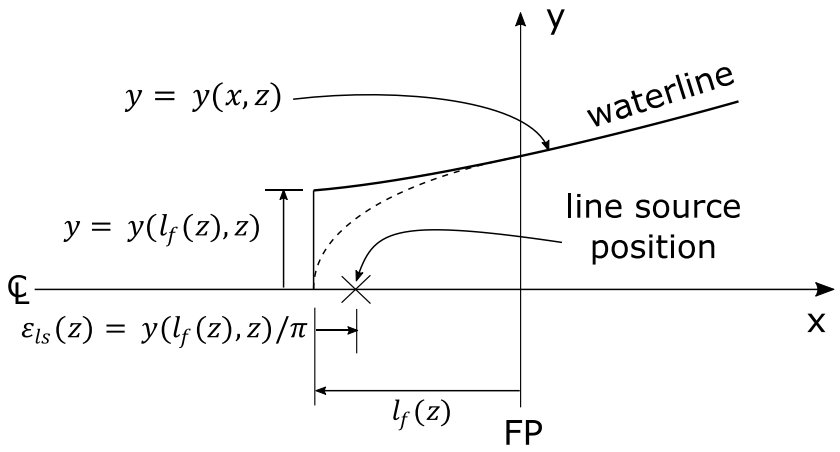

Source: FABRÍCIO FILHO, SHINOHARA; YAMANO (2019b).

The singularity distribution for the above (a) is a source distribution on the hull centerline plane (plane "xz") with a density given by equation (7); for (b), a line source located a little aft of the fore end (line $x(z) = -l_f(z) + \varepsilon_{ls}, y(z) = 0$) with a density given by equation (11), where $\varepsilon_{ls}(z) = y(l_f(z),\ z)/\pi$:

$$\sigma(x,z) = \frac{V}{2\pi}\frac{\partial y(x,z)}{\partial x} \tag{7}$$

$$\sigma\big(l_f(z) + \varepsilon_{ls}, z\big) = \frac{V}{2\pi} y\big(l_f(z), z\big) \tag{11}$$

(Equation (7) is first presented in 2.6.2. The reader may refer to there. Equation (11) comes from equation (8) in 2.6.1).

4.4.2 Calculation procedures

In the following, the calculation procedures for the calculation as part of the theoretical analysis of "Study 1" are presented.

4.4.2.1 Bow form to be discussed

For the longitudinal direction, we discuss the hull part fore from the SS 9 ¾ because we focus our attention on the bow. For draft-ward direction, we discuss the hull part below 15WL, because the deepest draft the resistance test is conducted is 14.66m.

4.4.2.2 How to calculate wave-making resistance from the bow form

(a) *Mathematical representation of the hull form*: First, we express the hull form data in the non-dimensional coordinates ξ, η and ζ: $\xi = x/\ell$, $\eta = y/b$, $\zeta = z/\ell$, where $\ell = L_{pp}/2$. Second, we approximate the waterlines with third or fourth-order polynomials $\eta(\xi)$. Third, if necessary, we interpolate a waterline at any draft using three of the above-approximated waterlines near the draft.

(b) *Division of the bow*: to precisely take the bow form into the calculation, we divide the bow draft-wise into small calculation units, as shown in Figure 21. The interval between two waterlines Δz is changed from 0.25 m to 1 m according to the bow form near the waterlines.

Figure 21 – Division of bow for calculation.

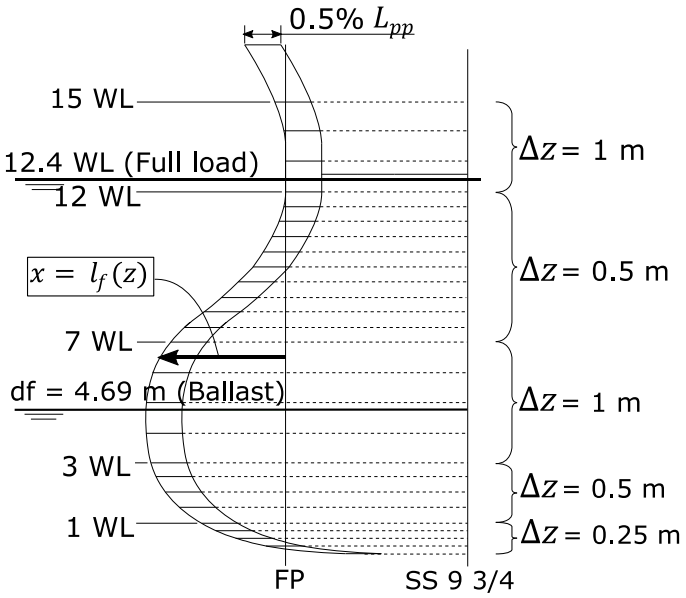

Source: FABRÍCIO FILHO, SHINOHARA; YAMANO (2019b).

(c) *Calculation of a divided unit*: The section form of a divided unit between the two waterlines – equations. (12) and (13):

$$y_{n+1} = f_{n+1}(x, z_{n+1}) \tag{12}$$

$$y_n = f_n(x, z_n) \tag{13}$$

is approximated with a form of a trapezoid as shown in Figure 22. Therefore, a waterline between the two waterlines above can be expressed as follows – equation. (14):

$$y = f(x,z) = f_n(x,z_n) + \frac{f_{n+1}(x,z_{n+1}) - f_n(x,z_n)}{z_{n+1} - z_n}(z - z_n) \tag{14}$$

The fore end of a divided unit is approximated with a vertical line as also shown in Figure 22.

Figure 22 – Transverse section and fore end profile of a divided unit.

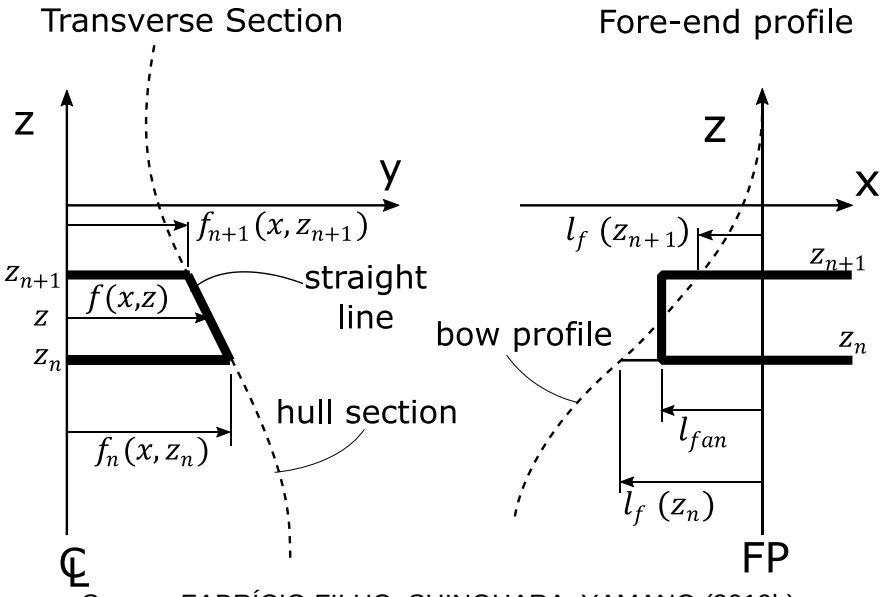

Source: FABRÍCIO FILHO, SHINOHARA; YAMANO (2019b).

The longitudinal position of the fore end is expressed with equation (15):

$$l_{fan} = \frac{1}{2}[l_f(z_{n+1}) + l_f(z_n)] \tag{15}$$

The section form at $x = l_{fan}$, which can be obtained from equation (14) at $x = l_{fan}$, decides the equivalent line source density. The line source is positioned a little after the fore end, at $x = l_{fan} + \varepsilon_{lsn},\ y = 0$, where $\varepsilon_{lsn} = [\varepsilon_{ls}(z_{n+1}) + \varepsilon_{ls}(z_n)]/2$.

From equations (6), (7), and (14), we can get the amplitude functions by the side hull of a divided unit – equation (16):

$$\left.\begin{matrix} C_{shn}(\theta) \\ S_{shn}(\theta) \end{matrix}\right\} = \frac{2\chi}{\pi}\sec^3\theta \int_{l_{fan}}^{x_n}\int_{z_n}^{z_{n+1}} \frac{\partial y(x,z)}{\partial x}\, e^{z\chi\sec^2\theta} \begin{matrix} cos \\ sin \end{matrix}(\chi x \sec\theta)\, dz\, dx \tag{16}$$

where the upper limit of the integral in x, is $x_n = \begin{cases} c_1 \\ l_{fan} + c_2 \end{cases}$, for any constants $c_1, c_2 \leq x_{SS\,9\,3/4}$ (x position of SS 9 ¾).

From equations. (6), (11), (14) and (15), we can get the amplitude functions by the fore end of a divided unit – equation (17):

$$\left.\begin{matrix} C_{fen}(\theta) \\ S_{fen}(\theta) \end{matrix}\right\} = \frac{2\chi}{\pi} \sec^3\theta \int_{z_n}^{z_{n+1}} y\left(l_{fan}, z\right) e^{z\chi \sec^2\theta} \begin{matrix} cos \\ sin \end{matrix}\left(\chi l_{fan} \sec\theta\right) dz \tag{17}$$

The total amplitude functions by a divided unit are obtained as follows – equations (18):

$$\begin{aligned} C_n(\theta) &= C_{shn}(\theta) + C_{fen}(\theta) \\ S_n(\theta) &= S_{shn}(\theta) + S_{fen}(\theta) \end{aligned} \tag{18}$$

(d) *Summing up of the divided units*: The amplitude functions by the area to be taken into calculation can be obtained by summing up those by a divided unit as follows – equations (19):

$$\left.\begin{matrix} C_x(\theta) \\ S_x(\theta) \end{matrix}\right\} = \sum_{n=1}^{N} \begin{Bmatrix} C_{xn}(\theta) \\ S_{xn}(\theta) \end{Bmatrix} \tag{19}$$

4.4.3 Calculation results of preliminary study

In the preliminary study, the wave-making resistance $r_w \cdot \nabla_s^{2/3} = R_{ws}/\rho_s V_s^2$ at F_n=0.15 was calculated for the following two cases, “Case a” and “Case b”, where the range of the bow to be taken into calculation is different from each other.

Case a: From the fore end to 0.5% L_{pp} aft at each waterline (see Figure 21)

Case b: From the fore end to 1% L_{pp} aft at each waterline

The calculation results are shown in Figure 23, compared with the resistance test results.

"Case a" takes into calculation only the real fore end (the real fore end corresponds nearly to the imaginary half breadth of the waterline fore end "b_e" and the entrance half-angle of the waterline, "i_e"). In "Case b", the range is extended to 1% L_{pp}.

From Figure 23, we know that the calculated wave-making resistance due to the side hull seems larger than the wave-making resistance obtained by the resistance tests.

The calculation results of "Case a" is nearest to the resistance test results, both in amount and tendency. So, in the discussion hereafter, for example in Figure 24 and Figure 25, the results of the "Case a" are referred to as the calculation results.

Figure 23 – Comparison of wave-making resistance between calculation results ("Case a" and "Case b") and test results at F_n=0.15 (7m-long model)

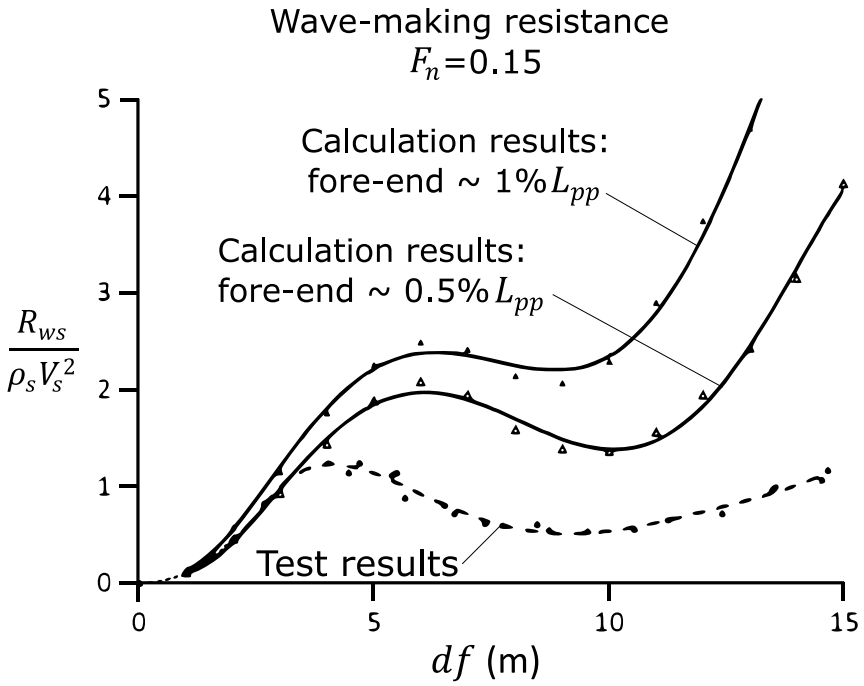

Source: FABRÍCIO FILHO, SHINOHARA; YAMANO (2019b).

4.4.4 Discussion of results of preliminary study

In Figure 24, the wave-making resistance $\frac{R_{ws}}{\rho_s V_s^2}$ at F_n = 0.15 obtained by the resistance test conducted by Yamano (1994) with a 7m-long model is compared with the results of our theoretical calculation by the method described in section 4.4.1.

Figure 24 – Comparison of wave-making resistance between calculation results and test results by Yamano (1994) at F_n=0.15 (7m-long model ship, tested by Yamano (1994))

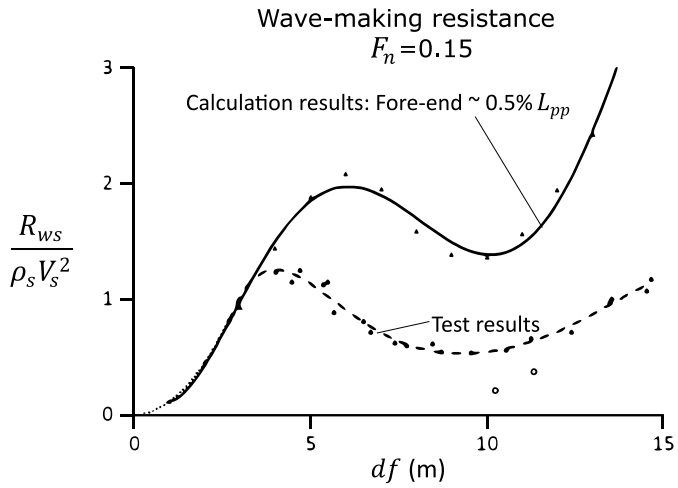

Source: FABRÍCIO FILHO; SHINOHARA; YAMANO (2019b).

The results of the theoretical calculation shown in Figure 24 are different from the resistance test results in its amount. However, its tendency is similar to that of the resistance test results. That is, the peak around d_f = 5 m, the bottom around d_f = 10m and the resistance increase over d_f = 10 m are seen in both results.

In Figure 25, two contents of the wave-making resistance calculated by linear wave-making resistance theory at F_n = 0.15 are shown in the form of $\frac{R}{\rho_s V_s^2}$. One is the wave-making resistance due to the imaginary breadth of fore end, and the other is that by the side hull.

Figure 25 – Calculated components of wave-making resistance at F_n=0.15

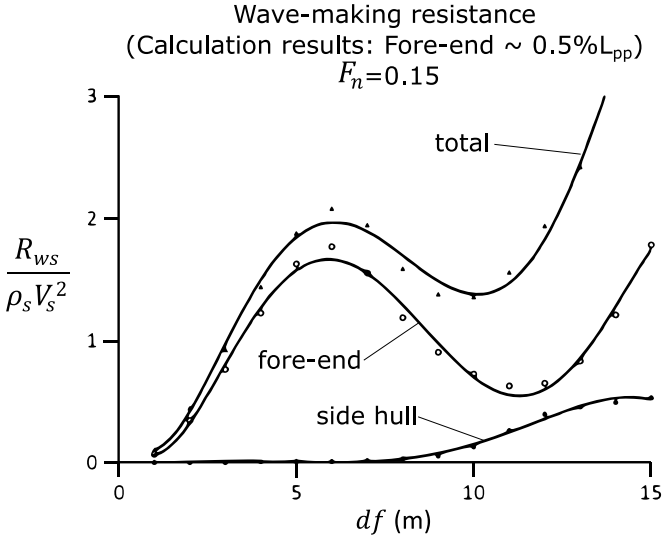

Source: FABRÍCIO FILHO; SHINOHARA; YAMANO (2019b).

From Figure 25, we can know that

a) The peak around fore draft d_f = 5 m is caused by the largest imaginary half breadth of the waterline fore end.

b) The bottom around fore draft d_f = 10 m is caused by the smallest imaginary half breadth of the waterline fore end and the not-so-large entrance angle of the side hull.

c) The increase of resistance over fore draft d_f = 10 m is caused by the increase of the imaginary half breadth of the waterline fore end and of the entrance angle of the side hull waterline.

That is, what we estimated in 4.3 (Figure 18) has been confirmed by the preliminary theoretical analysis.

4.4.5 Implications of results of preliminary study

As shown in Figure 23, the calculation results for “Case a” – from the fore end to 0.5% L_{pp} aft – is nearest to the resistance test results in its amount and in its tendency.

This result at least shows that:

a) The wave-making resistance of a full ship is largely related to the far fore end of “from the fore end to 0.5% L_{pp} aft”.

b) The calculated wave-making resistance by the side hull is larger than that by the resistance tests.

These results seemed to imply something important to us. This motivated us to further study in order to find the bow form parameters which are most strongly related with wave-making resistance.

4.5 RELATION BETWEEN BOW FORM AND WAVE-MAKING RESISTANCE

In this section, we proceed with a detailed study to clarify the relation between bow form and wave-making resistance. In 4.5.1, we search for bow form parameters which are strongly related with wave-making resistance. As a result, we find that wave-making resistance can be almost explained with only one bow form parameter. Based on our finding, in 4.5.2, we develop an equation to estimate the wave-making resistance.

4.5.1 Search for bow form parameters which are strongly related with wave-making resistance

In the preliminary study, we calculated the wave-making resistance with changing the length of side hull. As a result, we found that the calculation result for the case of side hull with length 0.5% L_{pp} is fairly near to the resistance test results by Yamano (1994).

We further search for the bow form parameters which are strongly related with wave-making resistance in the following.

4.5.1.1 Evaluation of influence of water depth and side hull on wave-making resistance

In the following, the effect of water depth and side hull on wave-making resistance.

a) *Water depth*

Figure 26 shows the calculation results for the cases where depth of the hull taken into calculation is changed “from water surface to BL, 6m, 4m and 2m below” on the condition that side hull length is 0.5%L_{pp}.

From Figure 26, we know that the calculation result for water depth “from water surface to 2m below” is nearest to the resistance test results in its amount and tendency.

Figure 26 – Water depth effect at F_n = 0.15 (7m-long model ship, tested by Yamano (1994))

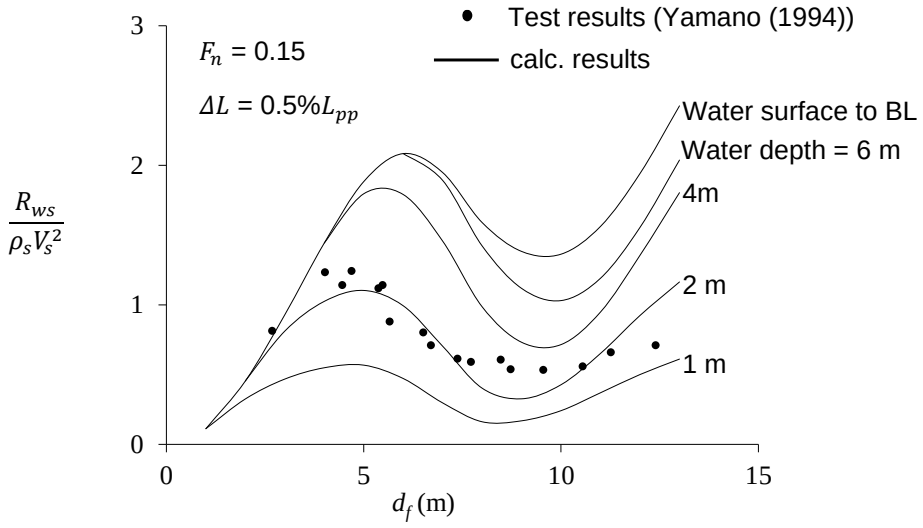

Source: FABRÍCIO FILHO et al (2020).

b) *Side hull*

Figure 27 shows the calculation results for the cases where the side hull length is “2.5%, 2%, 1%, 0.5% L_{pp} and 0” from the fore end, on the condition that the water depth is “from water surface to 2m below”.

From Figure 27, we know that “side hull length ΔL = 0%” is nearest to the model test results in its amount and tendency.

Figure 27 – Side hull length effect at F_n = 0.15 (7m-long model ship, tested by Yamano (1994))

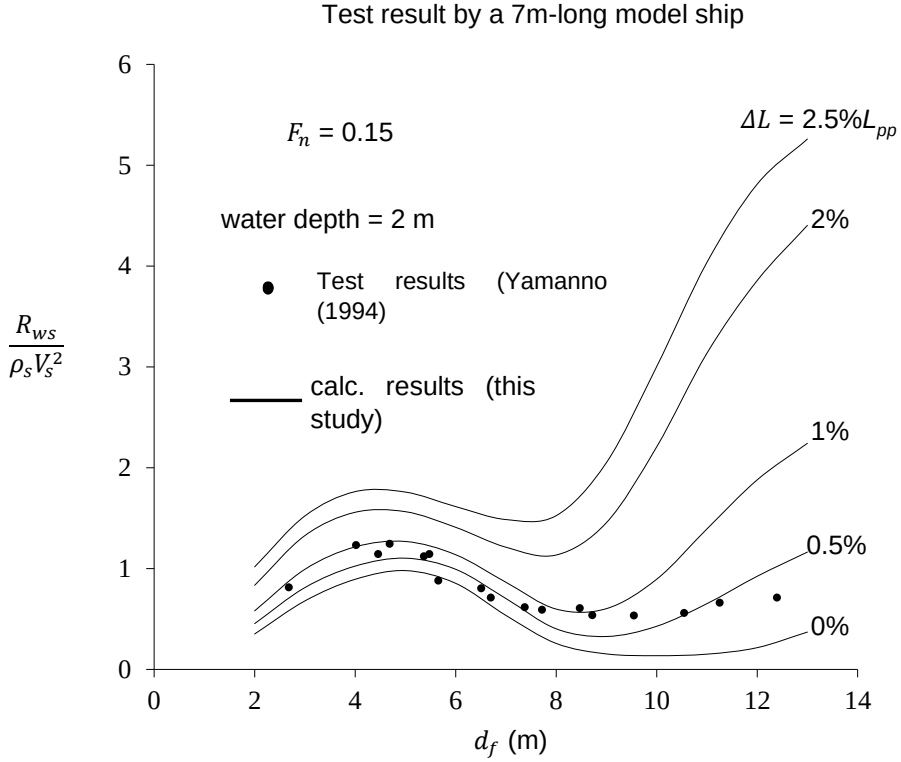

Source: FABRÍCIO FILHO *et al.* (2020).

4.5.1.2 Evaluation of influence of “b_e”, “i_r” and “i_e” on wave-making resistance

The three bow form parameters “b_e”: imaginary half breadth of waterline fore end, “i_r”: stem rake angle and “i_e”: entrance half angle of the waterline, on the water surface, are illustrated in Figure 28.

Figure 28 – Illustration of "b_e", "i_r" and "i_e"

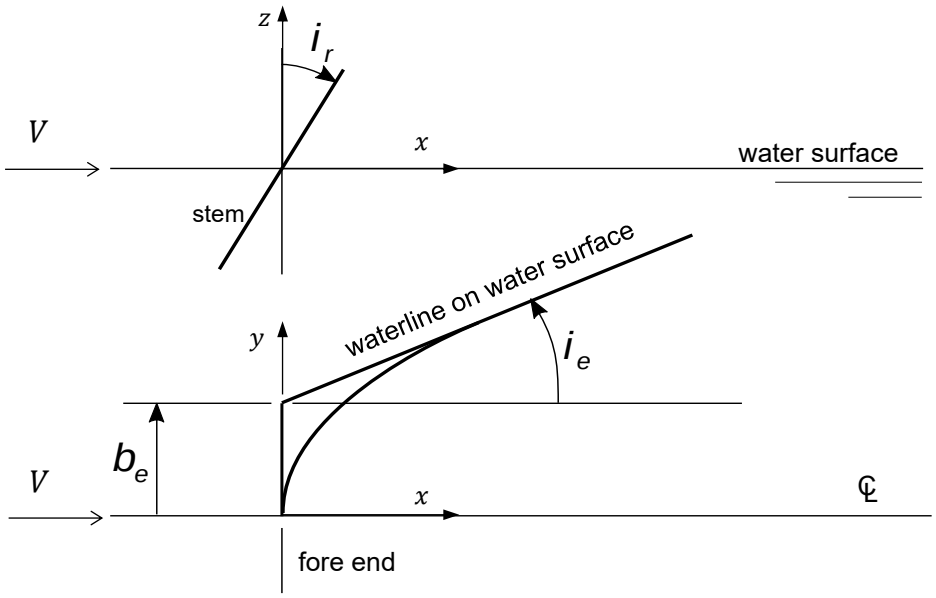

Source: FABRÍCIO FILHO *et al.* (2020).

From 4.5.1.1, item "*(b)*", we know that we need not take the side-hull into consideration in the calculation of wave-making resistance due to the bow. That is, only a line source with density $\sigma(z) = \left(\frac{V}{2\pi}\right) b_e(z)$ and with depth of about 2m is enough for the calculation. It implies no influence of "i_e". However, we will confirm the "no influence" by another way and discuss the reason for the "no influence" in the following.

(a) Calculation of wave-making resistance due to a vertical line source

The depth of a line source, which is used for calculation of wave-making resistance, is only about 2m. So, the "b_e" on the water surface is used for the whole depth about 2m. Then, the wave-making resistance due to a vertical line source with depth d_{ls} can be calculated by the following equation (20):

$$\frac{R_{ws}}{\rho_s V_s^2} = \pi \int_0^{\pi/2} [S^2(\theta) + C^2(\theta)] \cos^3\theta \, d\theta \tag{20}$$

Where

$$\left.\begin{matrix} S(\theta) \\ C(\theta) \end{matrix}\right\} = \frac{4V\chi^2}{g}\sec^2\theta \left\{\begin{matrix} \sin \\ \cos \end{matrix}\right\}(\chi x_1 \sec\theta) \int_{-d_{ls}}^{0} \sigma(z_1)\exp(z_1\chi\sec^2\theta)\,dz_1 \qquad (21)$$

With $\sigma(z_1) = \frac{V}{2\pi} b_e$, $-d_{ls} = -\tau\ell$, $x_1 = 0$, $z_1 = \ell\zeta_1$, then:

$$\begin{aligned} S(\theta) &= 0 \\ C(\theta) &= \frac{2b_e}{\pi}[1 - \exp(-\tau\chi_0\sec^2\theta)] \end{aligned} \qquad (22)$$

Therefore, the wave-making resistance due vertical line source with depth d_{ls}, $\left(\frac{R_{ws}}{\rho_s V_s^2}\right)_{LS}$, is calculated with equations (20) and (22).

(b) Influence of "b_e" on wave-making resistance

Figure 29 shows the relation of resistance test results $\frac{R_{ws}}{\rho_s V_s^2}$ by Yamano (1994) with a 7m-long model of Ship ISNI, at F_n = 0.15 and "b_e" at each draft. Almost all the test results by Yamano are nearly on a line. Only No. 11 is largely deviated. The reason is its smaller d_f (2.68 m) which will be explained later in Figure 33. The d_f of the other data is more than 4.5 m. The No. 11 data corrected to the condition with d_f more than 4.5m is shown as "No. 11m".

Figure 29 – $b_e - R_{ws}/\rho_s V_s^2$ test results at F_n = 0.15 (7m-long model ship, tested by Yamano (1994))

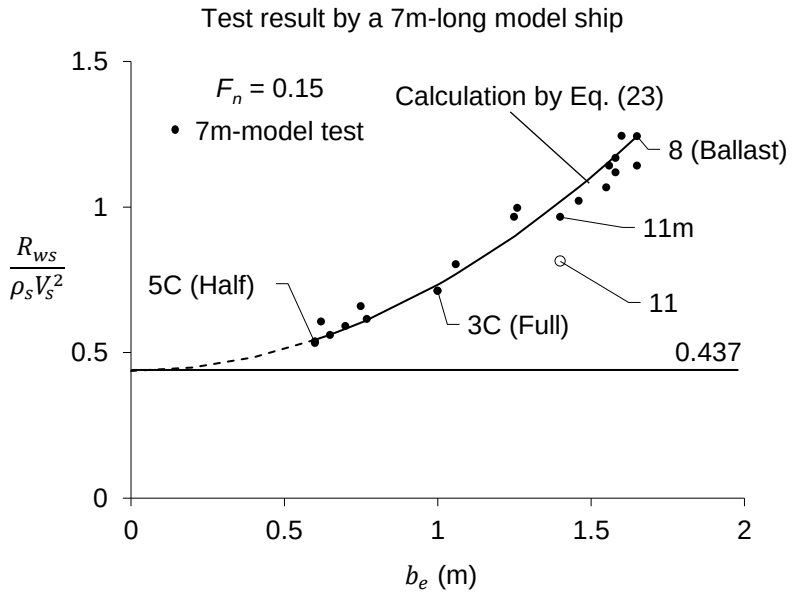

Source: FABRÍCIO FILHO *et al*. (2020).

The mean line can be expressed with equation (23).

$$\frac{R_{ws}}{\rho_s V_s^2} = \left(\frac{R_{ws}}{\rho_s V_s^2}\right)_{LS} + 0.437 \tag{23}$$

Where

$\frac{R_{ws}}{\rho_s V_s^2}$: wave-making resistance of Ship ISNI at F_n = 0.15

$\left(\frac{R_{ws}}{\rho_s V_s^2}\right)_{LS}$: $\frac{R_{ws}}{\rho_s V_s^2}$ due to a vertical line source, positioned at waterline fore end, with density $\sigma = \frac{V}{2\pi} b_e$ and with depth 1.5 m at F_n = 0.15 which can be calculated by equations (20) and (22).

$d_f \geq 4.5$m

Equation (23) and Figure 29 can be considered to mean that:

a) The wave-making resistance at F_n = 0.15 at a draft consists of two components.
b) One is that due to bow fore end with depth 1.5m. Its amount is decided only by be on the water surface. We need not consider the interference with other part. Its amount can be calculated as wave-making resistance of a vertical line source with density $\sigma = \frac{V}{2\pi} b_e$ and with depth 1.5 m.
c) Another is that due to the hull below 1.5m water depth. Its amount has a constant 0.437 and is same at any draft.

(c) Influence of "i_r" on wave-making resistance

Figure 30 shows the relation between the deviation of each test result of $\frac{R_{ws}}{\rho_s V_s^2}$ by Yamano (1994) from the mean line in Figure 29 and "i_r". From Figure 30, we can say that there is no influence of "i_r" on $\frac{R_{ws}}{\rho_s V_s^2}$.

Figure 30 – "i_r" – $\Delta\left(\frac{R_{ws}}{\rho_s V_s^2}\right)$ (measured one – mean line in Figure 29) (7m-long model ship, tested by Yamano (1994))

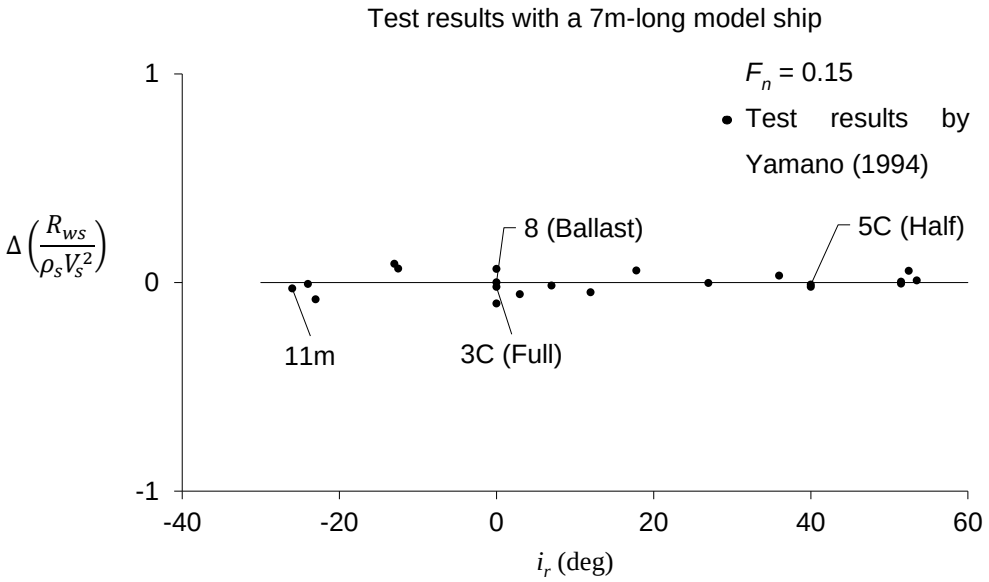

Source: FABRÍCIO FILHO *et al.* (2020).

We check the influence of "i_r" by another way. We calculate the wave-making resistance due to a raked line source shown in Figure 31.

Figure 31 – Raked stem for R_w calculation

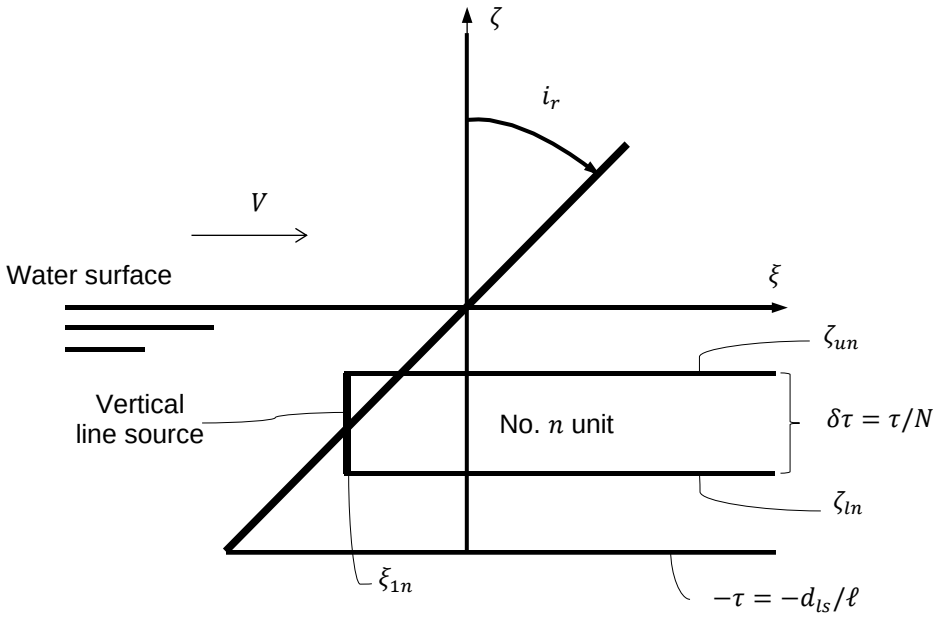

Source: FABRÍCIO FILHO *et al.* (2020).

The raked line source was divided draft-wards into 1,000 units. Each unit has a vertical line source at the fore end as shown in Figure 31. The amplitude functions S(θ) and C(θ) by the divided units can be calculated as follows:

For a unit No. n:

$$\begin{matrix} S_n(\theta) \\ C_n(\theta) \end{matrix} = \frac{2}{\pi} b_e \sec\theta \left\{ \begin{matrix} \sin \\ \cos \end{matrix} (\xi_{1n} \chi_0 \sec\theta) \right\} \left[e^{\zeta_{un} \chi_0 \sec^2\theta} - e^{\zeta_{ln} \chi_0 \sec^2\theta} \right] \quad 24)$$

where $\tau = d/\ell$, $\delta\tau = \tau/N$, $\zeta_{un} = -(n-1)\,\delta\tau$, $\zeta_{ln} = -n\,\delta\tau$, $\xi_{1n} = \frac{\zeta_{un}+\zeta_{ln}}{2} \tan(i_r)$. Then,

$$\begin{matrix} S(\theta) \\ C(\theta) \end{matrix} = \sum_{n=1}^{N} \begin{matrix} S_n(\theta) \\ C_n(\theta) \end{matrix} \quad 25)$$

Calculation was conducted for the "i_r" range from 53.5 deg to –26 deg which covers "i_r" of 21 drafts of Ship ISNI. The result is shown in Table 4.

Table 4 – Calculated $\frac{R_{ws}}{\rho_s V_s^2}$ for line sources with different rake angle "i_r" at F_n = 0.15

No.	6C		5C		11	
Condition	Max. aft-ward rake		Half		Max. fore-ward rake	
b_e (m)	0.7		0.6		1.4	
i_r (deg)	0	53.5	0	40	0	-26
$\left(\frac{R_{ws}}{\rho_s V_s^2}\right)_{estimated}$	0.582	0.575	0.544	0.542	1.017	1.013

Source: FABRÍCIO FILHO *et al.* (2020).

Remarks:
1. Line source depth d = 1.5m, N = 1,000
2. Estimation by equations (20), (24), (25) and (23).

From Table 4, we know that the influence of "i_r" is negligibly small. This result confirms what Figure 30 shows.

(d) Influence of "i_e" on wave-making resistance

Figure 32 shows the relation between the deviation of each test result of $\frac{R_{ws}}{\rho_s V_s^2}$ from the mean line in Figure 29 and "i_e". The mean line in Figure 32 has no inclination. Therefore, we can say that there is no influence of "i_e" on $\frac{R_{ws}}{\rho_s V_s^2}$.

Figure 32 – "i_e" – $\Delta\left(\frac{R_{ws}}{\rho_s V_s^2}\right)$ (measured one – mean line in Figure 29) (7m-long model ship, tested by Yamano (1994))

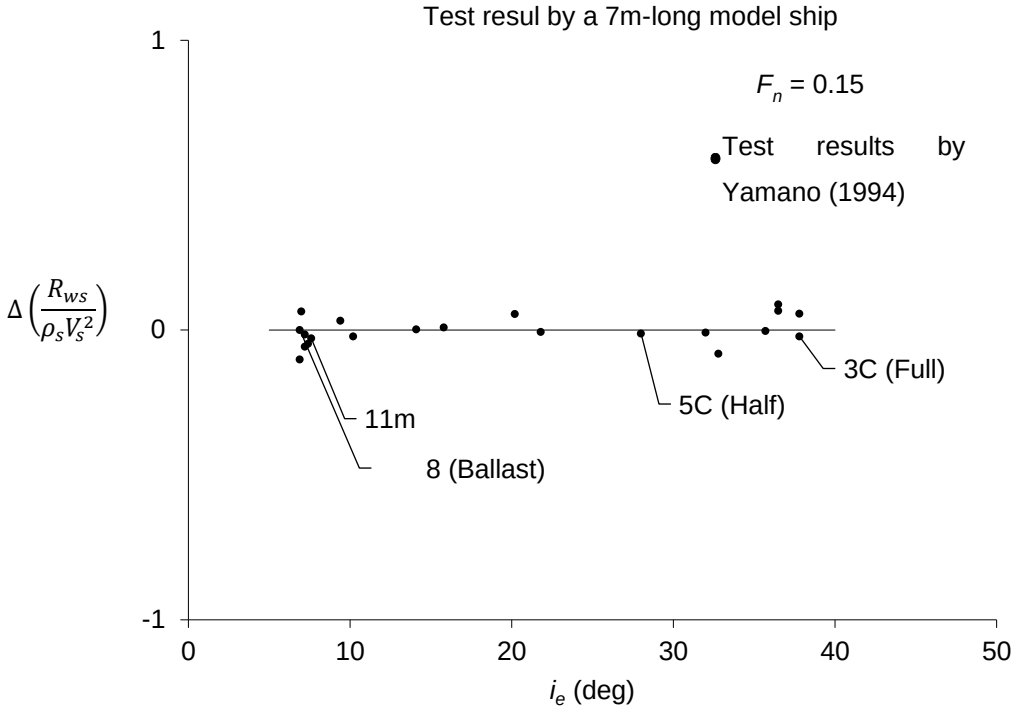

Source: FABRÍCIO FILHO *et al.* (2020).

As a reason for no influence of "i_e", we can point out the fact that, except OF2 (36.5 deg), 3B, 3C and 4 (37.8 deg), 3D (36.5 deg) and 5D (35.7 deg), "i_e" is lower than the maximum allowable "i_e" = 35 deg at F_n = 0.15 by Lewis (1988) and even the maximum "i_e" value 37.8 deg is only 2.8 deg over the maximum allowable value. Probably, this fact has resulted in the no influence of "i_e".

Figure 33, extracted from Yamano *et al.* (1996), shows the maximum allowable "i_e" values for several kinds of ship, according to Lewis (1988).

Figure 33 – Maximum allowable "i_e" for several kinds of ship

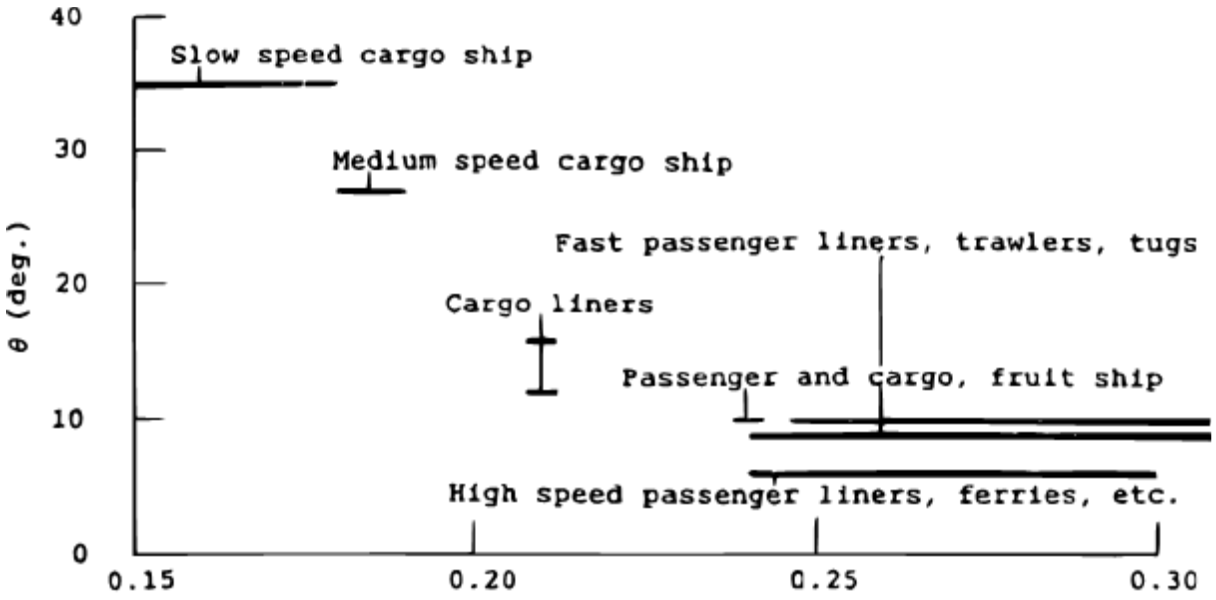

$$F_n = \frac{V}{\sqrt{g \cdot L_{WL}}}$$

Source: YAMANO *et al.* (1996)

4.5.2 An equation to estimate wave-making resistance of the subject ship

As a summary of the above discussion, the wave-making resistance of Ship ISNI at F_n = 0.15 can be estimated by equation (26):

$$\frac{R_{ws}}{\rho_s V_s^2} = \left(\frac{R_{ws}}{\rho_s V_s^2}\right)_{LS} + \alpha \qquad 26)$$

Where

$\frac{R_{ws}}{\rho_s V_s^2}$: wave-making resistance at F_n = 0.15

$\left(\frac{R_{ws}}{\rho_s V_s^2}\right)_{LS}$: wave-making resistance due to a vertical line source, positioned at waterline fore end, with density $\sigma = \frac{V}{2\pi} b_e$ and with depth 1.5 m

α: $\frac{R_{ws}}{\rho_s V_s^2}$ due to the hull below 1.5 m water depth

α = 0.437: $d_f \geq 4.5$ m

α = the curve shown in Figure 34: $1.5 \text{ m} \leq d_f \leq 4.5 \text{ m}$

α = 0: $d_f \leq 1.5$ m

At $d_f \leq 1.5\,\mathrm{m}$, $\alpha = 0$, because there is no hull below the line source. The curve at $1.5\mathrm{m} \leq d_f \leq 4.5\mathrm{m}$ was decided by using the $\frac{R_{ws}}{\rho_s V_s^2}$ value of condition No.11. Figure 34 shows the line estimated by equation (26) compared with resistance test results by a 7m-long model ship, by Yamano (1994).

Figure 34 – $d_f - \frac{R_{ws}}{\rho_s V_s^2}$ at F_n = 0.15 (7m-long model ship, tested by Yamano (1994))

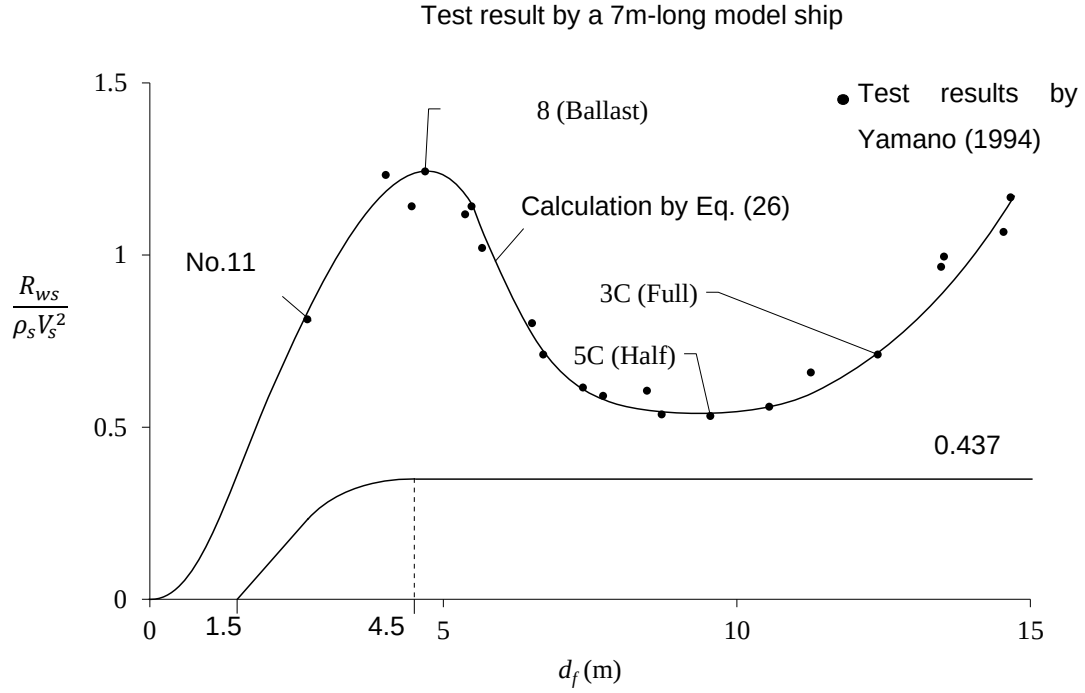

Source: FABRÍCIO FILHO *et al*. (2020).

We can use equation (26) to any other ships, if the two parameters in it:

a) The depth of the line source, d_{ls}

b) The constant α

are adapted to the ship using the base data of the ship.

4.6 DESIGN OF BOW FORMS TO REDUCE WAVE-MAKING RESISTANCE AT BALLAST CONDITION

In order to reduce the larger wave-making resistance at Ballast condition of Ship ISNI, we design two modified bow forms, M1 and M2, using equation (26). Original bow form O is that of Ship ISNI.

4.6.1 Design of bow forms

From equation (26) and Figure 29, we know that a smaller "b_e" makes the wave-making resistance smaller on the condition "i_e" is lower than 35 deg. The "b_e" at Ballast condition of original bow O is 1.65 m. So, we design "b_e" of modified bows M1 and M2 as follows to reduce the wave-making resistance of bow O:

M1: "b_e" = 0.6 with the same bow profile as O, "i_r" = 0 deg, "i_e" = 20 deg

M2: to extend waterline fore end of M1 to the point where "b_e" becomes equal to 0.1 m, "i_r" = 0 deg, "i_e" = 20 deg.

Comparison of bow forms among bow models O, M1 and M2 is shown in Figure 35.

Figure 35 – Comparison of bow forms among bow models O, M1 and M2

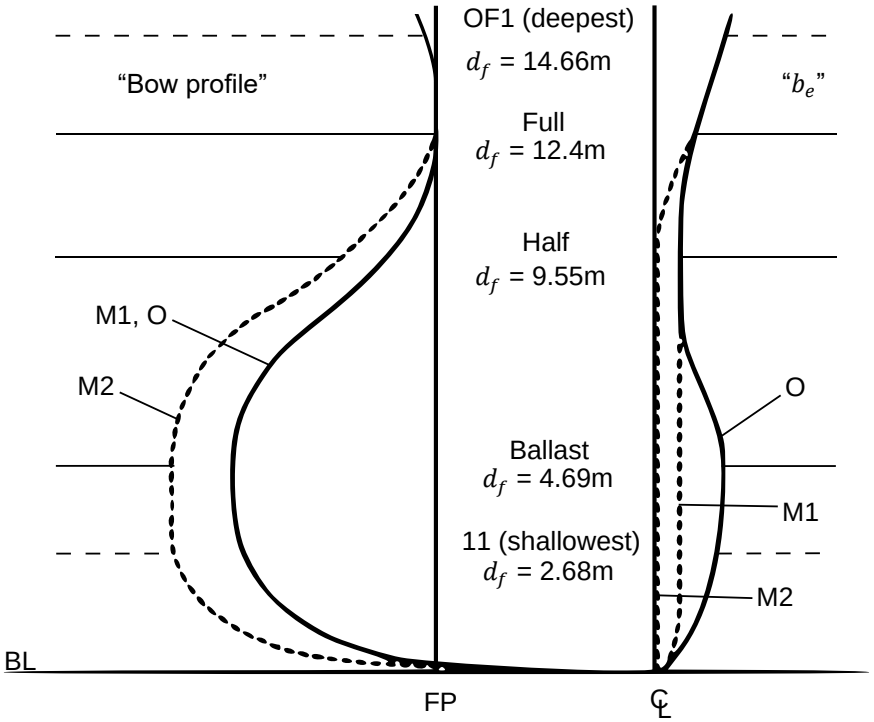

Source: FABRÍCIO FILHO *et al*. (2020).

(a) Comparison of "bow profile" and "b_e" among bow models O, M1 ans M2

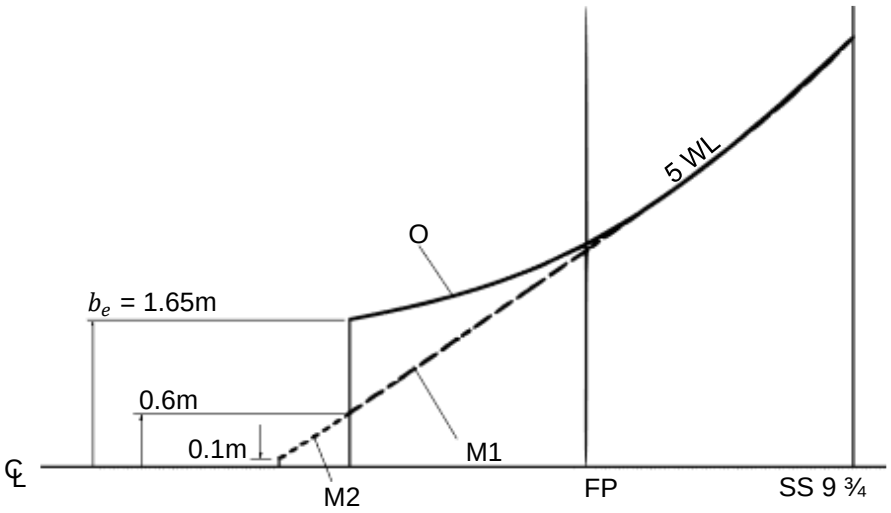

(b) Comparison of 5 m waterline fore end among bow models O, M1 and M2.

4.6.2 Estimation of reduction of wave-making resistance by designed bow forms

We have estimated the $\frac{R_{ws}}{\rho_s V_s^2}$ at F_n = 0.15 of bow models O, M1 and M2 with equation (26). The results are shown in Table 5. The estimated EHP reduction by M1 and M2 is 7.3% and 8.3%, respectively.

Table 5 – Estimation of resistance reduction by M1 and M2

Bow	$R_{ws}/\rho_s V_s^2$	R_{ws}/R_{tsO} (%)	$\Delta R_{ws}/R_{tsO}$ (%)
O	1.243	*12.9	0
M1	0.544	5.65	-7.3
M2	0.440	4.57	-8.3

Source: FABRÍCIO FILHO *et al*. (2020).

Remarks:
1. $R_{ws}/\rho_s V_s^2$: estimation by equation (26)
2. *: test result by a 7m-long model ship
3. Suffix O: Bow O

4.7 MODEL TESTS OF DESIGNED BOW FORMS

To confirm the usefulness of the developed bow form design method, 2m-long model ships of bow forms O, M1 and M2 were prepared and tested for this study, by Oshima Shipbuilding Co., Ltd. This section reports the model tests and the results got by them.

4.7.1 Outline of model tests

In order to confirm the usefulness of equation (26), we conducted model test of the three bow models: O, M1 and M2.The outline of the model test conducted for this study is repoted below.

4.7.1.1 Model tank

The circulating water channel of Oshima Shipbuilding Co., Ltd. with the following particulars was used.

Observation part: L =6,000 mm, B = 2,000 mm, Water depth = 1,000 mm

Max. waterflow speed = 2.5 m/s.

4.7.1.2 Model test

Model ships with L_{pp} = 2,000 mm without rudder and bilge keels were used. Resistance tests at three conditions – Full, Half, and Ballast – were conducted on each of the bow models – O, M1, and M2 – as shown in Table 6. At the same time, wave photos were taken.

Table 6 – Model ship and test condition (2m-long model)

	Full-scale ship (m)	Model Ship (m)		
Name	ISNI	O, M1, M2		
L_{pp}	212	2		
B	32.2	0.3038	Condition	Tested F_n
$d_a/d_m/d_f$	12.4/12.4/12.4	0.1170/0.1170/0.1170	Full	0.05 – 0.18
	9.55/9.55/9.55	0.0901/0.0901/0.0901	Half	0.05 – 0.18
	6.50/5.60/4.69	0.0613/0.0528/0.0443	Ballast	0.05 – 0.18

Source: FABRÍCIO FILHO *et al*. (2020).

4.7.2 Test results

The results of the resistance tests conducted for this study are reported below.

4.7.2.1 Results of resistance tests

Figure 36 shows the comparison of $F_n - \frac{R_{ws}}{\rho_s V_s^2}$ curves among bow models O, M1 and M2. At Full and Half conditions, there is no difference. At Ballast condition, there is difference among the three bow models at the F_n range from 0.1 to 0.18. Figure 37 shows the comparison of V_s' – EHP curves among the three bow models. The

average EHP reduction in the F_n range from 0.1 to 0.18 by M1 is 3.1% and that by M2 is 5.5%.

Figure 36 – Test results $F_n - R_{ws}/\rho_s V_s^2$ of O, M1 and M2 (2m-long mode ships, tested for this studyl)
Test results by 2m-long model ship

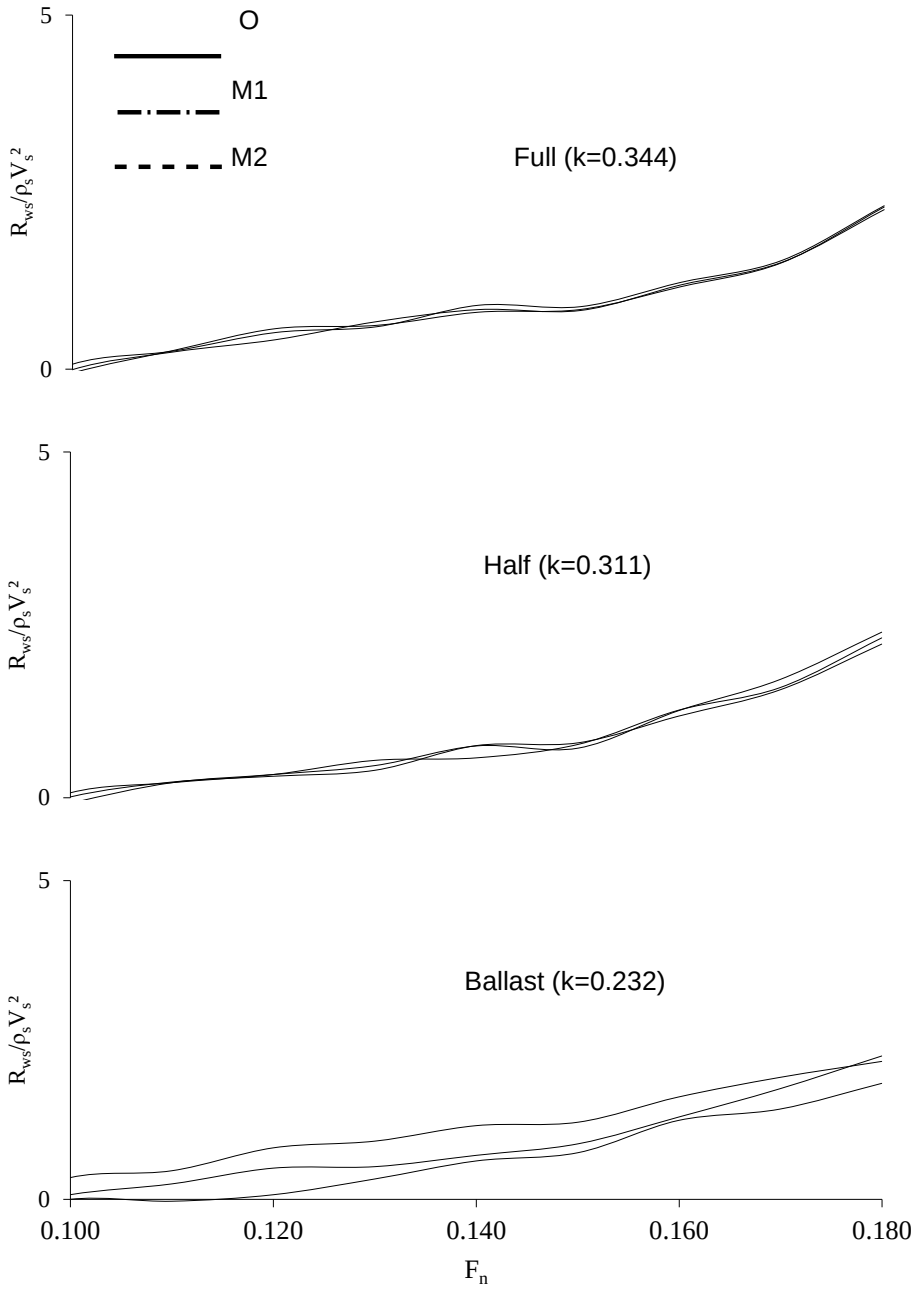

Source: FABRÍCIO FILHO *et al*. (2020).

Figure 37 – Test results V_s'– EHP of O, M1 and M2 (2m-long model ships, tested for this study)

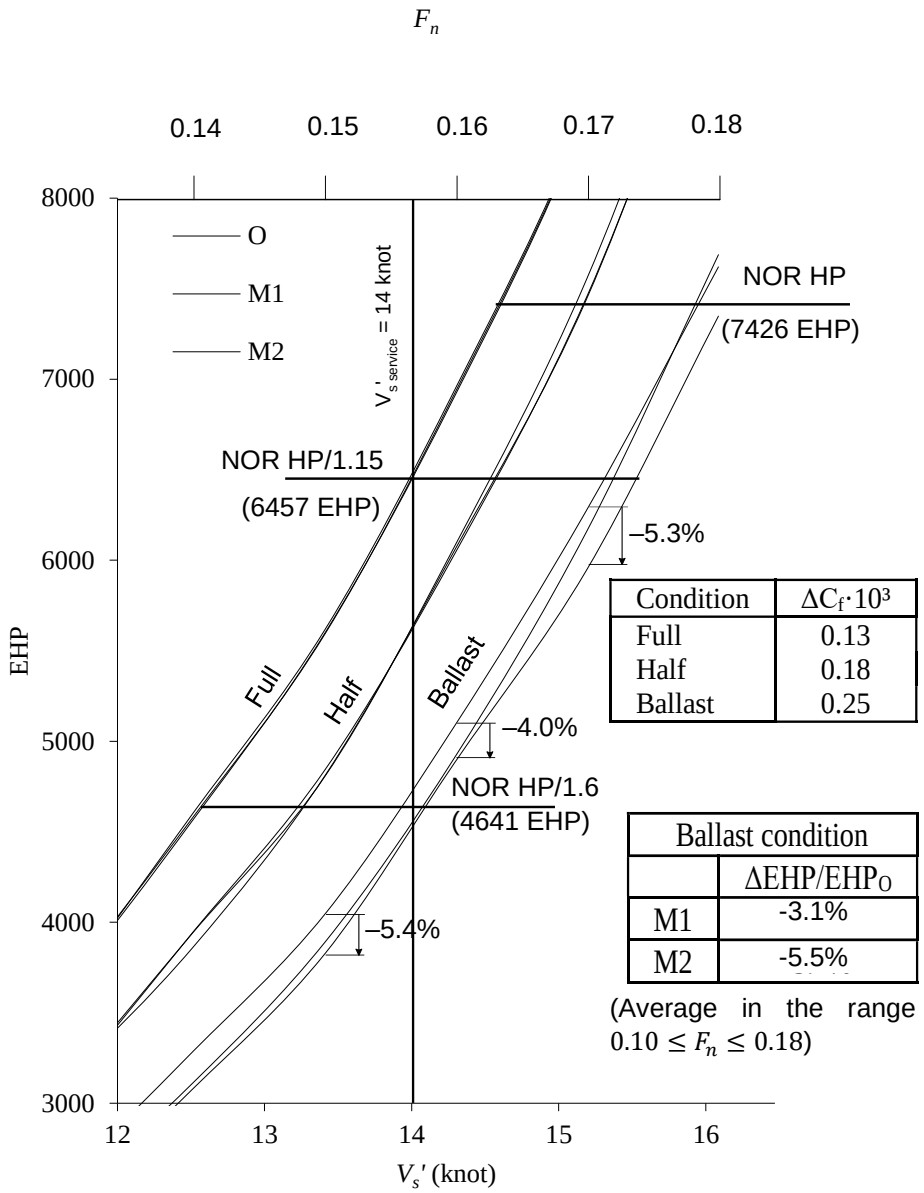

Source: FABRÍCIO FILHO *et al*. (2020).

4.7.2.2 Wave photos

Photos for each F_n at three conditions for three bow models were taken. Figure 38 shows photos of bow wave of bow models O, M1 and M2 at F_n = 0.15 at Ballast condition. From Figure 38, we can know that bow wave is improved to the direction from OB through M1 to M2.

Figure 38 – Bow waves of bow models O, M1 and M2 at F_n = 0.15 at Ballast condition (2m-long model ships, tested for this study)

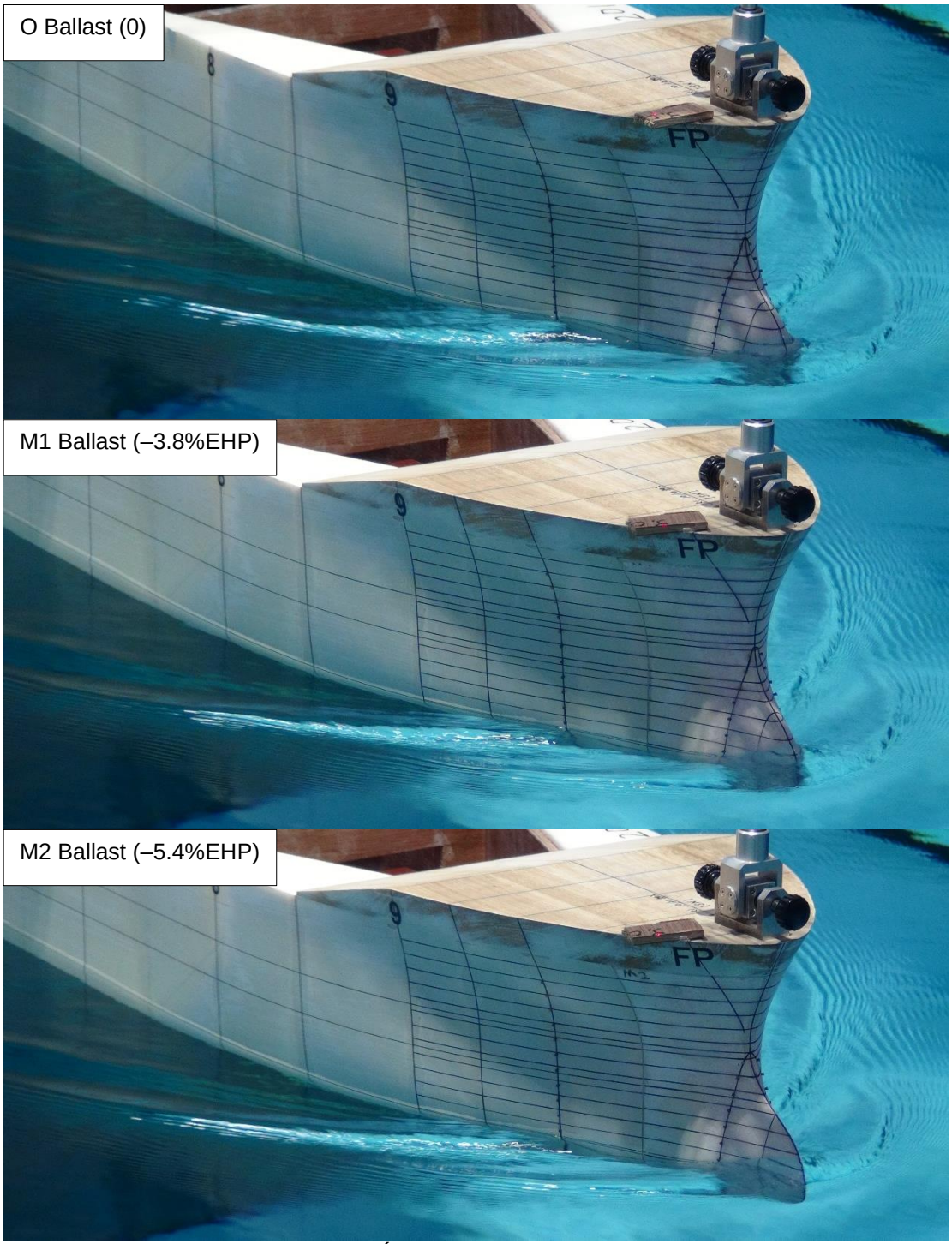

Source: FABRÍCIO FILHO *et al.* (2020).

4.8 DISCUSSION OF “STUDY 1”

In 4.8.1, we discuss the EHP reduction by M1 and M2 measured in the resistance test with the 2m-long model ships prepared for this study, comparing it

with the estimation with our developed equation. In 4.8.2, we discuss the change of $\frac{R_{ws}}{\rho_s V_s^2}$ with Froude number F_n.

4.8.1 Comparison of measured EHP reduction by M1 and M2 with estimation

The comparison of the measured EHP (R_{ts}) reduction by M1 and M2 with estimation is shown in Table 7.

Table 7 – Comparison of EHP (R_{ts}) reduction by M1 and M2 at F_n = 0.15 between estimation and 2m-long model test

	Estimation			2m-long model test		
Bow	$R_{ws}/\rho_s V_s^2$	$R_{ws}/R_{tsO}(\%)$	$\Delta R_{ws}/R_{tsO}(\%)$	$R_{ws}/\rho_s V_s^2$	$R_{ws}/R_{tsO}(\%)$	$\Delta R_{ws}/R_{tsO}(\%)$
O	1.243	*12.9	0	1.211	13.7	0
M1	0.544	5.65	-7.3	0.872	9.87	–3.8
M2	0.440	4.57	-8.3	0.733	8.30	–5.4

Source: FABRÍCIO FILHO *et al*. (2020).

Remarks:
1. *: estimation
2. **: Estimation by equation (26)
2. Suffix O: Bow O

The measured EHP reduction is smaller than the estimation as shown in Table 7. The difference between the test results by 2m-model ships and estimation is also shown in Figure 39.

Figure 39 – Comparison of EHP (R_{ts}) reduction by M1 and M2 between estimation and test results by 2m-long model ships (tested for this study)

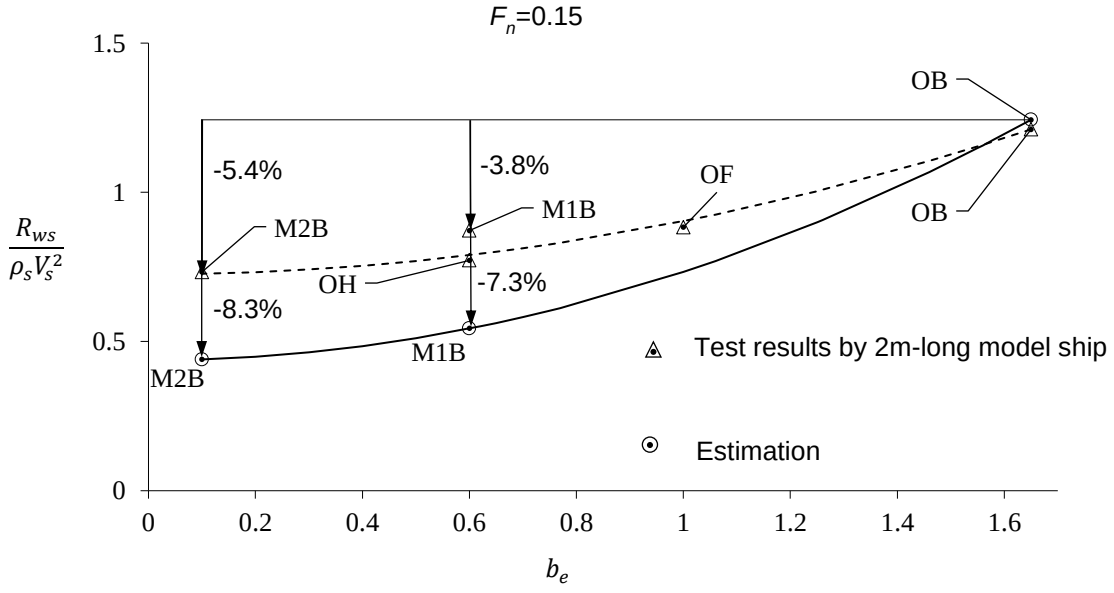

Source: FABRÍCIO FILHO *et al.* (2020).

From Figure 39, we know the followings. The points OB, OH, OF, M1B and M2B obtained by the tests by 2m-long model ships are on another line (dotted line corresponding to WAVE-MAKING RESISTANCE due to a line source with 0.9m depth) different from that of the estimation (solid line corresponding to WAVE-MAKING RESISTANCE due to a line source with 1.5m depth). This difference caused the smaller EHP (R_{ts}) reduction by M1 and M2 in the tests by 2m-long model ships than estimation.

The reason why the line for OB, OH, OF, M1B and M2B obtained by the tests by 2m-long model ships has changed from that the estimation has not been found. However, the ratios Test result/Estimation of both models have, each other, near values, as shown in Table 8.

Table 8 – Comparison of EHP reduction ratio 2m-long model test result/estimation at F_n=0.15 between M1 and M2

	M1	M2
EHP reduction: Test result/Estimation	3.8/7.3=0.49	5.4/8.3=0.65

Source: FABRÍCIO FILHO *et al*. (2020).

This shows that equation (26) is qualitatively correct at least. On the other hand, the EHP reduction -5.4% by M2 at F_n=0.15 in the test by 2m-model ships can be said to be practically a large enough value compared with the rather smaller modification of M2 from O shown in Figure 35.

The estimation of the price of saved fuel per year with EHP reduction of 5.5% (which is the average EHP reduction by M2 in the test by 2m-model ships in the F_n range from 0.10 to 0.18) is shown in Table 9 for two ships: Ship ISNI, and one more ship, Ship IYNR. The price of saved fuel oil per year is estimated in 111 thousand US dollars for Ship ISNI and 272 thousand US dollars for Ship IYNR, for an average price of type C heavy oil. These are very large savings.

As a conclusion, we can say that the equation (26) is useful for the bow form design for a full ship.

Table 9 – Price of saved fuel per year with EHP reduction of 5.5%

	Unit	Ship 1	Ship 2
Ship name	-	ISNI	IYNR
Ship kind	-	Panamax bulk carrier	VLCC
Ship speed	knot	14	16
DWT	t	62,377	258,733

NOR BHP	hp	9,520	25,200
Fuel consumption rate of Main Engine*	gf/hp/h	131	121
Fuel consumption per day	t/day	29.9	73.2
Operation days per year (at ballast condition)	day/year	150	150
Fuel consumption per year	t/year	4487	10,977
fuel consumption reduction of 5.5% per year	t/year	246.9	603.7
Fuel price per ton	JPY/t	50,000	50,000
	USD/t	450	450
	BRL/t	1,950	1,950
Price of saved fuel per year	JPY/year	12,346,488	30,187,080
	USD/year	111,118	271,684
	BRL/year	481,513	1,177,296

Source: The Author (2019).

Remarks:
* Base calorific values=9,800 kcal/l, type C heavy oil

4.8.2 Change of $\frac{R_{ws}}{\rho_s V_s^2}$ value with Froude number F_n

Until now, we have discussed the data at F_n = 0.15. Next, we check how $\frac{R_{ws}}{\rho_s V_s^2}$ changes with Froude number F_n. In 4.8.2.1, we check whether we can use a line source to estimate $\frac{R_{ws}}{\rho_s V_s^2}$ at other F_n than 0.15. In 4.8.2.2, we check the part which does not come from line source, that is, the remaining part .

4.8.2.1 $\frac{R_{ws}}{\rho_s V_s^2}$ due to a line source

Figure 40 shows a comparison of $\Delta\left(\frac{R_{ws}}{\rho_s V_s^2}\right)_{M2B-OB}$ between the estimation with a line source and the test result over F_n. "$\Delta\left(\frac{R_{ws}}{\rho_s V_s^2}\right)_{M2B-OB}$" is the difference of $\frac{R_{ws}}{\rho_s V_s^2}$ between M2B and OB. Figure 41 is the same comparison between OH and OB.

Figure 40 – Comparison of $\Delta\left(\frac{R_{ws}}{\rho_s V_s^2}\right)_{M2B-OB}$ between test result and estimation with a line source

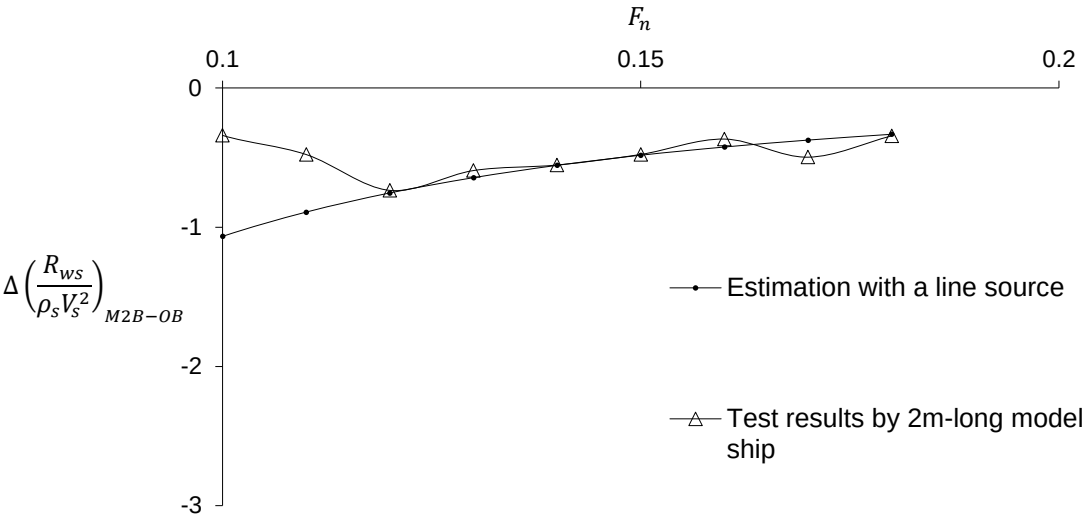

Source: FABRÍCIO FILHO *et al*. (2020).

Figure 41 – Comparison of $\Delta\left(\frac{R_{ws}}{\rho_s V_s^2}\right)_{OH-OB}$ between test result and estimation with a line source

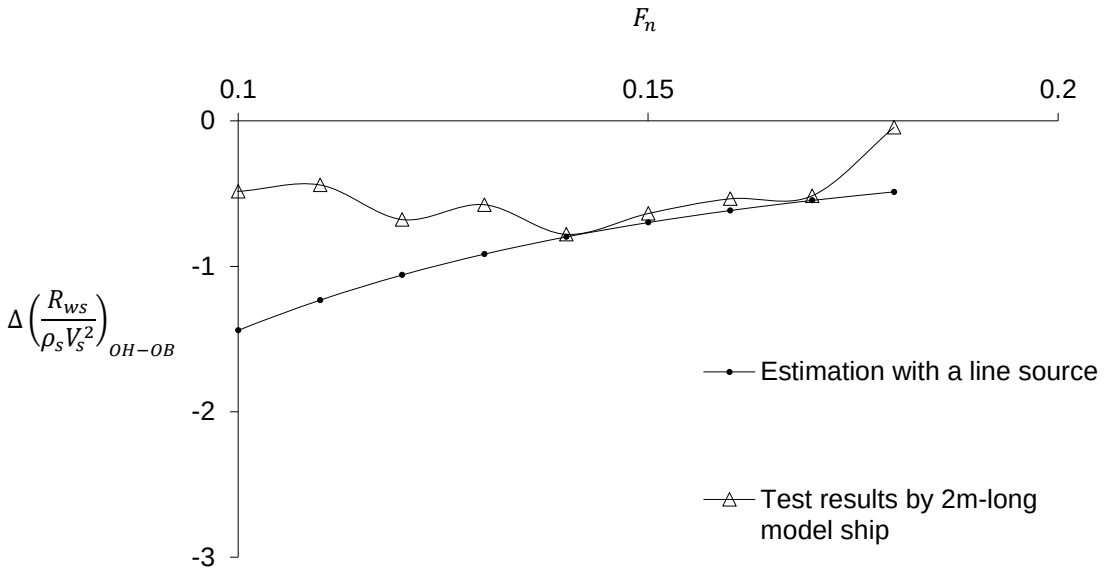

Source: FABRÍCIO FILHO *et al*. (2020).

In both of Figure 40 and Figure 41, at F_n from 0.12 to 0.18, the test result changes with F_n with the same amount and tendency as the estimation. It shows that at F_n from 0.12 to 0.18, we can estimate $\frac{R_{ws}}{\rho_s V_s^2}$ due to bow fore end with a line source which we used at F_n= 0.15. Therefore, $\frac{R_{ws}}{\rho_s V_s^2}$ due to bow fore end decreases with the increase of F_n as shown in Figure 42.

Figure 42 shows how $\frac{R_{ws}}{\rho_s V_s^2}$ due to bow fore end changes with F_n in case of OB. In Figure 42, the value of $\frac{R_{ws}}{\rho_s V_s^2}$ at F_n =0.15 is from the test result by the 7m-long model ship by Yamano (1994) and the change of $\frac{R_{ws}}{\rho_s V_s^2}$ with F_n is from the test result by the 2m-long model ship. At F_n =0.15, occupies about 65% of total $\frac{R_{ws}}{\rho_s V_s^2}$. However, it decreases to about 32% at F_n = 0.17.

Figure 42 – $\frac{R_{ws}}{\rho_s V_s^2}$ due to bow fore end (estimation with a line source) in total $\frac{R_{ws}}{\rho_s V_s^2}$ (OB, 7m-long model ship, tested by Yamano (1994))

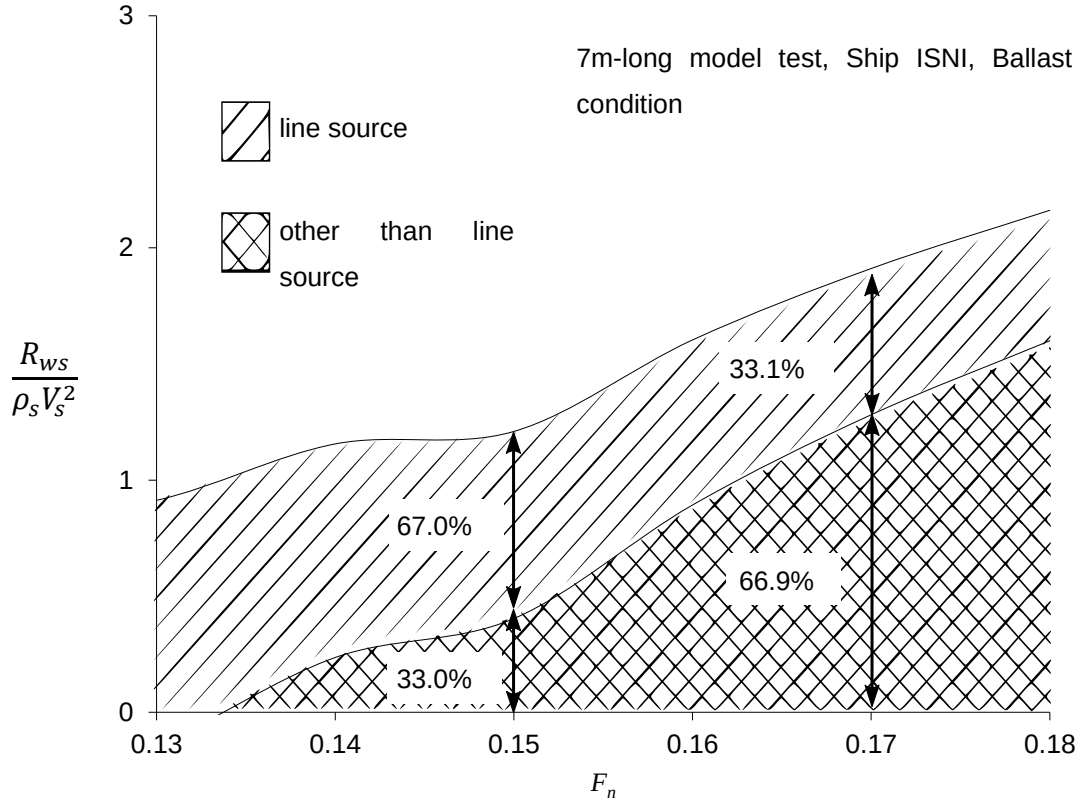

Source: FABRÍCIO FILHO *et al*. (2020).

4.8.2.2 Remaining $\frac{R_{ws}}{\rho_s V_s^2}$

The comparison of the remaining $\frac{R_{ws}}{\rho_s V_s^2}$ obtained using the following equation (27) among OF, OH and OB is shown in Figure 43.

$$\left(\frac{R_{ws}}{\rho_s V_s^2}\right)_{\text{remaining}} = \left(\frac{R_{ws}}{\rho_s V_s^2}\right)_{\text{7m-model test}} - \left(\frac{R_{ws}}{\rho_s V_s^2}\right)_{\text{LS 0.9m depth}} \quad (27)$$

$\left(\frac{R_{ws}}{\rho_s V_s^2}\right)_{\text{7m-model test}}$: the value at F_n=0.15 is from test result by the 7m-long model ship and the change of $\frac{R_{ws}}{\rho_s V_s^2}$ with F_n is from the test result by the 2m-long model ship. The mean line of OF, OH and OB shown with a dotted line in Figure 43 can be expressed by equation (28):

$$\left(\frac{R_{ws}}{\rho_s V_s^2}\right)_{\text{remaining}} = 3700\,(F_n - 0.1)^3 \quad (28)$$

Figure 43 – Comparison of $\left(\frac{R_{ws}}{\rho_s V_s^2}\right)_{\text{remaining}}$ (7m-long model ship, tested by Yamano (1994))

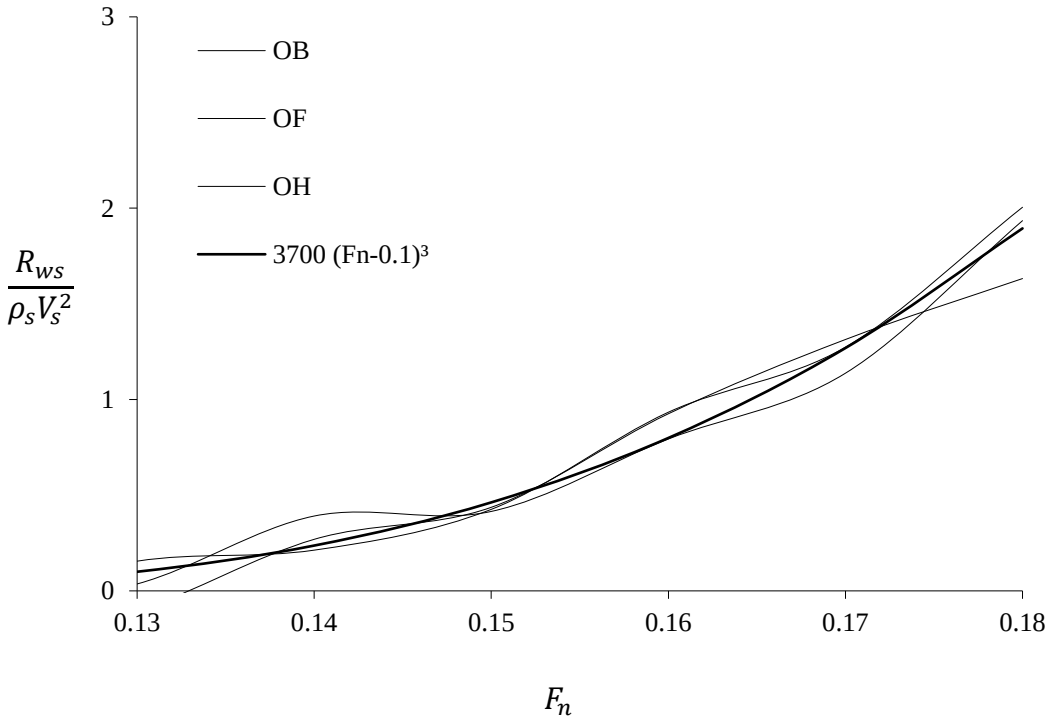

Source: FABRÍCIO FILHO *et al*. (2020).

4.9 BOW FORM DESIGN METHOD FOR A FULL SHIP

In 4.5.2, we have derived equation (26) to estimate wave-making resistance of a full ship at F_n = 0.15. In 4.8.2, we have clarified how the two components of the wave-making resistance change with F_n. Based on these results, we propose the following bow form design method for a full ship. This method is paying attention to

wave-making resistance due to bow fore end. Therefore, it is effective for a ship with design F_n lower than 0.17.

The design method is described in the following items (1) – (5).

(1) Base data:

Resistance test results at three drafts of a parent form or a similar ship – Full, Medium draft and Ballast (the largest "b_e" and the smallest "b_e" are preferable to be included in these conditions).

(2) Decision of b_e – $\left(\frac{R_{WS}}{\rho_S V_S^2}\right)_{\mathrm{LS}}$ curve in equation (26) based on the base data:

The depth of the line source which represents waterline fore end is decided by using the base data.

(3) Decision of F_n – $\left(\frac{R_{WS}}{\rho_S V_S^2}\right)_{\mathrm{remaining}}$ curve:

First, the curve F_n – $\left(\frac{R_{WS}}{\rho_S V_S^2}\right)_{\mathrm{remaining}}$ is made at each condition. Next, as a mean of those at three conditions, F_n – $\left(\frac{R_{WS}}{\rho_S V_S^2}\right)_{\mathrm{remaining}}$ curve is decided. This mean curve can be applied to every condition.

Now we have got equation (26). The α in equation (26) is the curve which we have got above as F_n – $\left(\frac{R_{WS}}{\rho_S V_S^2}\right)_{\mathrm{remaining}}$ curve. With the equation (26), we can estimate $\frac{R_{WS}}{\rho_S V_S^2}$ at any draft and at any F_n.

(4) Design of "b_e" distribution:

In principle, smaller "b_e" gives smaller $\frac{R_{WS}}{\rho_S V_S^2}$. We design d_f - "b_e" distribution on this principle.

(5) Design of "i_e" and bow profile:

If we try to decrease "b_e" on the condition that bow profile is kept as it is, "i_e" increases. We must compromise this issue. To solve the issue, we can use the recommended maximum "i_e" given in Lewis (1988) as a maximum allowable limit of "i_e". To keep the "i_e" smaller than the recommended maximum "i_e", we can adjust bow profile.

5 DEVELOPMENT OF A NEW RESISTANCE TEST METHOD FOR A FINE SHIP IN A CWC

The study reported in this chapter is designated “Study 2”. Here, we report the development of a New Resistance Test Method for a fine ship in a CWC. In section 5.1, the background necessary to understand “Study 2” is reported. In section 5.2, the proposal of the New Resistance Test Method is reported. In section 5.4, the design of models for a confirmation test in a CWC is reported. In section 5.5, a study on the manufacture of a model for a test in a CWC is reported.

5.1 BACKGROUND

In the following, the background necessary to understand “Study 2” is reported.

5.1.1 Traditional Resistance Test Method in a CWC

CWC – Circulating Water Channel – is a device used, among other purposes, for conducting resistance tests in model ships. For knowing more about CWC, the reader may refer to 2.1.4. In Figure 44, the CWC acquired by UFPE is shown.

Figure 44 – UFPE’s CWC (Circulating Water Channel), with an observation part with dimensions length × breadth × height = 2.00m × 0.50m × 0.50m, and with a maximum flow speed of 1.5m/s.

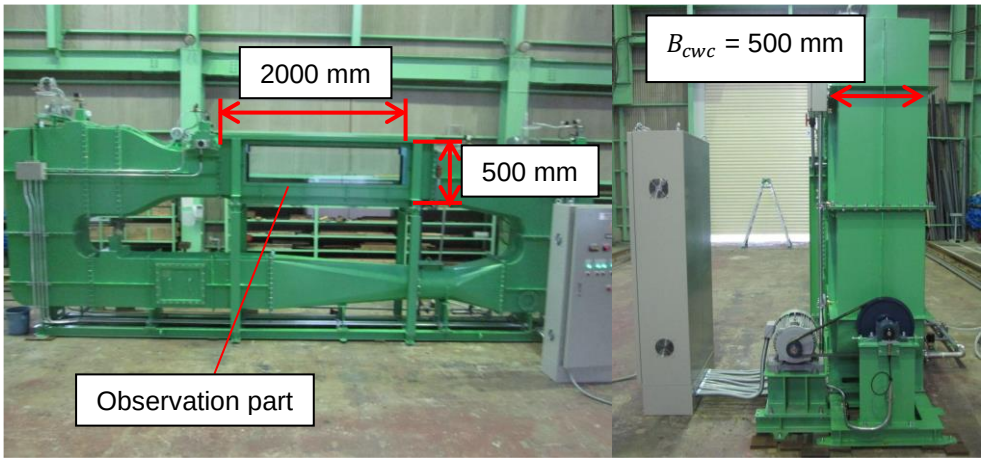

Source: West Japan Fluid Engineering Laboratory Co., Ltd. (2015).

In the Traditional Resistance Test Method, the length L_{pp} of a model ship used for a resistance test in a CWC is decided to be equal to the breadth B_{cwc} of the CWC. There are several types of CWCs with B_{cwc} varying from 0.3m to 2.0m. Therefore, the

length L_{ppm} of the model ship used in these CWCs ranges from 0.3 to 2.0m in the Traditional Resistance Test Method.

On the other hand, the length L_{ppm} of a model ship used in a towing tank (L = 200m, B = 13m, Water depth = 6.5m, for example) is about 7m. The total resistance of a model ship is proportional to ${L_{ppm}}^3$ at a Froude number. Therefore, the total resistance of the model ship used in a CWC is much smaller than that of the model in a towing tank, as shown in Table 10.

Table 10 – Model ship length L_{ppm} – total resistance of a model ship

Model tank	Towing tank	CWC			
Model ship length L_{pp} (m)	7	3	2	0.5	0.3
Ratio of total resistance	1	1/12.7	1/42.9	1/2744	1/12703
	12.7	1	1/3.4	1/216	1/1000
	42.9	3.4	1	1/64	1/296
	2744	216	64	1	1/4.6
	12622	994	294	4.6	1

Source: YAMANO (2019).

Especially in a CWC with smaller breadth B_{cwc} = 0.3 – 0.5m, the amount of the total resistance is from 1/64 to 1/296 of that of the model ship with L_{ppm} = 2m, as shown in Table 10. The smaller total resistance decreases the accuracy of the resistance measurement. This lower accuracy in resistance measurement in a smaller CWC, as well as the lower form accuracy of the smaller model ship for a smaller CWC are issues that the New Resistance Test Method for a Fine Ship in a CWC solves.

5.1.2 Advantages and disadvantages of test in a CWC

Chart 2 shows the Advantages and disadvantages of a test in a CWC.

Chart 2: Advantages and disadvantages of a test in a CWC.

Advantages	Disadvantages
Possible to keep a condition for a long time ↓ Preferable for observation of flow	Model scale is small $L_{ppm} = B_{CWC}$, usually 0.3 – 0.5m ↓ Low accuracy of measured resistance

Source: The Author (2019).

For observation of flow, compared with a towing tank, CWC is more convenient, since it can keep a condition for a long time. However, the demerit of CWC is that the model scale L_{ppm} is limited to the breadth of the observation part of the CWC, B_{cwc}, which is usually from 0.3 to 0.5m, what makes the accuracy of measured resistance low, as already explained in 5.1.1. Such demerit is an issue that the New Resistance Test Method is proposed to solve.

5.1.3 Models for a test

For the developed New Resistance Test Method, a model for a test in a CWC is necessary. However, we have had no experience of model manufacture by ourselves, and there are no makers around us who have such experience. Therefore, we decided to study the way how to prepare such a model by ourselves.

5.1.3.1 Conditions necessary for models and model manufacture

The model should satisfy the following conditions: for a model, 1) Accuracy, 2) Strength and 3) Water tightness; for model manufacture, 4) Accuracy control and 5) Time-schedule control should be possible.

5.1.3.2 Model manufacture through out-sourcing or by ourselves

Since there are no makers around UFPE who have the experience of the manufacture of such a model, it cannot be expected that the makers do the conditions 4) and 5) described above in at an acceptable level. We also have no such experience. Therefore, the best way we should take would be for us to manufacture the model by ourselves, at least first, and to find the issues that we might meet and to study the ways how to solve the issues by ourselves.

5.2 BASE FINDINGS THAT SUPPORT NEW RESISTANCE TEST METHOD

In 5.2.1, the two findings on which the New Resistance Test Method is based are presented, “Finding 1” and “Finding 2”. We confirm the reliability of “Finding 1” in 5.2.2. In 5.2.3, we discuss the dominance of wave-breaking near the bow (“Finding 2”).

5.2.1 Two findings that support the New Resistance Test Method

The New Resistance Test Method is based on two findings, which are described in the following.

“Finding 1”: Most of the wave-making resistance is generated by the bow: The studies on wave-making resistance of a ship (YAMANO *et al*., 1996, 1997; FABRÍCIO FILHO *et al*., 2018, 2019a) show that:

a) Each part of the forebody is not equally important for wave-making resistance.

b) Most of the wave-making resistance of a fine ship is that due to the bow (from about 3% aft of FP to the fore end of a ship’s hull)

“Finding 2”: Most of the wave-making resistance by the bow is due to wave-breaking near the bow: Wave-making resistance consists of wave-pattern resistance and wave-breaking resistance. Wave-pattern resistance is the resistance due to the waves propagating afterwards. Wave-breaking resistance is the resistance due to the wave-breaking just near the bow. In the two studies on wave-making resistance of a ship by Yamano *et al.* (1996, 1997), it has also been found that:

a) Wave-pattern resistance is very small.

b) Most of the wave-making resistance due to the bow is that due to wave-breaking just near the bow.

The reliability of “Finding 1” and “Finding 2” has been confirmed through the following:

For “Finding 1”: through theoretical analysis using the linear wave-making resistance theory (HAVELOCK, 1924; 1932), it can be understood how each part of the forebody affects the wave-making resistance. This approach is used in Fabrício Filho *et al*. (2018), where calculations are conducted for the overall forebody of the hull forms of two models of a 354,000ft³ refrigerated cargo ship, M.No.1 and M.No.5. The resistance test results of M.No.1 and M.No.5 show that the wave-making resistance of M.No.5 is much lower than that of M.No.1 in the range $0.20 \leq F_n \leq 0.26$. The same approach is used in Fabrício Filho *et al*. (2019), but in the latter, the calculations are conducted for the bow only of the same. The comparison of the results of both studies confirms the reliability of finding 1).

For “Finding 2”: through the model test results presented in Yamano *et al*. (1996,1997), it is shown that the main component of the difference in wave-making resistance is that in wave-breaking resistance.

5.2.2 Confirmation of the reliability of “Finding 1”

We confirm the reliability of “Finding 1” below by theoretical analysis with linear wave-making resistance theory, in 5.2.2.1, and discussion with other related model test results, in 5.2.2.2.

5.2.2.1 Theoretical analysis with linear wave-making resistance theory

About fundamental explanation on the linear wave-making resistance theory, the reader may refer to 2.6. The used coordinate system xyz is shown in Figure 45: origin is at the fullest section, hull centerline plane and load waterline plane of a ship with length 2ℓ and draft d;. the x-axis is in the load waterline plane and hull centerline plane, and points to the aft of ship; y-axis is in the load waterline plane and fullest section plane, and points to the starboard direction; z-axis is in the fullest section plane and hull centerline plane, and points to the upward direction). V is the speed of a uniform flow towards the positive direction of the x-axis.

The wave-making resistance, according to the linear wave-making resistance theory, can be calculated by equations (5) and (6) (HAVELOCK, 1934):

$$R_w = \pi\rho V^2 \int_0^{\pi/2} [S^2(\theta) + C^2(\theta)] \cos^3\theta \, d\theta \tag{5}$$

$$\left.\begin{matrix} C(\theta) \\ S(\theta) \end{matrix}\right\} = \frac{4V\chi^2}{g} sec^3\theta \cdot \int_{x_1}^{x_2}\int_{z_1}^{z_2} \sigma(x,z) e^{z\chi\, sec^2\theta} \begin{matrix} cos \\ sin \end{matrix} (\chi x \sec\theta) dz\, dx \tag{6}$$

(Equations (5) and (6) are first presented in 2.6.2. For further explanation on these equations, the reader may refer to section 2.6).

Figure 45 – (a) Coordinate system definition. (b) The direction θ.

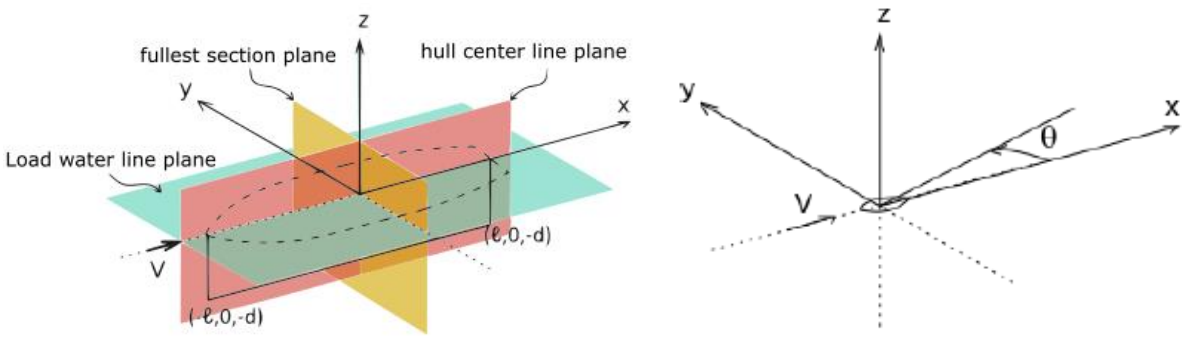

(a) (b)

Source: FABRÍCIO FILHO; SHINOHARA; YAMANO (2019a).

For convenience of calculation, the following non-dimensional coordinates ξ, η and ζ are used: $\xi = x/\ell$; $\eta = y/(B/2)$; $\zeta = z/\ell$, where ℓ is the entrance length (the length from FP to the fullest section), $B/2$ is the half breadth of the ship. To input the forebody hull form into the theoretical calculation, the hull form is simplified and represented with just three important parameters: sectional area curve, load waterline, and fore end half breadth. Polynomial approximations are used for the sectional curve $\eta_1(\xi)$ – equation (29) – and the load waterline $\eta_0(\xi)$ – equation (30).

$$\eta_1(\xi) = 1 - \sum_{n=1}^{5} a_{2n}\xi^{2n} \qquad for -1 \le \xi \le 0 \tag{29}$$

$$\eta_0(\xi) = \begin{cases} 1 - \sum_{n=1}^{5} l_{2n}\left(\xi + 1 - \frac{\ell_e}{\ell}\right)^{2n} & for -1 \le \xi \le -1 + \frac{\ell_e}{\ell} \\ 1 & for -1 + \frac{\ell_e}{\ell} \le \xi \le 0 \end{cases} \tag{30}$$

The simplification of a transverse section form of the forebody is illustrated in Figure 46.

Figure 46 – Simplification of a transverse section form.

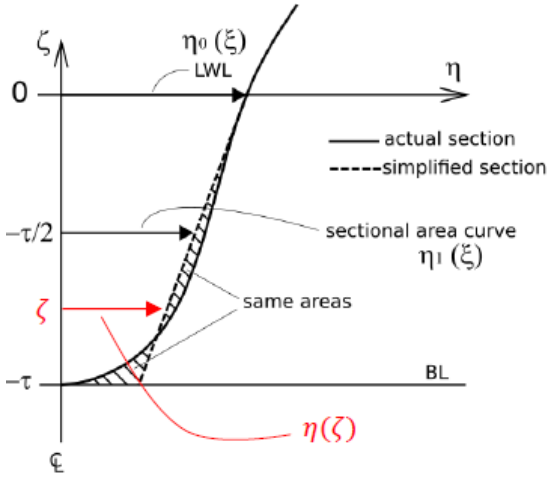

Source: FABRÍCIO FILHO; SHINOHARA; YAMANO (2019a).

The polynomial simplified hull surface $\eta(\xi,\zeta)$ (main hull) expressed with sectional area curve $\eta_1(\xi)$ and LWL curve $\eta_0(\xi)$ is shown in Figure 47.

Figure 47 – Simplified hull surface $\eta(\xi,\zeta)$ (main hull) expressed with sectional area curve $\eta_1(\xi)$ and LWL curve $\eta_0(\xi)$.

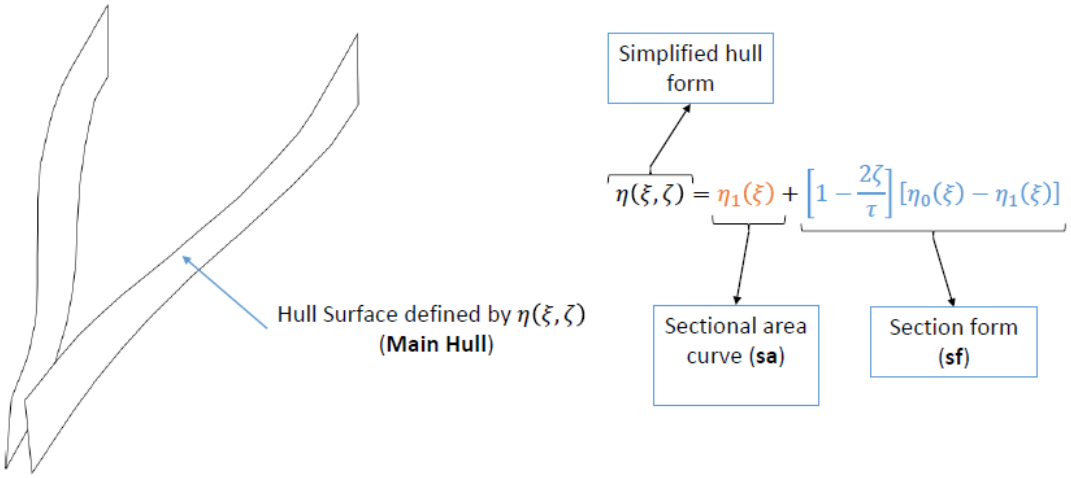

Source: FABRÍCIO FILHO; SHINOHARA; YAMANO (2019a).

To calculate $S(\theta)$ and $C(\theta)$, the hull form is represented with singularities (sources, sinks, and doublets) distributed over the hull center line plane. In the present case, the forebody main hull is represented with a source distribution over the hull centerline plane ($-1 \leq \xi \leq 0, -\tau \leq \zeta \leq 0$) and the fore end part with a line source located a little aft FP ($\xi = -1 + \varepsilon_{ls}, -\tau \leq \zeta \leq 0$). Figure 48 shows the relation between source density $\sigma(\xi,\zeta)$ and hull form $\eta(\xi,\zeta)$. Figure 49 shows the equations to calculate $S(\theta)$ and $C(\theta)$ for each of the three hull form parameters (sectional area curve, section form, and fore end form). The integration of these $S(\theta)$

and $C(\theta)$ squared over θ from $-\pi/2$ to $\pi/2$ with equation (5) gives the wave-making resistance due to each of these parameters separately or also due to all of them.

Figure 48 – The relation between source density $\sigma(\xi,\zeta)$ and hull form $\eta(\xi,\zeta)$.

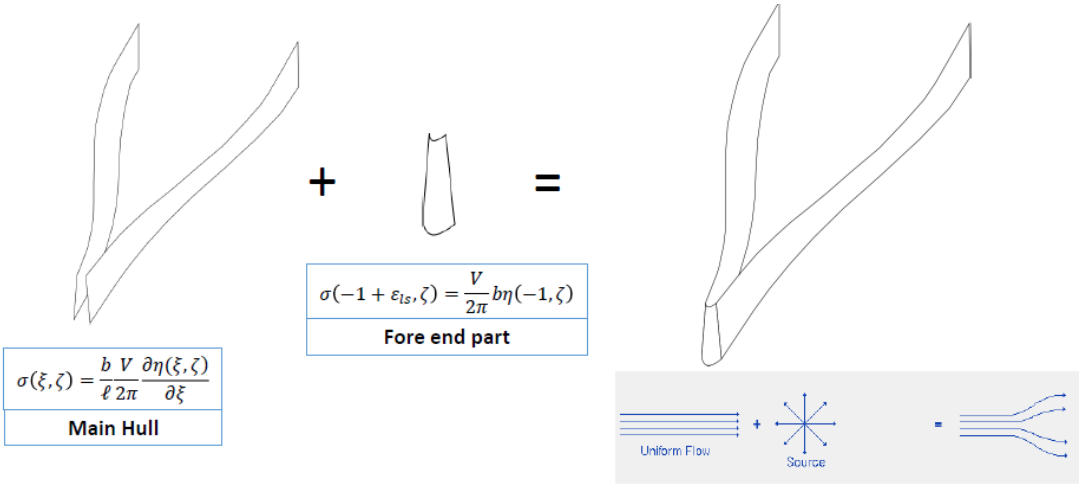

Source: FABRÍCIO FILHO; SHINOHARA; YAMANO (2019a).

Figure 49 – Equations to calculate $S(\theta)$ and $C(\theta)$ of forebody hull.

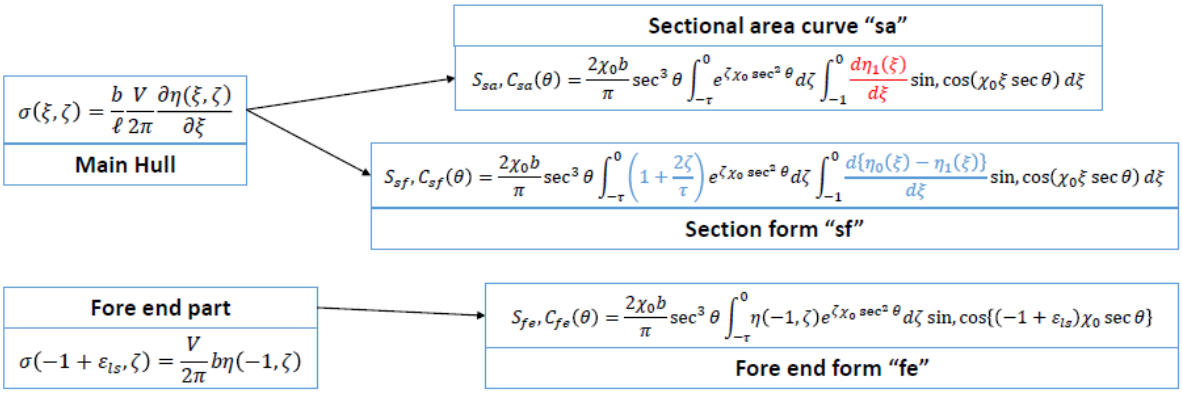

Source: FABRÍCIO FILHO; SHINOHARA; YAMANO (2019a).

Concerning the calculation procedure, the wave-making resistance due to each of the three parameters (sectional area curve, section form, and fore end form) and due to all of them was calculated, using the equations shown in Figure 49 above, integrating in ξ from FP ($\xi = -1$) to the Fullest Section ($\xi = 0$). Fabrício Filho *et al.* (2019a), the wave-making resistance was calculated for the same parameters as before, but with the integration range in ξ from FP ($\xi = -1$) to Square Station No. 9 ½ ($\xi = -0.90654$).

Figure 50, Figure 51 and Figure 52 show the calculated results in terms of wave-making resistance coefficient, $r_w = \frac{R_w}{\rho \nabla^{2/3} V^2}$.

Figure 50 – Comparison of the calculated wave-making resistance coefficient due to the sectional area curve.

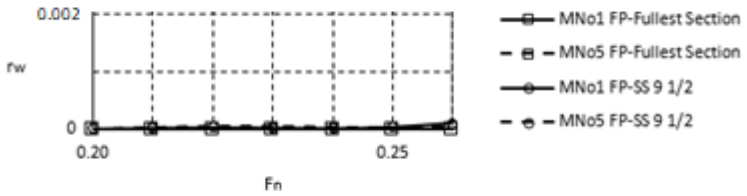

Source: FABRÍCIO FILHO; SHINOHARA; YAMANO (2019a).

Figure 51 – Comparison of the calculated wave-making resistance coefficient due to the section frame.

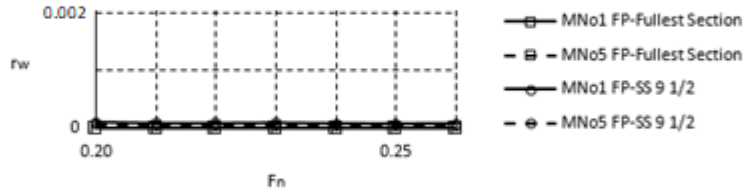

Source: FABRÍCIO FILHO; SHINOHARA; YAMANO (2019a).

Figure 52 – Comparison of the calculated wave-making resistance coefficient due to the fore end form.

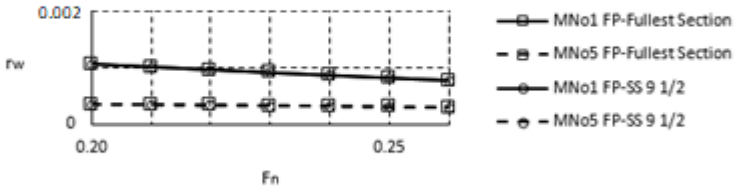

Source: FABRÍCIO FILHO; SHINOHARA; YAMANO (2019a).

From these figures, the wave-making resistance due to the sectional area curve and section form is small compared with that due to the fore end. Therefore, the difference in wave-making resistance between due to the integration range in ξ from FP to SS No. 9 ½ and due to the integration range from FP to the fullest section is also small.

The wave-making resistance due to the fore end form, represented by a line source a little aft FP is the same for the above both cases. The wave-making resistance coefficient due to the fore end form is shown in Figure 52.

From the above analysis, it has been theoretically confirmed that the bow form of a fine ship has an outstanding importance in wave-making resistance at the Froude number range below 0.26.

5.2.2.2 Discussion with other related model test results

The following discussion relies on model test results presented in Yamano *et al*. (1996,1997). The effect of the bow form and the effect of LWL entrance angle on wave-making resistance and

(a) On the effect of the bow form on wave-making resistance: Yamano at el. (1996, 1997) investigated five stem forms of a container ship with L_{pp} = 206.0 m shown in Figure 53 (a) by resistance tests. Form ① is the base form. The part from the fore end up to 6 m (2.9%L_{pp}) aft of FP was mainly modified. The results show that the stem form difference makes a very large difference in EHP, as it can be seen in Figure 53 (b): at 22.5 knots, there is an EHP increase ratio of up to 18% from form ① and a ship speed drop up to 1 knot from form ①. This data clearly shows that the form of the bow part with a length of only 2.9%L_{pp} largely controls the hull resistance.

Figure 53 – (a) Investigated bow forms: LWL fore end forms. (b) Comparison of EHP curves among the investigated bow forms – resistance results.

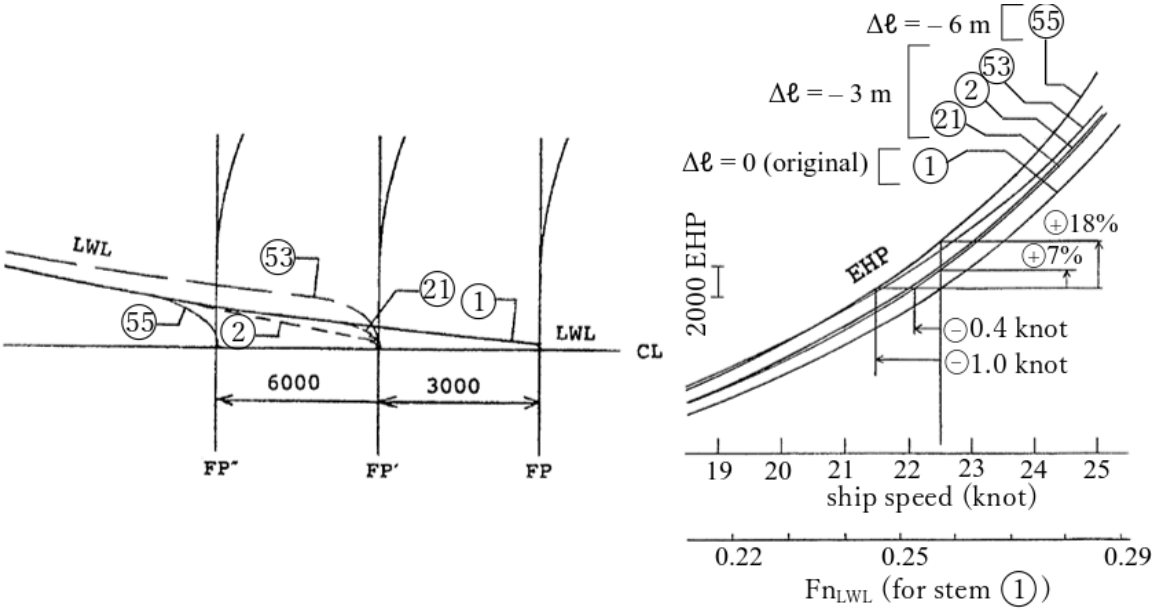

(a) (b)

Source: YAMANO *et al*., 1996.

(b) On the effect of LWL entrance angle on wave-making resistance of ten fine ships: The residual resistance coefficients of ten ships are compared in Figure 54 (a). The principal particulars of the ships are shown in Table 11. The five ships of Group A are designed by the shipbuilder A completely independently from those of group B designed by the shipbuilder B.

Table 11 – Hull particulars of the ten fine ships.

Group:	A					B				
Ship No.:	A1	A2	A3	A4	A5	B1	B2	B3	B4	B5
	6.67	6.90	7.14	7.00	6.72	6.72	6.65	6.60	6.60	6.90
	2.76	2.35	3.08	3.13	3.13	2.58	2.42	2.65	2.53	2.76
					0.57 ~ 0.61					
	72.1	79.6	70.0	89.3	87.4	79.6	76.9	82.4	81.6	104.0
	143.7	160.6	136.1	180.2	174.5	166.0	155.8	161.5	164.4	213.0
	11	7	7	6.5	4	10.5	9.5	12.5	12	13
	0.15	0.10	0.12	0.25	0.45	0.05	0.05	0.18	0.08	0.05

Source: Yamano *et al*., 1996.

Figure 54 – (a) Comparison of r_r of ten fine ships. (b) Correlation between LWL entrance half-angle θ and measured r_r.

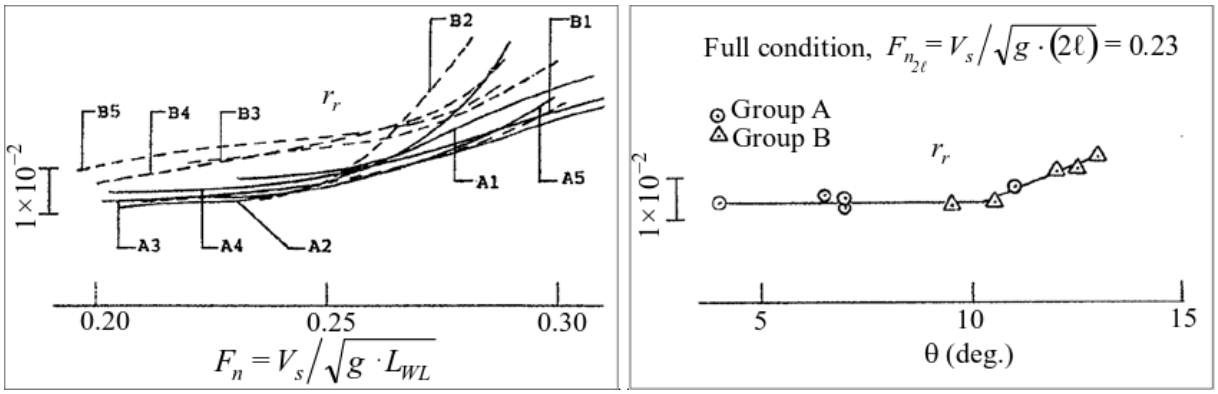

(a) (b)

Source: YAMANO *et al.*, 1996.

In Figure 54 (a), the three ships of Group B have a higher r_r (residual resistance coefficient) at Froude number lower than 0.26 compared with the other seven ships. The difference corresponds to about 8% of EHP. The authors of the paper have made all the efforts to find the cause of the large r_r difference. At the last, they found that the large r_r difference can be explained by only the difference of the LWL entrance angle as shown in Figure 54 (b). The ships of group A were designed independently from those of Group B as explained above. It means that many other hull form factors besides the LWL entrance angle are different from each other between the two groups of ships. Nevertheless, the large r_r difference can be explained only by the LWL entrance angle difference. It shows how large the influence of the LWL entrance angle to wave-making resistance is.

From the above discussion, we know that the above two resistance test results strongly support our previous study result that has pointed out the outstanding importance of bow form of a ship in wave-making resistance at Froude number below 0.26.

5.2.3 Dominance of wave-breaking near the bow (“Finding 2”)

In the bow form comparison in Yamano *et al*. (1996, 1997), EHP of Stem ㊺ is higher than that of Stem ① by 18%. The EHP difference is caused by the difference in wave-making resistance. Figure 55 shows that the main component of the difference in wave-making resistance coefficient (r_w) measured by resistance test is that in wave-breaking resistance (r_{wb}), since the difference in wave-pattern

resistance (r_{wp}) coefficient calculated from measured wave pattern following the model ship in negligibly small and $r_w = r_{wp} + r_{wb}$.

Figure 55 – Comparison of wave-making resistance coefficient r_w and its component wave-pattern resistance coefficient r_{wp}

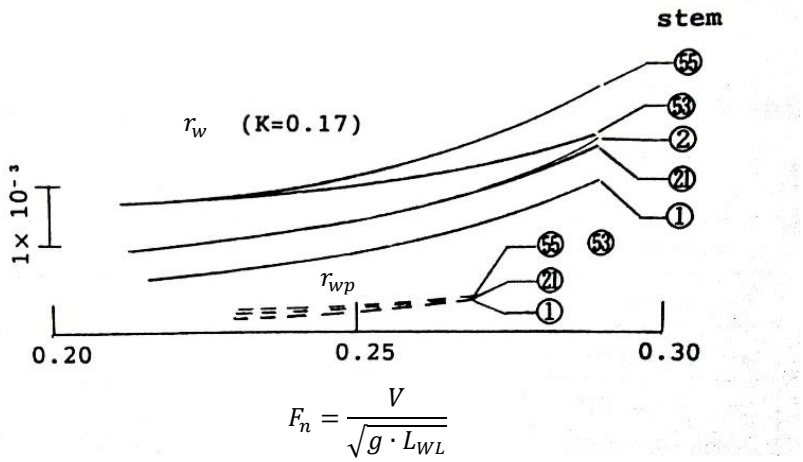

Source: YAMANO, 1996, 1997.

Figure 56 shows bow waves of Stem ① and Stem ⑤⑤.

Figure 56 – Comparison wave-breaking at bow between Stem ① and Stem ⑤⑤

Stem ①

Stem ⑤⑤

Source: YAMANO, 1996, 1997.

From Figure 56, we can know that the wave breaking, which is the main component of the above 18% of EHP difference, occurs just near the bow.

5.3 PROPOSAL OF A NEW RESISTANCE TEST METHOD FOR A FINE SHIP IN A CWC

In the following, the proposal of a New Resistance Test Method for a fine ship in a CWC, which intends to solve the issues presented in 5.1.2 is reported. In 5.3.1, the New Resistance Test Method is presented and explained. In 5.3.2, our evaluation of the New Resistance Test Method is reported.

5.3.1 The New Resistance Test Method for a fine ship in a CWC

In this section, the New Resistance Test Method is

In this section, the New Resistance Test Method is presented and evaluated.

5.3.1.1 Presentation of New Resistance Test Method

The components of a model according to the New Resistance Test Method are shown in Figure 57, represented in top view.

Figure 57 – Components of a model according to the New Resistance Test Method

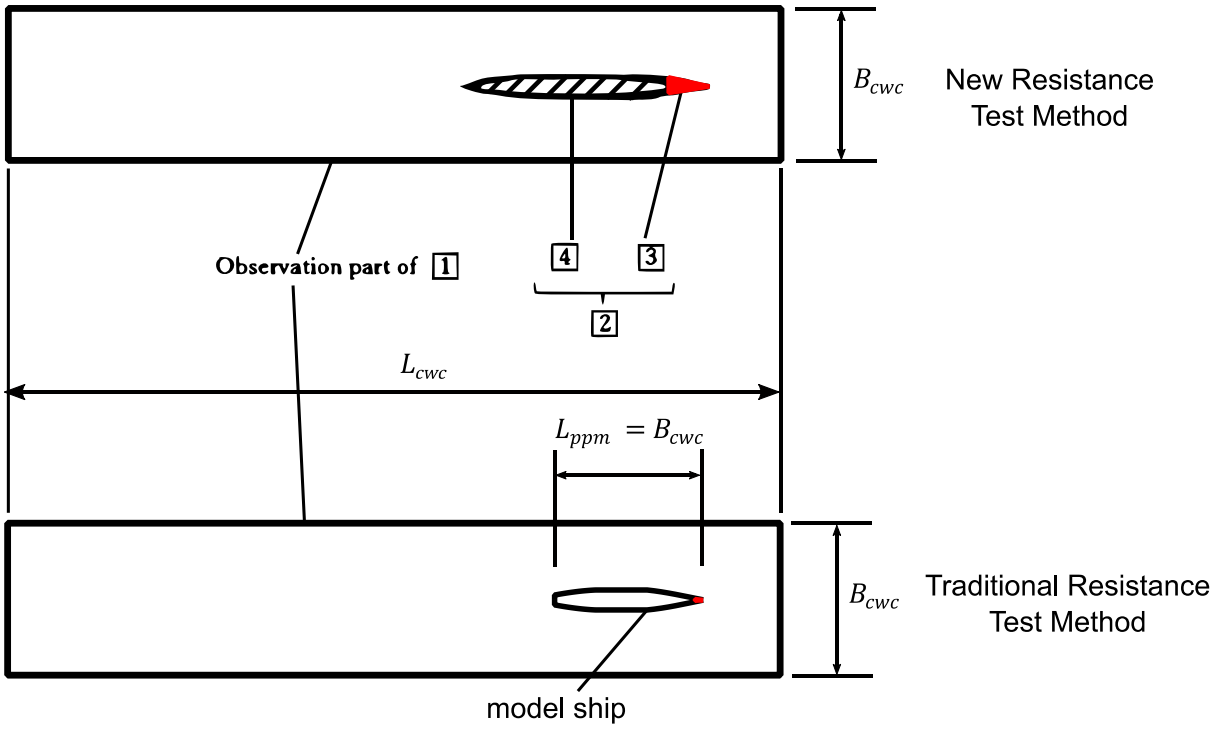

1: CWC, 2: Model to be tested, 3: Bow model, 4: Fairing part

Source: YAMANO (2019).

The rectangle indicated by [1] is the observation part of the CWC, where a model is placed for a test. The observation part [1] has length L_{cwc} and breadth B_{cwc}. In the New Resistance Test Method, a model such as [2] is used. The model [2] has two parts:

(a) a “bow part” model [3], of a much larger model ship.

(b) a “fairing part" [4], after the “bow part” model [3].

5.3.1.2 The way the New Resistance Test Method solves the issue

As described in 5.1.1 and 5.1.2, the issues that the New Resistance Test Method is proposed to solve are: the lower accuracy in resistance measurement in a smaller CWC and the lower form accuracy of the smaller model ship for a smaller CWC.

Based on the findings described in 5.2, it is known that the bow part is the most important hull part for wave-making resistance. So, in the New Resistance Test Method, a test is not done with the model of a whole ship from stern to bow like in the Traditional Resistance Test Method, but with the model of only the bow part, which is the most important hull part for wave-making resistance.

By using the model of only the bow part, instead of the model of a whole ship from stern to bow, for a resistance test in a CWC, we can increase the scale of the model. By increasing the scale of mode, the total resistance of the model increases. With the increase of total resistance, the accuracy of measuring total resistance is increase. As a result, by increasing the scale of model, the model can be manufactured more accurately. Therefore, the form accuracy of is also increased.

5.3.2 Evaluation of the New Resistance Test Method

In the following, we discuss the effect of CWC walls in our developed new resistance test method and evaluate effectiveness of our developed new resistance test method.

5.3.2.1 Discussion of effect of CWC side walls on the resistance of the model in New Resistance Test Method

A concern about the New Resistance Test Method is the effect of CWC side walls on the flow. In Figure 58, an example of a model [2], of a fine ship, designed according to the New Resistance Test Method is shown. The observation part of the CWC has length L_{cwc}=2.00m and breadth B_{cwc}=0.50m. The length of the assumed model ship is $L_{ppm} = 5.38B_{cwc}$=2.69m.

Figure 58 – Waves generated by model [2] at New Resistance Test Method in a CWC

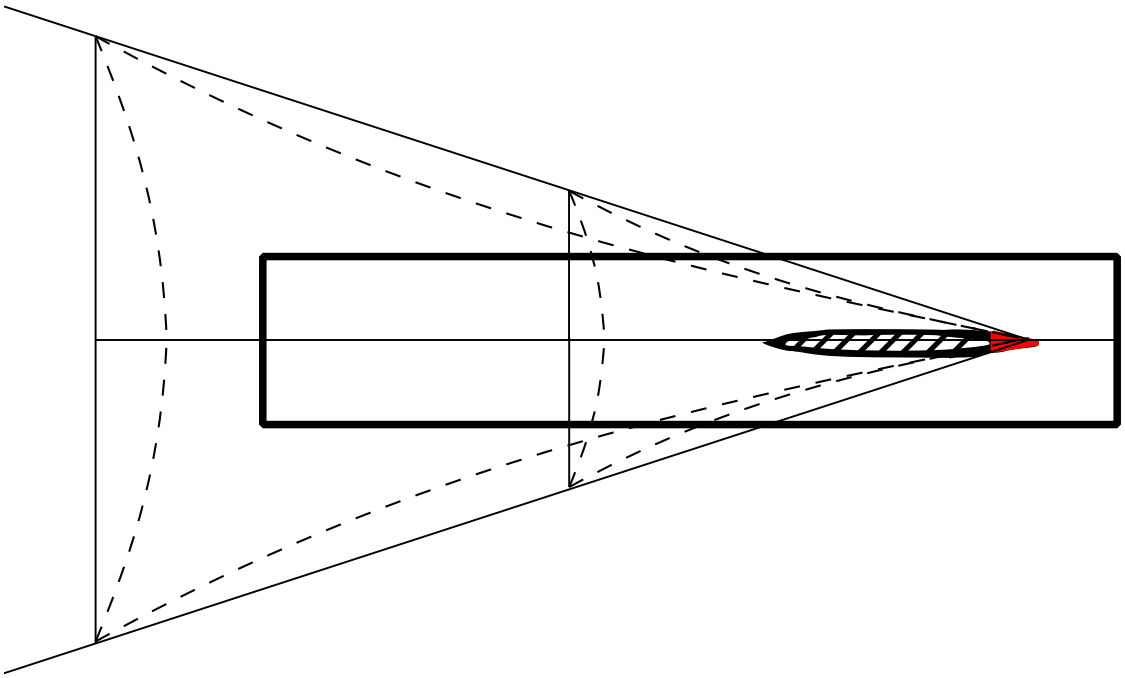

Source: YAMANO (2019).

Concerning wave-breaking, as discussed in 5.2.3, it occurs near the bow. The area around the bow in Figure 58 is enough for the wave-breaking. Therefore, we can say that the effect of CWC walls on wave-breaking near the bow is negligibly small.

Concerning wave pattern propagating afterwards, as discussed in 5.2.3, it is known that, in wave-making resistance, the component due to wave pattern is much smaller compared with that due to wave -breaking. Therefore, the concern about wave pattern is less important than that about wave-breaking.

In Figure 58, wave ridge lines of the 1st and 2nd waves generated by the model [2] are represented by the segment lines [6], at F_n=0.25. The diverging waves of the

two waves are reflected by the CWC. However, the reflected waves do not reach the tested model [2]. Therefore, the effect of CWC side walls to wave-making resistance due to wave pattern is considered small.

From the above discussion, it can be concluded that the effect of CWC side walls on wave-making resistance in the New Resistance Test Method is negligibly small.

5.3.2.2 Effectiveness of New Resistance Test Method

To evaluate the effectiveness of the New Resistance Test Method we consider two CWCs: “CWC 1” with breadth B_{cwc}=0.5m and “CWC 2” with B_{cwc}=2.0m. Other particulars of these two CWCs are shown in Table 12.

If we adopt the Traditional Resistance Test Method, the length L_{ppm} of a model ship to be used in a CWC should be equal to CWC breadth B_{cwc}. Therefore, L_{ppm}=0.5m for “CWC 1” and L_{ppm}=2.0m for “CWC 2”. However, if we adopt the New Resistance Test Method, we can test the bow part model of an assumed model ship with length L_{ppm}=3.0m for “CWC 1” and L_{ppm}=7.0m “CWC 2”, for example.

The total resistance of the bow part model in the New Resistance Test Method is 216 times larger than the resistance of the same bow part of a model ship according to the Traditional Resistance Test Method in “CWC 1” and 42.9 times in “CWC 2”. This shows that we can measure the resistance by the most important part (bow) of a hull with much higher accuracy with the New Resistance Test Method.

Table 12 – Comparison between Traditional Resistance Test Method and New Resistance Test Method

CWC		1		2	
		TRTM	NRTM	TRTM	NRTM
L_{cwc}	m	2.0		6.0	
B_{cwc}	m	0.5		2.0	
V_{max}	m/s	1.5		2.5	
L_{ppm}	m	0.5	3.0	2.0	7.0
$max\ F_n$	-	0.678	0.277	0.565	0.302
$R_{tm}\ ratio$		1	216	1	42.9

Source: YAMANO (2019).

Remarks:
TRTM: Traditional Resistance Test Method in a CWC
NRTM: New Resistance Test Method in a CWC

5.4 A DESIGN OF MODELS FOR A CONFIRMATION TEST IN A CWC

A complete model for a confirmation test of the New Resistance Test Method for a fine ship in a CWC was designed. The model has two parts that are connected each other and then, connected to the measuring apparatus of a CWC. In 5.4.1, the design of the complete model is reported. In 5.4.2, the design of the connection systems – one to connect the two parts each other and the other to connect the complete model to the measuring apparatus of a CWC – is reported. And, in 5.4.3, the complete model with two parts and the connection systems are shown all together.

5.4.1 Design of a complete model

The design of a complete model with two parts is shown in Figure 59.

Figure 59 – Designed complete model for a confirmation test in a CWC (M.No.1)

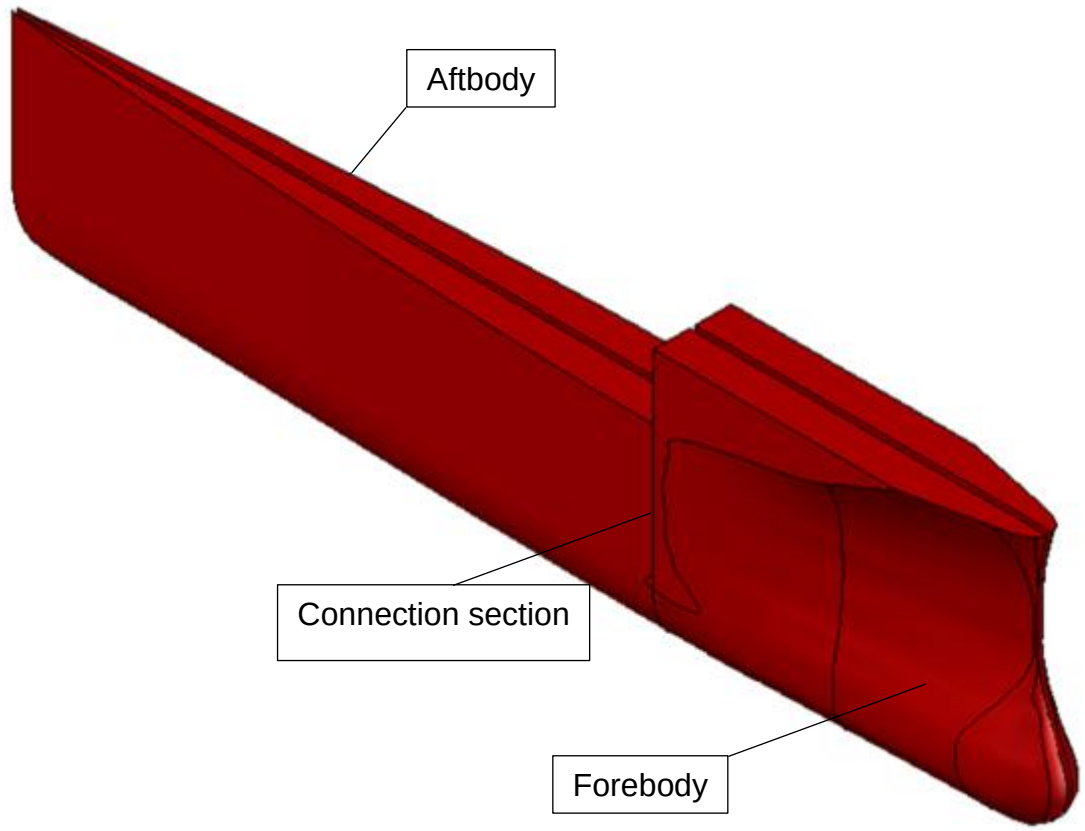

Source: The Author (2019).

In view of Figure 57 the model shown in Figure 59 above corresponds to “Model to be test [2]” in Figure 57, which consists of “Bow model [3]” and “Fairing part [5]”.

A model shown in Figure 57 was designed for the UFPE’s CWC, whose observation part – which corresponds to the rectangle “Observation part of [1]” in Figure 57 – has the dimensions: L_{cwc} = 2.00m × B_{cwc} = 0.50m × height = 0.50m (see Chart 1.1 and Figure 44).

Three bow models of a 354,000ft³ refrigerated cargo ship (L_{pps} = 134.5m) were intended to be designed: M.No.1, M.No.5 and M.No.7. So, the design was done in such a way that a body is separated into two parts: “Forebody” and “Aftbody” and the “Aftbody” is used connected to the three “Forebody”.

Figure 60 shows the dimensions of a complete model with the two parts: “Forebody” and “Aftbody”.

Figure 60 – Dimensions (in mm) of a complete model for a confirmation test in a CWC. In dimension label of “Forebody” length, $l_{f,\max}(mm)$ is the maximum longitudinal length of bow profile from FP.

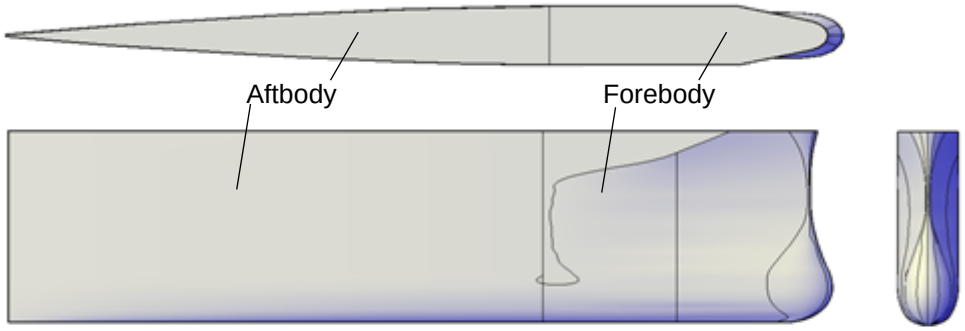

Source: The Author (2019).

At SS 9, which is the fullest section of the complete model – where all the waterlines are parallel to the centerline plane, the complete model is separated into two parts. The part from SS 9 to SS 7 in Figure 60 is the “Aftbody”, and the part from the fore end to SS 9 in Figure 60 is the “Forebody”. The “Aftbody” consists of the

“Fairing part 5” in Figure 57, which has a two-dimensional form based on NACA 0009, and the “Forebody” consists of:

1) from the fore end to SS 9 ½ , the bow part of one of the three models (M.No.1, M.No.5 or M.No.7), same as “Bow model 3” in Figure 57

2) from SS 9 ½ to SS 9 – a part of the “Fairing part 5” which is a transition between the “Aftbody” in SS 9 and the “Bow model 3” at SS 9 ½.

The “Assumed model ship 4” is a model for a Traditional Resistance Test with the hull form of one of the three models (M.No.1, M.No.5 or M.No.7), with L_{ppm} = 2.69m. So, the model scale is 1/50.

5.4.2 Design of connection systems

In the following, the design of the connection systems is reported.

5.4.2.1 Design of connection system between “Forebody” and “Aftbody”

“Aftbody” is attached to “Fixed center plate” shown in Figure 61. “Fixed center plate” is connected to the measuring apparatus of the CWC.

Figure 61 – Fixed center plate to which “Aftbody” is attached.

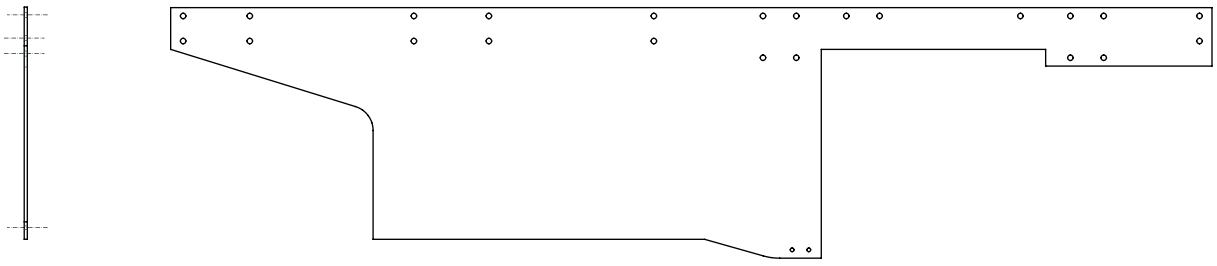

Source: The Author (2019).

“Forebody” is attached to “Movable center plate” shown in Figure 62. For each model, one “Movable center plate” is needed.

Figure 62 – Movable center plate to which “Forebody” is joined.

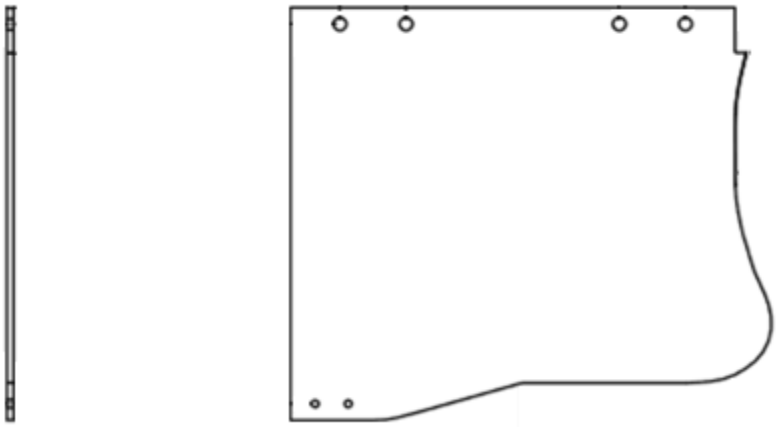

Source: The Author (2019).

“Movable center plate” is connected to “Fixed center plate” by an upper connection and a lower connection, as shown in Figure 63. As “Movable center plate” is connected only to “Fixed center plate”, to change the model, only changing “Movable center plate” is needed.

Figure 63 – “Movable center plate” connected to “Fixed center plate”.

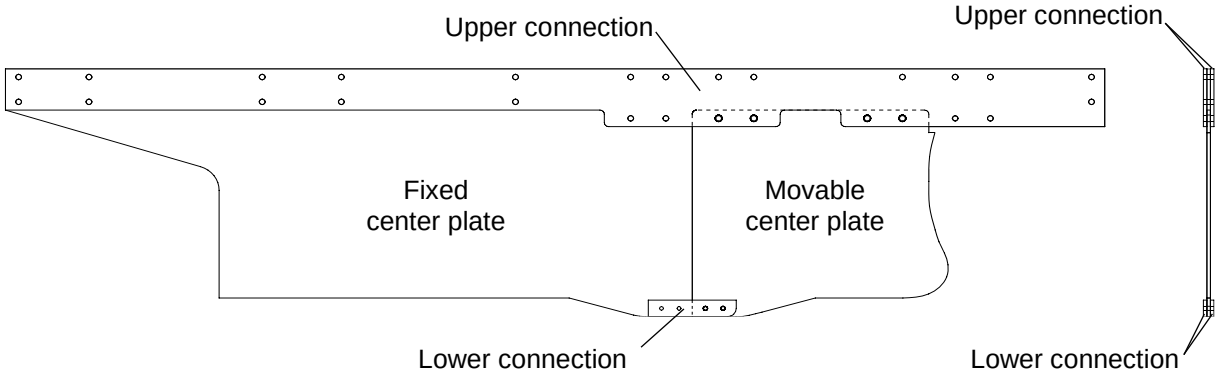

Source: The Author (2019).

5.4.2.2 Design of connection system between complete model and measuring apparatus of a CWC

The connection system described in 5.4.2.1, with the model attached to it, is connected to the measuring apparatus by clamps, as exemplified in Figure 64 with a flat plate. The connection system is positioned in the place where the flat plate is.

Figure 64 – Flat plate connected to measuring apparatus by clamps.

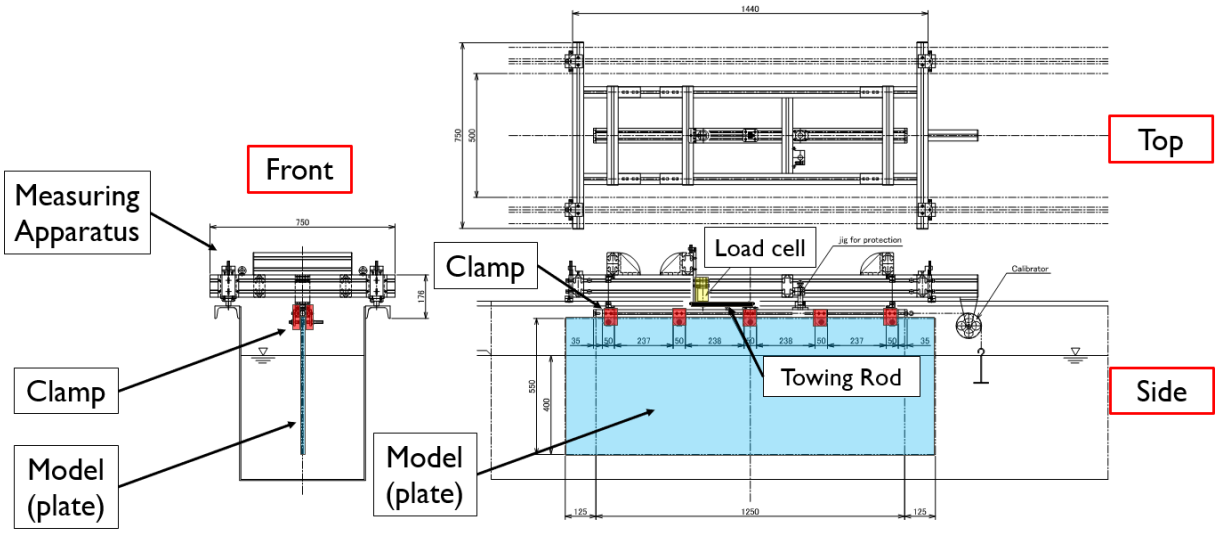

Source: FEL (2015). Adapted.

5.4.3 Complete model and connection system designed

Figure 65 shows the design of a model attached to connection system and immersed in the CWC observation part.

Figure 65 – Design of a model attached to connection system.

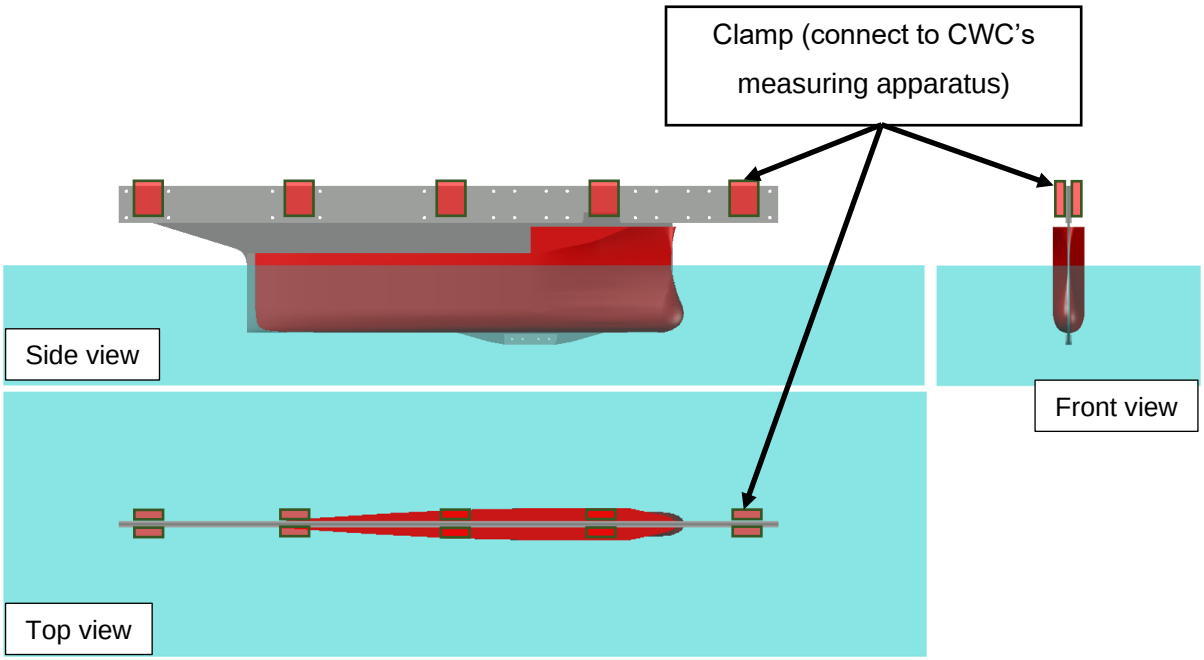

Source: The Author (2019)..

5.5 A STUDY OF MODEL MANUFACTURE FOR THE TEST IN A CWC

For the developed New Resistance Test Method, a model for a test in a CWC is necessary. Due to the lack of model suppliers, we decided to study the way how to

prepare such a model by ourselves. We manufactured a partial model and evaluated it in order to confirm whether it satisfies or not the conditions for a model and for model manufacture established in 5.1.3.

In the following, the study on the manufacture of a model for a test in a CWC is reported. In 5.5.1, the structure and manufacture process to manufacture a model is reported. In 5.5.2, the materials used to manufacture the partial model. In 5.5.3, the evaluation the manufacture partial model. In 5.5.4, the discussion of the results of this study.

5.5.1 Structure and manufacture process

The structure of the model consists of the following parts:

1) Center plane

2) Transverse frames with accurate section forms shown in Figure 66 (a), (b) and (c)

3) Horizontal members with accurate waterline forms shown in Figure 66 (a), (b)

4) Plastic to be inserted into the rectangular space surrounded with two transverse frames and two longitudinal members shown in Figure 66 (c).

Regarding the manufacturing process:

- The inserted plastic is shaped using the forms of the surrounding frames and longitudinal members as shown in Figure 66 (c).

Figure 66 – (a) Transverse frames and longitudinal members before cut, drawn in A4 papers. (b) Assembled frames and longitudinal members on a center plane. (c) Frames, longitudinal members and inserted “Plastic 1”.

(a) (b) (c)

Source: Author.

5.5.2 Materials

The materials used to manufacture the partial model are the following:

1) Paper with size A4 (210 mm × 297 mm) and with a density of 180 g/m² was used for the center plane, transverse frames, and longitudinal members.

2) “Plastic 1”, the material (styrofoam) used for a float in a swimming pool found in a supermarket is used as the plastic to be inserted between the frames and longitudinal members.

3) Glue gel was used for joining the paper members and joining “Plastic 1” to paper members.

4) Filler made of white glue and wood powder is used to fill gaps in the partial model.

5) Water-based paint usually used for cloth painting was used to paint the completed partial model.

Figure 67 – Tests of two plastics against polyester resin and oil paint. “1” refers to “Plastic 1” and ”2” to “Plastic 2”. (a) Samples with size: 20 mm × 20 mm × 15 mm before tests. (b-1), (b-2) Samples after polyester resin application. (c) Samples after oil paint application.

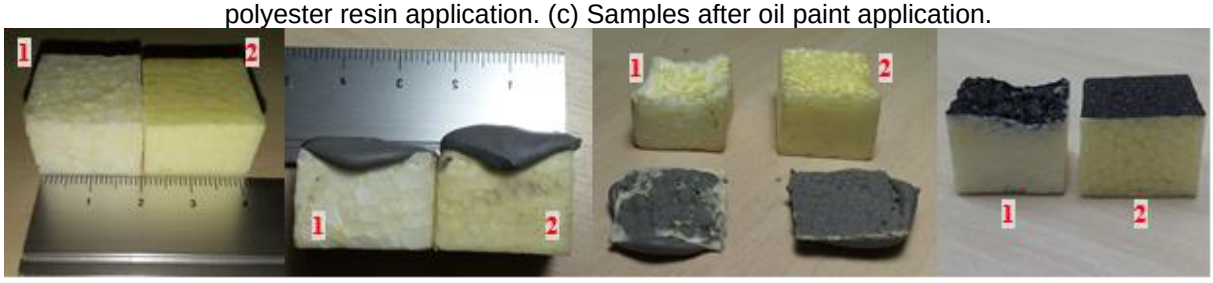

(a) (b-1) (b-2) (c)

Source: Author.

5.5.3 Test of a partial model

After the completion of the partial model, we evaluated it in order to confirm whether it satisfies or not the conditions for a model established in 3.1.3. The completed partial model is shown in Figure 68.

Figure 68 –Completed partial model before the water tightness test. Left and right photos show different views of the same model.

The evaluation is as follows:

1) Accuracy: We have confirmed that we can keep the accuracy of form by the way where we use transverse sections and horizontal sections even with papers. By increasing the number of sections and by using wood for transverse and horizontal sections, we can increase the form accuracy.

2) Strength: Material for the center plane, transverse frames, and horizontal members is paper. However, the completed partial model was rigid enough and seemed able to be used for the test in a CWC.

3) Water tightness: We have soaked the completed partial model in water for a day, to check its water tightness. As a result, it showed that the water had penetrated

the model as shown in Figure 69. It showed that the water-based paint used did not realize its water tightness.

Figure 69 – Partial model after the water tightness test.

Source: Author.

5.5.4 Discussion of the result

We discuss the result as follows:

1) Accuracy: We have confirmed that we can keep enough accuracy of the model by manufacturing the model by the method above described. If we need more accuracy, we can get it by increasing the number of transverse frames and horizontal members and by using wood instead of paper.

2) Strength: Even with structure members made of papers as described above, the completed partial model was rigid and seemed to have enough strength for the model test in a CWC. Therefore, if we use water-resistant wood for the center plane, transverse frames, and horizontal members, we can surely get a model with enough strength for the model test in a CWC. The wood will improve the accuracy of the model also compared with the paper.

3) Water tightness: To get water tightness, we need such material that can bear polyester resin and oil paint. We have searched for such material and found it. It is “Plastic 2”, the material used for a styrofoam block. We have tested whether “Plastic 2” can bear polyester resin and oil paint. The result is shown in Figure 67. The result shows that “Plastic 2” can bear them.

4) Our prospect of the model for a CWC: Through the above study, we have found that we can manufacture such a model that has enough accuracy, strength, and water tightness and so we can use for the model test in a CWC. It has strength members made with water-resistant wood, “Plastic 2” as material to be inserted among strength members, polyester resin and oil paint to be laid over the model.

6 CONCLUSIONS

The conclusions are stated below for each of the studies: “Study 1” and “Study 2”.

6.1 FOR “STUDY 1”

We have got the following conclusions:

(1) About the relation between the bow form parameters and the wave-making resistance of a full ship, we could clarify that:

(a) “b_e”: imaginary half breadth of fore end of waterline on the water surface decides the larger part of wave-making resistance at a draft, at F_n lower than 0.17.

(b) “i_e”: entrance half angle of waterline on the water surface has a negligibly small influence on the wave-making resistance at the draft, if its value is lower than the recommended maximum value in (LEWIS, 1988).

(c) “i_r”: stem rake angle on the water surface has a negligibly small influence on the wave-making resistance at the draft.

(2) To estimate the wave-making resistance of Ship ISNI, we have derived equation (26), which is a function of “b_e” and F_n. We can use it for any other ships by deciding two factors in the equation with their base data: depth of a line source and $F_n - \left(\frac{R_{ws}}{\rho_s V_s^2}\right)_{\text{remaining}}$ curve.

(3) We designed two modified bow models, M1 and M2, using equation (26), in order to reduce the larger wave-making resistance at Ballast condition of Ship ISNI. The EHP reduction by them we got by the resistance test with 2m-long model ship are 3.8% (M1) and 5.4% (M2) at F_n=0.15. The average EHP reduction in the F_n range from 0.10 to 0.18 are 3.1% (M1) and 5.5% (M2). These values are somewhat smaller than our estimation by equation (26). However, they are practically large enough as we explained in Table 9. Therefore, we can say that we have confirmed that we can use equation (26) for our bow form design of a full ship.

(4) We have developed a bow form design method for a full ship based on equation (26) as described in 2.8.4. We can apply it to bow form design for a full ship with any bow form and with design F_n less than 0.17.

6.2 FOR “STUDY 2”

(1) We have confirmed, by our additional theoretical analysis and further discussion with other related model test results, that the result of the undergraduate thesis (FABRÍCIO FILHO, 2018), which has pointed out the outstanding importance of bow form of a ship in wave-making resistance at Froude number below 0.26, is quite reliable.

(2) We developed a New Resistance Test Method for a fine ship in a CWC and evaluated its effectiveness. As considered in 3.2.3.2, the developed New Resistance Test Method in a CWC increases the value of the measured total resistance by 216 times compared to the Traditional Resistance Test Method in “CWC 1” and 42.9 times in “CWC 2”. This makes the New Resistance Test Method much more accurate than the Traditional Resistance Test Method.

(3) We have designed models and connection system for the confirmation test of the new resistance test method in the CWC.

(4) We have designed and manufactured a partial model for a test in a CWC, by ourselves. Through these studies, we have clarified the issues we meet in the model manufacture. Then, we have studied the ways how to solve the issues and clarified them.

(5) As a result, we are now ready for the manufacture of models including connection system and for the confirmation test in the CWC.

7 FINAL CONSIDERATIONS

Master's: 2019/03~2020/03

What we did in one year

Until the end of May/2019, we had done:

1. New Resistance Test Method for a fine ship in a CWC

a) Base: undergraduate thesis result (2018, resulted in one paper to SOBENA)

b) Proposal of a New Resistance Test Method for a fine ship in a CWC

c) Design of models and connection system for a confirmation test in a CWC

d) A study on model manufacture (this was done because we confirmed that we cannot rely on outsourcing for model manufacture: the makers nearby cannot manufacture a model according to our expectation; so, we had to study how to do a model by ourselves)

e) We have finished preparation for confirmation test in the CWC

On May 31st, 2019, Oshima Shipbuilding Co., Ltd. (OSY) confirms their decision to hire me on April 1st, 2020. This meant I must finish master's in one year.

CWC: since the end of August/2018, CWC was successfully installed at UFPE. However, at the end of May/2019, we could not have such prospect that we can use the CWC normally and conduct the confirmation test of the method soon there. So, we added one more theme: development of bow form design method for a full ship.

We could benefit from the added theme because:

- We could develop a useful design method also for a full ship
- Since OSY works with bulk carriers, the additional theme is useful for them. So, we proposed to OSY to cooperate with us in the realization of my master's thesis. They have accepted our proposal and we are very much thankful to them.

We can conclude that to add one more theme was a very wise choice.

From the end of May/2019, until January/2020, we have done:

1. Development of bow form design method for a full ship

a) Base: undergraduation thesis result

b) Preliminary study (resulted in one paper to SOBENA)

c) Detailed study (resulted in one paper to JMST)

The unhappy situation that we could not use CWC at UFPE in our research did not make us stop. Instead, we did more than what was initially planned, could have the support by OSY and could directly contribute to the company with our study. We could take advantage of an unhappy situation and finish very much satisfied. And we did it in one year, not in two.

This master's was a nice life experience for me. Such experience taught me not only about design of ship's hull form. It also taught me how to live in such a world where we have limited time, limited budget, some accidents, but we, anyway, must do our work there. Such a world is the real world, and even in it, we can find a way to be happy.

This is the last but most important message. I have done much work in one year for my master's thesis study and could get enough results as described. However, they have not been completed only by me. Without good cooperation with the people around me including the people of Oshima Shipbuilding Co. Ltd., I could not have done it. Now, I know that good enough cooperation with the people around me is a key to accomplish a big project.

REFERENCES

BABA, E. A new component of viscous resistance of ships. **J Soc Nav Archit Jpn** 125: 23-34, 1969.

EBIRA, K.; IWASAKI, Y.; KOMURA, A. Development of a new stem to increase the propulsive performance of LPG carriers. **J Kansai N A Jpn** 241: 1-8, 2004.

EYRING, V. *et al*. Emissions from International Shipping: 1. The Last 50 years. **Journal of Geophysical Research**, 110, 2005.

FABRÍCIO FILHO, L.C**. Estudo de uma forma de casco com menor resistência de formação de ondas para número de froude abaixo de 0,26.** 2018. 67 p. Graduate (monography) – Universidade Federal de Pernambuco, 2018.

FABRÍCIO FILHO, L.C.; CARBAJAL, M.A.C.; SHINOHARA, A.H.; YAMANO, T. A Study on a Hull Form with Lower Wave-Making Resistance at Froude Number Lower Than 0.26. *In*: INTERNATIONAL CONGRESS OF WATERWAY TRANSPORTATION, SHIPBUILDING AND OFFSHORE CONSTRUCTION, 27., 2018, Rio de Janeiro. **Proc.** [...]. Rio de Janeiro: SOBENA, 2018. DOI 10.17648/sobena-2018-87514

FABRÍCIO FILHO, L.C.; SHINOHARA, A.H.; YAMANO, T. **A Further Study on Relation between Wave-Making Resistance and Hull Form in Froude Number Range Less than 0.26**. Proc. of 25th ABCM International Congress of Mechanical Engineering – COBEM, 2019.

FABRÍCIO FILHO, L.C.; OKAMOTO, K.; SHINOHARA, A.H.; PENGFEI, G.; ARITA, K.; YAMANO, T. **A Study on Bow Form Design for a Full Ship**. 2020. Not published.

FABRÍCIO FILHO, L.C.; SHINOHARA, A.H.; YAMANO, T. A Study of the Relation between Wave-Making Resistance and Bow Form of a Full Ship in the Draft Range from a Shallow Draft to an Over-Full Draft**.** In: Proc. of 11th International Seminar on Inland Waterways and Waterborne Transportation, 2019, Brasília. **Anais eletrônicos...** Campinas, GALOÁ, 2019.

FEL. **UFPE CWC Manual.** FEL – West Japan Fluid Engineering Laboratory Co., Ltd. Manual.

HAVELOCK, T. H. The Calculation of Wave Resistance. **Proc. Royal Society**, p. 514-521, 1934.

HAVELOCK, T. H. The Theory of Wave Resistance. **Proc. Royal Society**. Vol. 138, A, p. 339-348. August 1932.

HAVELOCK, T. H. **Wave Patterns and Wave Resistance.** TINA, p. 430-446, 1924

IMO. **Prevention of Air Pollution from Ships:** Updated 2000 Study on Greenhouse Gas Emission from Ship. London, 2008.

INUI, T. **Wave-making resistance of ships.** T SNAME 70: 283-313, 1962.

KRACHT, A.M. **Design of bulbous bow.** T SNAME 86:197-217, 1978.

LAP, A.J.W.; VAN MANEN, J.D. **Fundamentals of Ship Resistance and Propulsion.** Netherlands Ship Model Basin, NSMB. 1958.

LEWIS, E.V. **Principles of Naval Architecture**. Vol. 2 Resistance, Propulsion and Vibration. SNAME: 70-71, 1988.

LUNDE, J.K. **On the Linearized Theory of Wave Resistance for Displacement Ships in Steady and Accelerated Motion.** The Society of Naval Architects and Marine Engineers, p.25-85, 1951.

MAN DIESEL & TURBO. **Basic Principles of Ship Propulsion.** Copenhagen, Denmark. 2011

MFAME TEAM. **Wave-making resistance – best example – from the IMarEST condition based maintenance conference**. 2016. Available from: http://mfame.guru/wave-making-resistance-best-example-from-the-imarest-condition-based-maintenance-conference/. Accessed in: Feb 11, 2020.

MICHELL, J.H. Wave–Resistance of a Ship. **Philosophical Magazine**, vol. 45, Ser. 5, p. 106-123. 1898.

MUNTJEWERF, J.J. **Methodical series experiments on cylindrical bows.** T RINA: 199-223, 1967.

OECD. **The Ocean Economy in 2030**. OECD Publishing, Paris. 2016 http://dx.doi.org/10.1787/9789264251724-en

RESEARCHGATE. **Numerical analysis of influence of ship hull form modification on ship resistance and propulsion characteristics Part III Influence of hull form modification on screw propeller efficiency** - Scientific Figure on ResearchGate. 2009. Available from: https://www.researchgate.net/figure/Body-lines-of-the-analyzed-hull-form-of-B-573-ship_fig1_259561496. Accessed in: Feb 12, 2020.

SCHILLER, RODRIGO ACHILLES. **Análise da eficiência energética em navios mercantes e estudo de caso do consumo de combustível em navio aliviador do tipo Suezmax**. Dissertação (Mestrado) - Escola Politécnica, Universidade de São Paulo, São Paulo, 2017.

SEATRADE MARITIME. **K Line reports full year profit.** May, 2013. Available from: https://www.seatrade-maritime.com/asia/k-line-reports-full-year-profit. Accessed in: Feb 12, 2020.

SHARMA, R.; SHA, O.P. Practical hydrodynamic design of bulbous bows for ships. **Nav Engineers J Winter**: 57-75, 2005.

SHIGEMITSU, M.; KAI, K. The wave-cancelling effects of waveless bulb on the high-speed passenger coaster M/S “KURENAI MARU”: Part II – The full-scale experiment. **J Soc Nav Archit Jpn** 110: 91-104, 1961.

TAKEKUMA, K.; KAYO, Y. A study on structure of wave breaking at bow of a full ship. **Mitsubishi Tech Bull** 18-5: 78-81, 1981.

TANEDA, S. Observation of viscous flow around an obstacle**.** Proc Symposium on Viscous Resistance, **Soc Nav Archit Jpn**: 35-58, 1975.

UEURA, T.; HINO, T.; SUZUKI, K. Study on CFD simulation of hydrodynamic phenomena with vortex flow around the blunt bow. **J Jpn Soc Nav Archit and Ocean Eng** 19: 9-18, 2014.

UNITED NATIONS. **Review of Maritime Transport 2017.** Geneve, 2017.

VAN MANEN, J. D.; VAN OOSSANEN, P. **Principles of Naval Architecture,** Vol. 2. The Society of Naval Architects and Marine Engineers. EUA. 1988.

WORLDCOAL. **Coal carrier wins 'Bulk Ship of the Year' award**. Dec, 2014. Available from: https://www.worldcoal.com/handling/04122014/coal-carrier-wins-ship-of-the-year-award-1641/. Accessed in: Feb 12, 2020.

YAMANO, T. **Hull form design data.** 1994. Not published.

YAMANO, T. **Hydrodynamics design of a ship**: DWG. 3-1 Class (3). April 5, 2018. 7 p. Class notes.

YAMANO, T.; FUNENO, I.; SAITO, Y.; AND IWASAKI, Y. **Stem Form for Fine Ships:** Ease of Construction or Improved Propulsive Performance, Proc. of 6th IMDC, pp. 361-375, 1997.

YAMANO, T.; SAITO, Y.; IWASAKI, Y; FUNENO, I. A Consideration on Stem Form for Fine Ships. **J. of Kansai Soc. N. A., Japan**, No.225, pp. 25-35, 1996.